藥學 博士 學位 論文

Proton-mediated modulations of Anoctamins

수소이온에 의한 아녹타민 활성 조절 기전

2015年 8月

서울大學校 大學院

藥學科 病態生理學 專攻

千 惠 娟

Abstract

Ca^{2+}-activated Cl^- channels are involved in fluid and electrolyte secretion in epithelial cells. It is closely related to intracellular pH. Anoctamin1 is known to mediate Ca^{2+}-activated Cl^- currents. However, little is known whether ANO1 can be modulated by change of intracellular pH. Here, we demonstrated that both ANO1 and ANO2 are inhibited directly by acidic intracellular pH using the inside-out patch clamp technique. The acid-induced modulations of other ANOs were also tested. ANO6 and ANO7 were inhibited by intracellular acid. But intracellular acid failed to block the current of ANO9. Intracellular acid also inhibit the voltage-dependent activation.

Intracellular acid induce the decrease of the Ca^{2+} sensitivity in ANO1. The higher Ca^{2+}-activated ANO1 current required more protons to inhibit. But the voltage-activated and heat-activated ANO1 current was not inhibited by intracellular acid.

To identify the location of the acid-induced inhibition, mutagenesis studies were performed. Mutations were made on His residues in cytoplasmic side of ANO1. However, there was no His mutant that showed the reduction of the acid-induced inhibition. Some clusters of Glu and Asp are also dispensable for the acid-induced inhibition. Recently, the Ca^{2+}-binding site of a fungal anoctamin (*nh*TMEM16) was uncovered by crystallography. The Ca^{2+}-binding residues are present in α6, α7 and α8

helix. The reference helix located between α6 and α7 helix are also essential for the Ca^{2+}-mediated activation due to its repulsive movement. Mutagenesis was performed in the Ca^{2+}-binding site and the reference helix. Indeed, we identified that Glu, Asp or Asn residues (650N, 654E, 702E, 705E, 734E and 738D) which are essential for Ca^{2+} binding are crucial sites for inhibition of ANO1 by intracellular proton. But reference helix does not affect the acid-induced inhibition of ANO1. This result suggests that proton in this region interfere binding of Ca^{2+}.

Our findings provide that molecular mechanism of ANO1 regulated by the internal pH. Intracellular proton inhibits the Ca^{2+}-mediated ANO1 activation by competitive manner or structural modification, acting on the Ca^{2+} binding site.

Keywords: Intracellular acid; Intracellular pH; ANO1; ANO2; chloride channel; fluid secretion; epithelial transport.

Student number: 2008-21813

Table of Contents

List of Figures

List of Tables

Introduction

1. Fluid and electrolyte secretion

1.1. The physiological roles of fluid secretion

Fluid and electrolyte secretion in epithelia serves various functions in different organs such as the airways, intestines, pancreas and salivary glands (Barrett and Keely, 2000; Verkman et al., 2003; Melvin et al., 2005; Lee et al., 2012). The maintenance of the adequate fluid compartment is important for normal functions of organs. For example, viscosity affects the rate of mucociliary clearance. Appropriate pH is essential for activating digestive enzymes. In cystic fibrosis, pathological symptoms are due to deficits of the luminal fluid.

1.1.1. Airways

The airways (trachea and bronchi) have numerous submucosal glands (Fig. 1). The epithelial cells in the airway contribute to produce airway surface liquid (ASL) (Verkman et al., 2003). The ASL is an aqueous solution composed of ions, glycoproteins such as mucins and other proteins like lactoferrin, defensins, lysozyme, IgA. It plays an important role in airway hydration, innate immunity and antimicrobial defense (Tarran et al., 2006). In cystic fibrosis, the increase in viscosity of ASL induces the occlusion of

the airways and bacterial infection (Chmiel and Davis, 2003; Gibson et al., 2003). The airway epithelia have polarity due to localizations of transporters and channels (Boucher, 1994). Due to transporters and channels, it is permeable to water and has a low transepithelial resistance (Farinas et al., 1997). Absorbing Na^+ and secreting Cl^- produce efficient ASL volume for mucus clearance (Verkman, 2001). It has been known that the epithelial Na^+ channel (ENaC) mediates absorbing Na^+ and Ca^{2+}-activated chloride channel (CaCC) or cystic fibrosis transmembrane conductance regulator (CFTR) mediates secreting Cl^- at the apical membrane (Chambers et al., 2007). These channel regulate ASL volume to response shear stress (Tarran et al., 2006). Shear stress through the airway surface increases ATP release and intracellular Ca^{2+} (Lazarowski et al., 2000; Tarran et al., 2005). ATP inhibits ENaC whereas it activates CaCC via G protein-mediated increase of intracellular Ca^{2+} (Cressman et al., 1999; Devor and Pilewski, 1999).

1.1.2. Intestines

The intestine secretes ~8 L a day. The secretory fluid contains the diverse digestive enzymes and it is adequate for digestive processing (Barrett and Keely, 2000). Fluid and electrolyte secretion in the intestine is specialized. In the proximal duodenum, the high level of HCO_3^- sustained to protect itself from the gastric acid (Hogan et al., 1994). To protect the epithelia from physical damage, lubricating the epithelia with mucous is important (Cooke, 1994). Throughout the gastrointestinal tract, fluid

secretion is dependent to movement of electrolytes. The predominant driving force of water secretion is Cl^-. HCO_3^- is the secondary source of flud secretion in the intestinal tract (Hogan et al., 1997). A monolayer of the epithelial cells lines along the intestine. Similar to other epithelia, diverse transporters and ion channels are involved to fluid and electrolyte secretion. Na^+-K^+-ATPase, $Na^+/K^+/2Cl^-$ cotransporter (NKCC) 1 and K channels are located at the basolateral membrane (McRoberts et al., 1985; Payne and Forbush, 1995; Lomax et al., 1996; Pressley, 1996). At the apical membrane, Cl^- exits through CFTR or CaCC (McEwan et al., 1994; Ameen et al., 1995). Excessive Cl^- secretion causes diarrhea (Turvill and Farthing, 1999). Distinct to that, patients in cystic fibrosis suffer from intestinal obstruction and digestive defects because of the insufficient Cl^- secretion (Cohn et al., 1998; Quinton, 1999).

1.1.3. Pancreas

Fluid from the pancreas is an alkaline fluid, which is a HCO_3^--rich fluid (Kuijpers and De Pont, 1987). The fluid contains digestive enzymes and releases into the duodenum. Similar to other exocrine glands, the exocrine pancreas is composed of the acinar and duct cells. The acinar cells are polarized epithelial cells, which are capable of secreting fluids and electrolytes (Lee et al., 2012). HCO_3^- is critical for fluid secretion in pancreas (Kuijpers and De Pont, 1987). Pancreatic secretion is controlled by hormones such as cholecystokinin and bombesin and neurotransmitters such as acetylcholine (Ashton et al., 1991; Ashton et al., 1993; Saluja et al.,

2008). The increase of cAMP and intracellular Ca^{2+} is occurred. Various transporters and channels are coordinated to the fluid secretion. Na^{+}-K^{+}-ATPase, Na^{+}-HCO_3^{-} cotranspoter (NBC) are expressed at the basolateral membrane (Petersen, 1986; Morth et al., 2011). Different to other secretary epithelia, the ENaC is not existed in pancreatic duct (Lee et al., 2012). NHE1 and AE2 are expressed in the basolateral membrane to maintain and regulate intracellular pH (Muallem and Loessberg, 1990; Zhao and Muallem, 1995a, b). CFTR, anion exchangers (AEs) and CaCCs are located in the apical membrane to secrete the fluid to the apical side (Zsembery et al., 2000; Steward et al., 2005; Ishiguro et al., 2009).

1.1.4. Salivary glands

Salivary glands are composed of three major parts, the parotid gland, the submandibular gland and the sublingual gland (Melvin et al., 2005). The secretory fluid of salivary glands contains water, electrolytes and a mixture of proteins. It is quite viscous because of large molecular weight mucins (Nauntofte, 1992). We usually secrete more than 1 L of saliva each day. It is responsible for the protection and the hydration of the oral cavity, oropharynx and esophagus (Turner and Sugiya, 2002). The viscosity of saliva affects mucosiliary clearance. The acinar cells in salivary glands have Na^{+}-K^{+}-ATPase, NKCC, Ca^{2+}-activated K^{+} channel and CaCC. Na^{+}-K^{+}-ATPase, NKCC and Ca^{2+}-activated K^{+} channel are located in the basolateral membrane, whereas CaCC are expressed in the apical membrane. Like other epithelial cells, Cl^{-} is accumulated due to NKCC. Cl^{-}

and HCO_3^- efflux is mediated by CaCC. Fluid secretion in salivary gland is modulated by acetycholine (Ach), which is released during parasympathetic stimulation. Ach induce the increase of Ca^{2+} and then Cl^- and HCO_3^- efflux is occurred. Simultaneously, intracellular pH is decreased. The decrease is diminished by HCO_3^- depeletion or chloride channel blocker (Melvin et al., 1988; Nguyen et al., 2000).

1.1.5. Eyes

The entire exposed surface of the eye is covered by tears, a fluid film. Tears are derived from the epithelial cells. Tears play a role in the protection of the cornea and conjunctiva (Dartt, 2002). Fluid is continuously secreted due to the various stresses, such as desiccation, bright light, cold, mechanical stimulation, physical injury, noxious chemical and infections (Dartt, 2002). To maintain optimal nutrients levels and pH, many transporters and channels are coordinated. Na^+-K^+-ATPase, NKCC, NHE1 and AE2 are located in the basolateral membrane (Turner et al., 2000; Turner et al., 2001). The adrenergic agonist, epinephrine enhances the fluid secretion (Shi and Candia, 1995). In conjunctiva, β_2-adrenergic receptors are mediated to stimulate the secretion (Kompella et al., 1996). Purinergic receptors, such as $P2Y_2$ and $P2Y_4$ are also related (Hosoya et al., 1999). Through these receptors, the level of cAMP and intracellular Ca^{2+} is increased. It induces the Cl^- efflux to the apical side (Shiue et al., 1998).

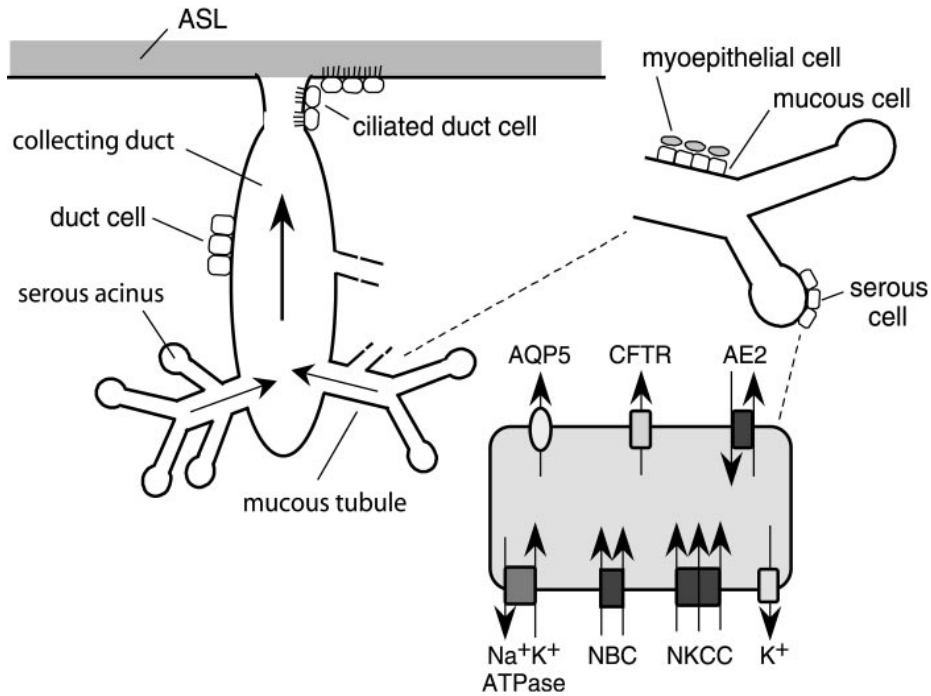

Fig. 1. Scheme of submucosal gland fluid secretion in human airways
(Verkman et al., 2003)

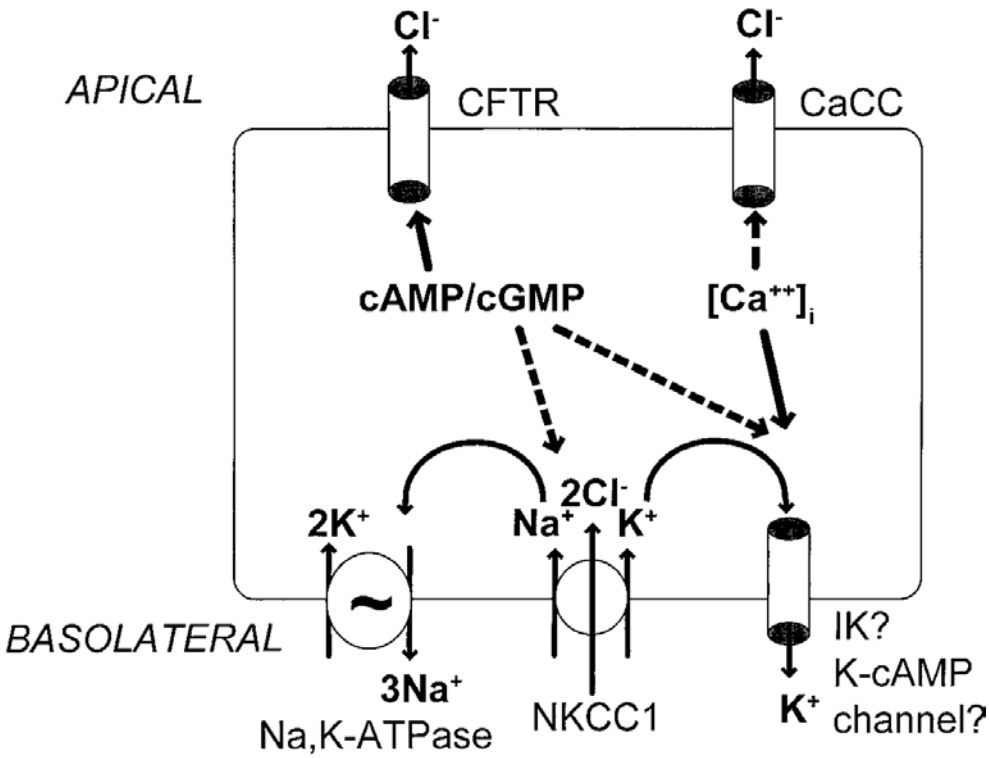

Fig. 2. Model of the fluid secretion in the epithelial cells

(Barrett and Keely, 2000)

1.2. Transporters and channels involved in the fluid secretion

Fluid and electrolyte secretion is highly regulated (Begenisich and Melvin, 1998; Jang and Oh, 2014). As shown in Fig. 2, transporters and channels are arranged asymmetrically in the secretary epithelia (Barrett and Keely, 2000; Melvin et al., 2005). In the epithelial cells, intracellular Cl^- is accumulated by an electroneutral NKCC located in the basolateral membrane. Concentration of intracellular Cl^- is higher than that of other cells (Foskett, 1990). Na^+-K^+-ATPase pumps out 3 Na^+ in exchange for 2 K^+ by using ATP in the basolateral membrane(Pressley, 1996). Na^+ is used as a source of Cl^- movement through the NKCC. And the pumps depolarize the membrane. More than two types of K^+ channels are located in the basolateral membrane (Petersen, 1986). Influx and reuse of K^+ maintain the depolarized membrane potential, which facilitates the electrical driving force for Cl^- exit. Thus, Cl^- efflux is occurred when the Cl^- channel is activated. Cl^- is a major determinant of the fluid secretion. 4 types of Cl^- channels are expressed in the apical membrane. They are classified by their activators; intracellular cAMP, cell swelling, membrane potential and intracellular Ca^{2+} (Begenisich and Melvin, 1998). HCO_3^- efflux is mediated by Cl^- channels at the apical membrane. It also regulates the fluid secretion, similar to Cl^- efflux. Intracellular carbonyl anhydrase generates HCO_3^- by catalyzing the reversible reaction of water and CO_2 (Fujikawa-Adachi et al., 1999). The constant HCO_3^- efflux induces the acidification of the epithelial cells.

Although, the protons produced by the catalytic reaction are pumping out via NHE, it is suggested that there are other mechanisms to avoid the acidification by the excessive Cl^- and HCO_3^- efflux. Because the acidification is prevented by HCO_3^- depletion or Cl^- channel blocker, it is plausible that Cl^- channel function is modulated by intracellular acid (Melvin et al., 1988; Nguyen et al., 2000).

1.2.1. The role of CFTR for the fluid secretion

The CFTR gene encodes the cAMP-activated Cl^- channel (Riordan et al., 1989). Mutation in the CFTR gene causes cystic fibrosis, a lethal and autosomal recessive disorder. CFTR plays important roles in many organs, such as the pancreas, intestine, lung, sweat gland, liver, gallbladder and genital tract (Quinton, 1999). In intestinal epithelia, CFTR is the main pathway for apical Cl^- efflux (Barrett and Keely, 2000). CFTR is localized at the apical membrane of secretory epithelia (Marino et al., 1991; Denning et al., 1992). As the anion channel, CFTR mediates the fluid and electrolyte secretion in the epithelia and also affects other transport processes. The defects on CFTR cause the pathological symptoms, such as airway obstruction, meconium ileus, focal biliary cirrhosis and exocrine pancreatic destruction porcine (Ianowski et al., 2007; Rogers et al., 2008). The patients with cystic fibrosis are more susceptible for the bacteria infection in the airways (Pilewski and Frizzell, 1999). The defense mechanism is disrupted because the abnormality of NaCl concentration in the fluid reduces the bacterial killing activity of ASL (Smith et al., 1996).

1.2.2. The role of VRAC for the fluid secretion

The current of volume-regulated anion channel (VRAC) has been measured at various epithelial cells (Hazama et al., 1999; Al-Nakkash et al., 2004; Stott et al., 2014). The identity of VRAC is unclear. Recently, LRRC8 is proposed as an essential component of VRAC (Qiu et al., 2014; Voss et al., 2014). But the evidence that LRRC8 plays a role in the epithelia as VRAC is insufficient.

1.2.3. The role of voltage-gated Cl^- channel for the fluid secretion

ClC family, composed of 9 members, is identified as voltage-gated Cl^- channels (Jentsch et al., 1990). ClC-2 is expressed and regulates the fluid and electrolyte secretion in the secretory epithelia (Lipecka et al., 2002; Catalan et al., 2004). The current of ClC-2 is activated by negative membrane potential (< -20 mV) and inhibited by Zn^+, 9-AC and DPC. But it is not blocked by DIDS (Thiemann et al., 1992; Staley et al., 1996).

1.2.4. The role of CaCC for the fluid secretion

Although diverse chloride channels such as CFTR are involved, CaCC has the priority to fluid and electrolyte secretion in the salivary and lacrimal gland (Cook et al., 1988; Begenisich and Melvin, 1998). Even in CFTR-mediated secretory cells, CaCC is observed in cells from patients with cystic fibrosis and CFTR defected mice (Frizzell et al., 1986; Anderson and Welsh, 1991). Because the secretion via CaCC is independent to CFTR,

agonists of CaCC has been proposed as the treatment target of cystic fibrosis (Namkung et al., 2011b).

Increase of intracellular Ca^{2+} is essential to evoke the current of CaCC. Diverse receptors are involved in Ca^{2+} mobilization, including muscarinic, α -adrenergic, substance P, P2Y and P2X receptors. For example, muscarinic receptor M3 at the basolateral membrane is activated by acetylcholine. The receptor is coupled to G proteins, which subsequently activates phospholipaseCβ (PLCβ). And then, PLCβ cleaves the phosphatidylinositol 1,4-bisphosphate (PIP_2) to the diacylglycerol (DAG) and the inositol 1,4,5-trisphosphate (IP_3). IP_3 binds to IP_3 R in the endoplasmic reticulum (ER) and the level of Ca^{2+} in the cytosol is increased by the IP_3 R activation (Lee et al., 1997).

2. CaCC

Calcium activated chloride currents were first described about 30 years ago in Xenopus oocytes (Barish, 1983). It is elicited by the increase of intracellular Ca^{2+}(0.2-5 μM). It has been observed in various cell types, such as neurons; epithelial cells; olfactory and photo-receptors; cardiac, smooth, and skeletal muscle cells; immune cells; brown fat adipocytes and hepatocytes (Hartzell et al., 2005). CaCCs mediates numerous physiological roles (Fig.3). The characteristics of CaCC have been described by many researchers for decades (Fig.4).

2.1. Physiological roles of CaCC

2.1.1. Sensory transduction

CaCC participates in the transduction of olfactory stimuli in the olfactory receptor neurons (Delay et al., 1997). G protein coupled receptor (GPCR) in the ciliary membrane is activated by odorants. The level of cAMP is increased. Subsequently, the influx of Na^{+} and Ca^{2+} is occurred by cyclic-nucleotide-gated (CNG) channels (Lowe and Gold, 1993). The membrane is depolarized further through CaCC activation by increase of intracellular Ca^{2+} (Kleene, 1997). Thus, CaCC may serve as the signal amplification in the olfactory receptor neurons.

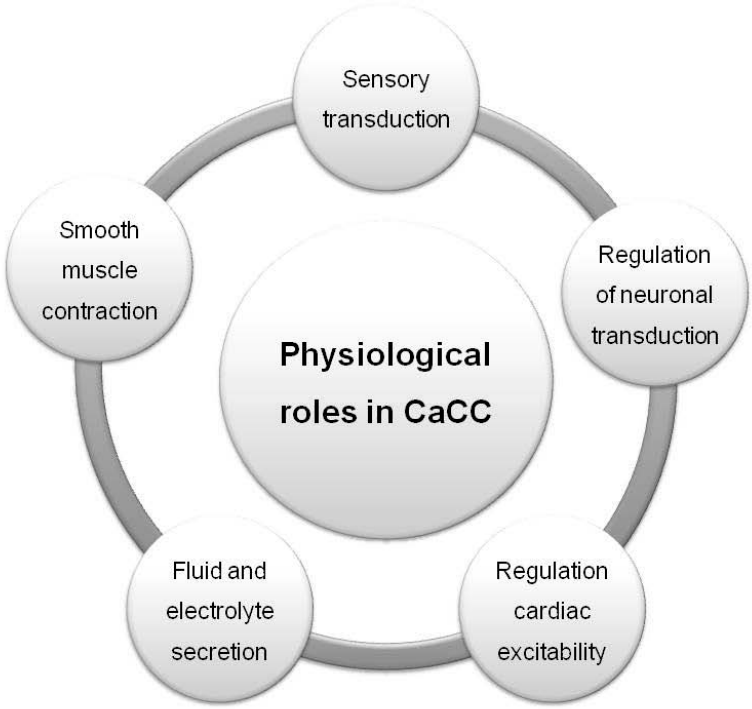

Fig. 3. CaCCs are involved in diverse physiological roles.

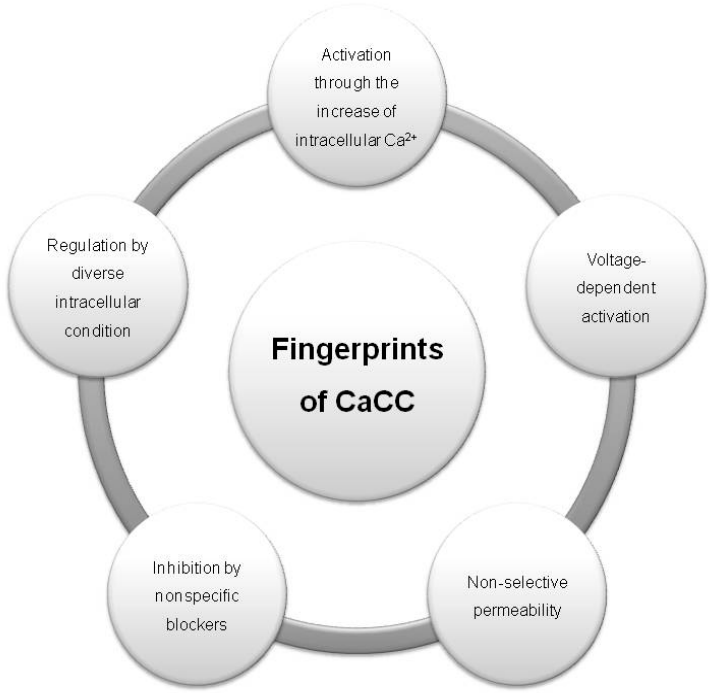

Fig. 4. There are specific characteristics in CaCC.

The taste receptors express CaCC (Herness and Sun, 1999). Taste stimuli induce the membrane depolarization. Because the current is outward-rectifying and inhibited by DIDS, SITS, and niflumic acid, it may be mediated by CaCC. And β-adrenergic agonist elicits the Cl^- current. The membrane depolarization via CaCC is critical for the transduction of gustatory stimuli.

CaCC has been also described in the cone photoreceptors (Maricq and Korenbrot, 1988; Barnes, 1994). And CaCCs are also present in the synaptic bipolar cells (Okada et al., 1995). In the dark, the photoreceptor is depolarized consistently by the activation of CNG (Rattner et al., 1999). Light induce the degradation of cGMP to close the CNG channels. The photoreceptors are hyperpolarized to produce the action potential. Even though the precise role of CaCC in the photoreceptor is elusive, it is proposed that CaCC is responsible to the membrane potential stabilization (Yau, 1994).

2.1.2. Neuronal and Cardiac excitability

Numerous types of neurons including dorsal root ganglion (DRG) neurons, spinal cord neurons, and autonomic neurons possess CaCCs. It has been suggested that CaCCs are involved in the action potential repolarization, generation of after-polarizations and membrane oscillatory behavior (Hartzell et al., 2005). In DRG neurons, CaCC may play a role in after-depolarizations following action potentials (Mayer, 1985). Because the

concentration of intracellular Cl^- is estimated at 30 mM (E_{Cl} = -35 mV), Cl^- exits via CaCC. It induces the depolarization (Deschenes et al., 1976; Duchen, 1990). CaCCs are also present in spinal cord neurons (Hussy, 1992). E_{Cl} of spinal cord neurons is -60 mV (Owen et al., 1984). Thus, it may participates in the repolarization during the action potential, limited to repetitive firing and trains of action potentials (Barker and Ransom, 1978).

CaCCs are essential components of repolarization after cardiac action potentials. In cardiac myocytes, the transient outward currents are found at the initial phase of repolarization. They are composed of the K^+ current inhibited by 4-aminopyridine and the Cl^- current activated by Ca^{2+} (Zygmunt and Gibbons, 1992; Zygmunt, 1994; Papp et al., 1995). The E_{Cl} determines whether the membrane potential is depolarized or repolarized by CaCC. CaCCs are also related to the cardiac arrhythmia. Ca^{2+} overload evoke the arrhythmogenic transient inward current (January and Fozzard, 1988; Hiraoka et al., 1998). The removal of anion or the application of Cl^- channel blocker prevents the reperfusion and ischemia-induced arrhythmias (Ridley and Curtis, 1992; Tanaka et al., 1996).

2.1.3. Smooth muscle contraction

CaCCs serve as the regulation of myogenic tone and the contraction stimulated by agonists in the smooth muscle. Ca^{2+} to evoke the current of CaCC is derived from the VGCC and IP_3R activation (Large and Wang, 1996; Davis and Hill, 1999). The E_{Cl} of smooth muscle cells is positive at resting state. Thus, the membrane is depolarized when CaCCs are

activated (Chipperfield and Harper, 2000). For example, the norepinephrine-induced increase of Ca^{2+} by the GPCR activation leads to membrane depolarization (Bolton, 1979). It is suggested that CaCC mediates the depolarization (Byrne and Large, 1985). The fact that the depolarization is almost disappeared by removal of Cl^- is evidence for the role of CaCC (Large, 1984). The depolarization leads to increase in the open probability of VGCCs. Subsequently, murscle contracts further. Cl^- channel blockers such as anthracene-9-carboxylic acid (A9C) and NFA reduce the contraction of portal vein strips, aorta, renal arteries, and arterioles induced by norepinephrine, endothelin, and angiotensin II (Pacaud et al., 1991; Carmines, 1995; Greenwood and Large, 1995; Criddle et al., 1996; Lamb and Barna, 1998).

2.1.4. Fluid secretion

The fluid secretion via CaCC has been described. It will not be mentioned in this section.

2.2. Fingerprints of CaCC

2.2.1. Mechanism of activation

The increase of intracellular Ca^{2+} evokes CaCCs. Ca^{2+} is areised from Ca^{2+} influx through diverse cation channels such as VGCCs, TRP channels and CNG channels or from intracellular stores via IP_3R (Hartzell et al., 2005). CaCC couples of different types of VGCC selectively in mouse

sympathetic neurons. Ca^{2+} from L- and P-typre channels activates CaCC, whereas Ca^{2+} from N-type channels activates Ca^{2+}-activated K^+ channel (Martinez-Pinna et al., 2000). The current of CaCC activated by the low Ca^{2+} concentration is outward-rectifying. But the current activated by the high Ca^{2+} concentration has linear I-V curve, non-rectifying (Koumi et al., 1994; Kuruma and Hartzell, 2000). The open probability (P_o) of CaCCs is voltage-dependent. Less Ca^{2+} is required for the CaCC activation at the positive membrane potentials (Arreola et al., 1996; Kuruma and Hartzell, 2000). Whether CaMKII affects the CaCC activation or not is controversial. The current is not decreased by KN-62, CaMKII inhibitor in rat parotid acinar cells (Arreola et al., 1998). However, KN62 blocks the activation of CaCCs in T84 cells (Nishimoto et al., 1991). The hill coefficients are estimated to 2-5 from dose-response curves. It suggests the presence of multiple Ca^{2+} binding sites in a channel protein (Arreola et al., 1996; Kuruma and Hartzell, 2000).

2.2.2. Permeability and selectivity

Compared to voltage-gated K^+ channels, most Cl^- channels including CaCCs are relatively nonselective (Jentsch et al., 2002; Hartzell et al., 2005). And there is no relationship between ionic radius and permeability in CaCCs (Hartzell et al., 2005). The selectivity of CaCC is $SCN^- > NO_3^- > I^- > Br^- > Cl^- > F^-$ (Evans and Marty, 1986; Large and Wang, 1996; Nilius et al., 1997). Moreover, the cation permeability of CaCCs is relatively large. P_{Na}/P_{Cl} is 0.1 (Qu and Hartzell, 2000).

CaCCs may have a relatively large pore because ions as large as $C(CN)_3^-$ are highly permeable. From dimensions of various blockers such as A9C and NFA, the pore dimension of CaCC is estimated (Qu and Hartzell, 2001).

2.2.3. Pharmacology

NFA and flufenamic acid are the most common blockers for endogenous CaCCs (White and Aylwin, 1990). NFA inhibits the current at 10 μM (Qu and Hartzell, 2001). However, NFA has an undesirable effect, which is inducing the enhancement of CaCC (Piper et al., 2002). It also blocks VRACs and K^+ channels (Xu et al., 1997). And Ca^{2+} currents are affected by NFA (Reinsprecht et al., 1995; Doughty et al., 1998). Other Cl^- channel blockers, such as tamoxifen, DIDS, SITS, NPPB, A9C, and DPC are less effective than flufenamic acid (Frings et al., 2000). Fluoxetine and mefloquine are more effective on VRAC than on CaCC (Maertens et al., 1999; Maertens et al., 2000a). Chlorotoxin, a small peptide isolated from the venom of the scorpion *Leiurus quinquestriatus*, blocks CaCC specifically in rat astrocytes (Dalton et al., 2003). However, chlorotoxin and its related peptides fail to block CaCC in T84 cells (Maertens et al., 2000b). A9C blocks CaCC voltage-dependently. It blocks the outward current, whereas the inward current is not modulated (Qu and Hartzell, 2001).

2.2.4. Regulation

Although it is controversial, CaMKII regulates CaCC by phosphorylation. inositol 3,4,5,6-tetrakisphosphate (IP_4) is involved in the CaMKII-mediated regulation (Vajanaphanich et al., 1994; Nilius et al., 1998; Xie et al., 1998). CaCCs of CFPAC-1 cells and T84 cells are stimulated by CaMKII and inhibited by IP_4 (Xie et al., 1998; Carew et al., 2000). The IP_4-mediated inhibition is found under only certain conditions. According to that, it is proposed that CaCCs have multiple phosphorylation sites. Thus, hyperphosphorylated CaCCs are not inhibited by IP_4 (Xie et al., 1998).

Annexins are phospholipid- and Ca^{2+}-binding proteins. It is present in the apical membrane of many secretory epithelia. Annexins inhibit CaCCs in epithelial cells (Chan et al., 1994; Kaetzel et al., 1994).

Intracellular acid inhibits CaCCs in acinar cells of lachrymal and parotid glands and in T84 cells (Arreola et al., 1995; Park and Brown, 1995). The physiological role and the mechanism of the acid-mediated inhibition in CaCCs are unclear. It is assumed that the acid-mediated inhibition prevents the excessive HCO_3^- efflux through CaCCs (Begenisich and Melvin, 1998).

CFTR and CaCC have a close relationship. The expression of CFTR reduces the current of CaCC in bovine pulmonary artery endothelial (CPAE) cells and mouse parotid acinar cells (Wei et al., 1999; Perez-Cornejo and Arreola, 2004). In contrast, the disruption of CFTR function increases the current of CaCC (Clarke and Boucher, 1992; Grubb et al., 1994; Colledge et al., 1995).

3. ANOCTAMIN family

The molecular identities of CaCC were elusive for decades. There were many attempts to find out the protein of CaCC. ClC-3, CLCA family, Bestrophin family and Tweety were proposed as the candidate of CaCCs. However, they represent the differences to the characteristics of the endogenous CaCCs (Hartzell et al., 2005).

Three independent research groups published that the orphan proteins, TMEM16A is a molecule of CaCC at about the same time (Caputo et al., 2008; Schroeder et al., 2008; Yang et al., 2008). It was named ANOCTAMIN1 (ANO1) because it was predicted to possess 8 transmembrane domains (Yang et al., 2008). Approches to discover the molecular identity of CaCCs are quite different depending on research groups.

First, TMEM16A was chosen by searching unknown proteins containing multiple transmembrane domains (Yang et al., 2008). It is activated by the increase of Ca^{2+} via the GPCR activation, such as endothelin, angiotensin, muscarinic and purinergic receptors. It has similar characteristics of endogenous CaCCs. It is outward-rectifying at the low Ca^{2+}-mediated activation, whereas non-rectifying at the high Ca^{2+}-mediated activation. Moreover, the permeability sequence of ANO1 is identical to that of CaCC. And the range of Ca^{2+} in activating and the single-channel conductance are same as those of CaCC described earlier. The further features of ANO1 were investigated. It localizes at the pancreas acinar cells, epithelial cells of

renal proximal tubules, bronchial epithelial cells, retinal cells, acinar cells of submandibular glands and DRG neurons. Knockdown of ANO1 in mouse acinar cells of submandibular glands *in vivo* reduces saliva secretion (Yang et al., 2008).

Second, TMEM16A was identified from *Xenopus* mRNA pools. It has been well-known that CaCCs are expressed in *Xenopus* oocytes. Because of the large endogenous current, *Xenopus* oocytes are not suitable for observing the exogenous current. Therefore, they used the new expression system, *Axolotl* oocytes. *Axolotl* oocytes present no current of CaCC, whereas heterologous expression of ANO1 induces the current of CaCC. It is similar to endogenous CaCC, Ca^{2+}-dependent outward-rectifying and activated by IP_3. After characterizing *Xenopus* ANO1, they confirmed mouse ANO1 (Schroeder et al., 2008).

Finally, ANO1 was discovered by the comparing gene-expression strategy. Interleukin-4 (IL-4) increases the current of CaCC in human bronchial epithelial cells. Up-regulated genes were selected as candidates by analysis of microarray. And then, screening was performed using YFP assay in the cells candidates. Knockdown of ANO1 reduce the function of CaCC. Short-circuit currents confirmed that ANO1 is a key component of CaCC. ANO1 has many different alternative splice sites. There are at least 4 variants, named (abcd), (abc),(ac) and (0) (Caputo et al., 2008).

3.1. The physiological roles of ANO1

Since the molecular identity has been discovered, the precise role of CaCC is extensively studied. The identification of ANO1 enables to use the genetic modulation *in vitro* and *in vivo*. As a result, the physiological roles of ANO1 are newly uncovered.

3.1.1. Epithelial cells

ANO1 regulates the secretion of saliva. The bronchial epithelial cells express ANO1 (Yang et al., 2008). IL-4 increases the expression level in the bronchial epithelial cells (Caputo et al., 2008). Expression of ANO1 is also up-regulated in epithelial cells from asthma mouse model and patients suffered from asthma. It is observed particularly in secretory cells. The application of a specific blocker reduces mucus secretion in human airway surface epithelial cells (Huang et al., 2012a).

A specific activator of ANO1, E_{act} evoke the current in epithelial cells of human salivary and airway submucosal gland (Namkung et al., 2011b). However, whether the E_{act} treatment *in vivo* increases saliva secretion is not confirmed.

3.1.2. Smooth muscle

ANO1 modulates the vascular contractility. Inhibition of ANO1 by the specific blocker reduces the airway smooth muscle contraction. Methacholine, a cholinergic agonist induces the airway smooth muscle contraction. However, it fails to induce the contraction after the treatment of an ANO1 specific blocker (Huang et al., 2012a). Disruption of ANO1

eliminates the current of CaCC in vascular smooth muscle cells. It reduces contractility in aorta, but not in mesenteric arteries. Thus, conditional knockout mice of ANO1 in vascular smooth muscle cells have lower systemic blood pressure and a hypertensive response by the application of vasoconstrictors. The result suggests that ANO1 might be a target of the hypertension therapy. (Heinze et al., 2014)

3.1.3. Nociceptive neurons

ANO1 is present mainly in nociceptors of DRG neurons (Cho et al., 2012). In DRG neurons, bradykinin increases the intracellular Ca^{2+} via the GPCR activation. It induces the current of CaCCs. The current is attenuated by knockdown of ANO1. CaCC blockers such as NFA and DIDS diminish the nociceptive behavior, such as licking, biting, and flinching. ANO1 may amplify the BK-induced excitatory effect in DRG neurons (Liu et al., 2010).

ANO1 is also activated at high temperature (above 44℃). Heat and Ca^{2+} activates ANO1 synergistically. Heat-mediated ANO1 activation depolarizes DRG neurons. Thus, it evokes the action potential spikes. Conditional knockout mice of ANO1 exhibit the defect in thermal nociception (Cho et al., 2012). Through several behavior tests on DRG-specific ANO1 knockout mice, it is concluded that ANO1 contributes to inflammatory and nerve-injury hypersensitivity (Lee et al., 2014a).

3.1.4. Cancer cells

Before the identification of ANO1 as CaCC, it was known that cancer cells from the gastrointestinal stromal tumor and oral squamous cell carcinomas highly express ANO1 (West et al., 2004; Huang et al., 2006). Recently, the relationship between ANO1 and cancer was extensively studied. ANO1 is also overexpressed in breat cancers (Britschgi et al., 2013). ANO1 regulates the cell proliferation and cell migration (Ruiz et al., 2012).

The mechanism is continuously studied. The phosphorylation of ERK1/2 and the levels of cyclin D1 are increased in ANO1-overexpressed cells. Mutant of ANO1, which defects in the channel function, fails to increase the phosphorylation of ERK1/2 (Duvvuri et al., 2012). It suggests that Cl^- movement is critical for the effect on cell cycle and proliferation. Another proposal refers that the migration is due to cell shrinkage. ANO1 is also related to the volume regulation (Ruiz et al., 2012). In the future, ANO1 would become a potent diagnostic and prognostic marker.

3.2. The physiological roles of ANO2

ANO2 also confers CaCC (Pifferi et al., 2009). When the molecular identities of CaCC were elusive, it is impossible to discriminate types of CaCCs. Nowadays it is noticed that ANO2 has slightly different characteristics. For example, it requires slightly higher Ca^{2+} to activate. Furthermore, it is feasible which physiological role is mediated by solely

ANO2.

3.2.1. Olfactory neurons

ANO2 is present in the olfactory cilial membrane. Olfactory sensory neurons contain a splice variant of ANO2. As a result of measuring ANO2 currents, the characteristics such as the permeability, desensitization and Ca^{2+} sensitivity are similar to the endogenous olfactory CaCCs. The results suggest that ANO2 is an essential component of olfactory CaCCs (Stephan et al., 2009).

ANO2 is localized to the main olfactory epithelium (MOE) and the vomeronasal organ (VNO). Disruption of ANO2 diminishes CaCC in the MOE and VNO. ANO2 knockout mice exhibit the moderate reduction of fluid-phase electro-olfactogram. However, olfactory behaviors of ANO2 knockout mice are normal. They can discriminate odorants, similar to wiltype mice. There is no compensatory upregulation of ANO1 and CNG channels, related to olfaction (Billig et al., 2011).

ANO2 is a key component of CaCC in olfactory organs, but it is dispensable for olfaction (Billig et al., 2011).

3.2.2. Photoreceptors

CaCC has been known that critical for regulating the synaptic transmission from photoreceptors to second-order neurons. ANO2 localizes in the photoreceptor synaptic terminals in mouse retina and interacts with PSD95, VELI3 and MPP4, components of a presynaptic protein complex. It

has a consensus PDZ class I binding motif. MPP4 knockout mice do not express ANO2 in the photoreceptor membranes. The localization and electrophysiological properties of ANO2 suggest that ANO2 serves as CaCCs in the photoreceptor synapse (Stohr et al., 2009).

3.2.3. Hippocampal neurons

Depolarization of hippocampal neurons by activating voltage-gated Ca^{2+} channels induces a tail current. The tail current is mediated by Cl^- and activated by Ca^{2+}. Because CaCC blockers such as NFA and NPPB inhibit the tail current, ANO family was proposed as the compartment of the tail current. Hippocampal pyramidal neurons express ANO2. Disruption of ANO2 reduces the tail current. Block of the tail current broadens the action potential. Thus, Disruption of ANO2 shortens action potentials. There is no change in the transmitter release at the axon termianls. The data reveals that ANO2 serves as a brake on neuronal excitability (Huang et al., 2012b).

3.3. The physiological roles of ANO3

ANO3 is expressed in DRG and spinal cord. The expression is focused in $IB4^+$ nociceptors. Knockout rats of ANO3 show the increase of the sensitivity of thermal and mechanical nociception. ANO3 facilitates sodium activated potassium current (Slack) in sensory neurons. ANO3 interacts with Slack and it modulates the channel activity of Slack. ANO3 is an important component of the pain modulation (Huang et al., 2013).

3.4. The functions of ANO6

ANO6 is known to be associated with scramblase activity. Lipids in the bilayer are asymmetrically distributed. Ca^{2+}-activated scramblase mediates the rapid externalization of PS, which are in the inner leaflet. It induces the coagulation of platelets and the apoptosis. (Suzuki et al., 2010; Yang et al., 2012). Knockout mice of ANO6 exhibit the reduction of Ca^{2+}-dependent PS exposure in platelets, erythrocytes and B-cells. They have impaired coagulation and prolonged bleeding. But the carotid aretery thrombosis is reduced in ANO6 knockout mice. The Ca^{2+}-activated outwardly rectifying current is disappeared in megakaryocytes from ANO6 knockout mice (Yang et al., 2012; Shimizu et al., 2013).

ANO6 also acts as a channel. ANO6 is an essential component of the outwardly rectifying Cl^- channel (ORCC). It is described at Jurkat lymphocytes during FasL-induced apopotosis. Knockdown of ANO6 reduces the current of ORCC (Martins et al., 2011). ANO6 is also suggested as CaCC. However, it requires higher Ca^{2+} to elicit the current and it is strongly outward-rectifying. ANO6 shows the delayed activation by Ca^{2+} (Grubb et al., 2013).

The permeability of ANO6 is controversial. ANO6 is permeable to Cl^-, But it also mediates cation current (Yang et al., 2012; Shimizu et al., 2013).

4. The mechanism of ANO1 activation

It is possible to consider ANO1 as a drug target, since the molecular identity of CaCC was uncovered. At the first time, they were known to have 8 transmembrane domains by the bioinformatical prediction (Yang et al., 2008). However, the topology was revised. Hemaglutinin (HA) was introduced to each fragments of ANO1. And then the-tagged fragments were detected by its antibody. As a result, 650-706 residues, which were known to be located in the extracellular region, is located in the intracellular region (Yu et al., 2012).

Recently, the crystal structure of *nh*TMEM16 was resolved (Brunner et al., 2014). TMEM16 of *nectria haematococcoa* is one of ANO family. It acts as a scramblase, whearas it doesn't have the channel activity. To take advantages, the mechanism of ANO1 activation has been clear.

4.1. Oligomerization

ANO1 is a homodimer (Fallah et al., 2011; Sheridan et al., 2011). Residues between 117 and 179 at N-terminus of ANO1 are dimerization domain. Mutant without the domain fails to elicit the current. Thus, we noticed that the dimerization is essential for the intact channel activation (Tien et al., 2013). The crystal structure of *nh*TMEM16 also shows a homodimer (Brunner et al., 2014). Two subunits form the interface, which are organized by the interface between N-terminus and C-terminus.

4.2. Calcium binding sites

It was controversial that ANO1 requires additional factors such as calmodulin to elicit the current by Ca^{2+}. However, only Ca^{2+} is sufficient to activate the purified ANO1 protein. Ca^{2+} directly evokes the currents of ANO1. Moreover, calmodulin and ANO1 do not form a stable complex *in vitro* (Terashima et al., 2013).

CaCC was thought to contain Ca^{2+} binding motifs such as EF-hands or C2 domains. As a result of searching EF-hand domain in ANO1, there is EF-hand like domain at N-terminus. But mutation on this region does not alter the Ca^{2+} sensitivity of ANO1. The Ca^{2+} sensitivity of ANO1 is in under micromolar range. Because the affinity for Ca^{2+} is generally lower than EF-hands or C2 domains, 'Ca^{2+} bowl model' like BK potassium channel was suggested. ANO1 contains clusters of Glu (5E). However, deletion of 5E abolishes the voltage dependence without altering the Ca^{2+} sensitivity (Xiao and Cui, 2014).

After many attempts, Ca^{2+} binding residues are uncovered. And because the X-ray structure of *nh*TMEM16 was resolved, they are confirmed as the Ca^{2+} site of ANO1. A fungal TMEM16 doesn't have CaCC function. But it acts as a scramblase as if ANO6. The scramblase activity also requires Ca^{2+}. Therefore, *nh*TMEM16 also contains the Ca^{2+} binding site. The residues in the Ca^{2+} binding site of *nh*TMEM16 are conserved in mouse ANO1. N650, E654, E702, E705, E734 and E738 are located at α6, α7

and α8 helix respectively. The residues are facing each other. The mutation on these residues induces the decrease of Ca^{2+} sensitivity of ANO1dramatically. Thus, it is concluded that these 6 residues are essential for Ca^{2+} binding to activate the channel (Yu et al., 2012; Brunner et al., 2014; Tien et al., 2014).

Reference helix located between α6 and α7 helix support the Ca^{2+}-induced ANO1 activation. Because it contains positive-charged residues, Ca^{2+} might repel the helix. Through the movement of this helix, Ca^{2+} might enter the Ca^{2+} binding site in the hydrophobic core region more easily (Lee et al., 2014b).

ANO1 is also activated by the other divalent cations, Ba^{2+}, Sr^{2+} and Ni^{2+} , But Mg^{2+} inhibits ANO1 by competitive manner (Yuan et al., 2013).

4.3. Voltage sensor

ANO1 is dually gated by intracellular Ca^{2+} and the membrane voltage. The current of ANO1 activated by lower Ca^{2+} is outward-rectifying. High voltage, more than +200 mV, activates ANO1 slightly without Ca^{2+}. 5E, which was located between α2 and α3 and suggested as 'Ca^{2+} bowl' in ANO1, mediates voltage sensing. Deletion of 5E fails to elicit the current at high positive membrane potential, unlike WT of ANO1 (Xiao and Cui, 2014).

4.4. Pore

ANO1 is permeable to diverse anions. The permeability sequence of ANO1 is NO_3^- > I_2^- > Br^- > Cl^- >F^-. It is also permeable to HCO_3^-, although the regulation mechanism is controversial. It was proposed that the calmodulin-binding increases HCO_3^- permeability (Jung et al., 2013). However, only increase of Ca^{2+} is sufficient to alter the permeability of ANO1 (Yu et al., 2014).

4 basic amino acids contribute to form a pore in ANO1. They are clustered around the external mouth of ANO1. Mutation on these residues decreases the preference for larger anions. Thus, they are suggested to decide the ion selectivity (Peters et al., 2015).

4.5. Activators and inhibitors

Specific blockers are important to identify a physiological function of the channel and to isolate specific currents from a mixture of currents. They are also useful for the affinity purification of a channel protein. However, there were no specific and potent blockers of CaCC. However, ANO1 is uncovered as a CaCC. To develop the specific blockers becomes possible. As a result, $CaCC_{inh}$-A01, $T16_{inh}$-A01 and MONNA were discovered by high-throughput screening (Namkung et al., 2011a; Oh et al., 2013). Tannic acids also inhibit ANO1 (Namkung et al., 2010). Eugenol was found in a Thai herbal preparation as an ANO1 inhibitor (Yao et al., 2012). The ANO1

inhibitors might be beneficial to the cardiovascular disease and the diarrhea.

To find out of activators of ANO1 was also attempted. The activator might be essential for treatment of salivary gland dysfunction, cystic fibrosis, dry eye syndrome, intestinal hypomotility and other Cl^--channel associated diseases. As a result, E_{act} was discovered. It activates ANO1 without the increase of intracellular Ca^{2+} (Namkung et al., 2011b).

Aim of study

Fluid and electrolytes secretion in epithelial cells is important to maintain normal function in the body. It is highly regulated by various transporters and ion channels. Among them, CaCCs are essential for Cl^- and HCO_3^- efflux. Epithelial cells contain more intracellular Cl^- than other cells because of NKCC transporters at the basolateral membrane. Due to electrochemical gradients, Cl^- is poised to exit the epithelial cells. CaCC-mediated Cl^- efflux induces water secretion to the lumen.

CaCC are also permeable to HCO_3^-. HCO_3^- is an important pH buffer of the cells. Efflux of HCO_3^- induces the acidification. Thus, the activation of CaCC increases the acidity and the increase of acidity is prevented by Cl^- channel blockers. It is plausible that intracellular acid may affect the CaCC activation. Indeed, the endogenous CaCC is inhibited by intracellular acid in parotid and lacrimal acinar cells and human colon carcinoma T84 cell line.

ANO1 refers CaCC. ANO1 plays critical roles in the fluid and electrolyte secretion and acid is a key regulator of the fluid and electrolyte secretion. However, it is unknown whether the intracellular acid affects the ANO1 activation. Thus, we attempts to confirm that intracellular acid inhibits ANO1 and ANO2, which were known as CaCCs. Other ANOs also have channel functions. Intracellular may modulate the activation of ANOs. Thus, we explored the acid-mediated modulations of ANOs.

The molecular mechanism of the acid-mediated ANO1 inhibition is

unknown. Studies of the precise mechanisms of the acid-mediated ANO1 modulation are meaningful to get insight of the ANO1 gating mechanism and to understand the regulation of fluid and electrolyte secretion.

Methods

1. Construction of ANO family and ANO1 mutants.

We used the construct of mouse ANO1, mouse ANO2, mouse ANO6, mouse ANO9 and human ANO7 in pEGFP-N1 vector. They were fused with enhanced green fluorescence protein (EGFP) at the C terminus.

All histidine mutants were generated by *in vitro* mutagenesis (Muta-direct site-directed mutagenesis kit, Intron). They were based on mouse ANO1 tagged EGFP at the C terminus. Primers for site-specific mutagenesis were designed by Quickchange Primer design website (http://www.genomics.agilent.com/primerDesignProgram.jsp). The list is shown in Table1. According to manufacturer's protocol, we performed PCR reaction. PCR conditions were 30 s of initial denaturation at 95℃, followed by 15 cycles of each 30 s at 95℃, 1min at 55℃ and 7 min at 72℃. And then, this PCR products were digested with Mutazyme™ enzyme at 37℃ for 1 hour. In case of mutants related to reference helix and calcium binding helix, we used previously reported ones. They were verified by DNA sequencing.

ANO1 5E deletion mutant and ED rich region mutant was generated by overlap-PCR method as previously used (Lee et al., 2014b).

H18R	a53g	forward	5'-ggaccgcagcgtccgcatcgtgaacatct-3
		reverse	5'-agatgttcacgatgcggacgctgcggtcc-3'
H69R	a206g	forward	5'-ctacatcttggtataccgtcacaagagagcctcag-3'
		reverse	5'-ctgaggctctcttgtgacggtataccaagatgtag-3'
H70R	a209g	forward	5'-catcttggtataccatcgcaagagagcctcaggga-3'
		reverse	5'-tccctgaggctctcttgcgatggtataccaagatg-3'
H120R	a359g	forward	5'-agtccccatggattaccgtgaagatgacaaacgct-3'
		reverse	5'-agcgtttgtcatcttcacggtaatccatggggact-3'
H151R	a452g	forward	5'-gacgaggataccaaaatccgtggtgtcgggtttg-3
		reverse	5'-caaacccgacaccacggattttggtatcctcgtc-3'
H159R	a476g	forward	5'-ggtttgtgaagatccgtgcgccctggcatgt-3'
		reverse	5'-acatgccagggcgcacggatcttcacaaacc-3'
H163R	a488g	forward	5'-catgcgccctggcgtgtgctctgtagg-3'
		reverse	5'-cctacagagcacacgccagggcgcatg-3'
H183R	a548g	forward	5'-cacaaagaaggtgtaccgcatcagtgagacgcgag-3'
		reverse	5'-ctcgcgtctcactgatgcggtacaccttctttgtg-3'
H212R	a635g	forward	5'-aaggtggctgagcgcaggccacagacc-3'
		reverse	5'-ggtctgtggcctgcgctcagccacctt-3'
H230R	a689g	forward	5'-cccgggagaagcaacgcctattcgacctgac-3'
		reverse	5'-gtcaggtcgaataggcgttgcttctcccggg-3'
H284R	a851g	forward	5'-ctgcataccctctgcgcgatggggactatga-3'
		reverse	5'-tcatagtccccatcgcgcagagggtatgcag-3'
H426R	a1277g	forward	5'-gccactttcatggagcgctggaaacggaagcag-3'
		reverse	5'-ctgcttccgtttccagcgctccatgaaagtggc-3'
H453R	a1358g	forward	5'-ggaagctgtcaaggatcgtcccagagcagagtatg-3'
		reverse	5'-catactctgctctgggacgatccttgacagcttcc-3'
H898R	a2693g	forward	5'-catcagccagcagatccgcaaagagaaggttctca-3'
		reverse	5'-tgagaaccttctctttgcggatctgctggctgatg-3'
H936R	a2807g	forward	5'-gccttgtaacaaccgcagccccacaaccc-3'
		reverse	5'-gggttgtggggctgcggttgttacaaggc-3'
H941R	a2822g	forward	5'-gccccacaacccgcccagaggcagg-3'
		reverse	5'-cctgcctctgggcgggttgtggggc-3'
H956R	a2867g	forward	5'-agctacgagtaccgtggggacgcgctg-3'
		reverse	5'-cagcgcgtccccacggtactcgtagct-3'

Table 1. Primers for ANO1 H/R mutants

2. Cell culture and functional expression in HEK293T cells

HEK 293T cells were maintained at 5% CO_2, 37℃ incubator in DMEM supplemented with 10% FBS, 10 units/mL penicillin, 10 μg/mL streptomycin. Cells were transiently transfected with Fu-geneHD according to the manufacturer's protocol (Promega). 1 μg plasmid was diluted in OptiMEM (GIBCO) with 3 μL transfection reagent, Fu-geneHD. Mixture was incubated 15min at room temperature and added to adherent cells. Cells were used for patch clamp experiments 24-48 hr after transfection.

3. Electrophysiology

Patch-clamp experiments were performed in inside-out or whole-cell configuration at room temperature (20-25℃). Patch pipettes were made of borosilicate glass (World Precision Instruments, Inc.) and pulled with a puller P-97 (Sutter instruments). The resistance of pipettes was approximately 3~5 MΩ after polishing tips with a microforge (MF820, Narishige). Cells were transferred into the bath on an inverted microscope (eclipse TE300, Nikon). Individual cell with GFP was targeted and applied gentle suction to form gigaseal. To make an inside out configuration, the attched membrane was excised rapidly. To form whole-cell configuration,

additional gentle suction was applied. Current were recorded with an Axopatch 200B amplifier. Output of the amplifier was filtered at 5 kHz and fed to Digidata 1440 (Molecular Devices). Data were acquired on a computer with pClamp 10.2 software.

For inside-out patch recordings, the pipette solution contained 140 mM *N*-Methyl-$_D$-glucamin (NMDG), 2 mM $MgCl_2$, 10 mM 4-(2-hydroxyethyl)-1-piperazineethanesulfonic acid (HEPES), 10 mM ethylene glycol tetraacetic acid (EGTA); pH was adjusted to pH 7.2 with HCl. The control bath solution contained 140 mM NMDG, 2 mM $MgCl_2$, 10 mM HEPES for pH 6.8, pH 7.2 and pH 8.0 or 10 mM 2-(*N*-morpholino)ethanesulfonic acid (MES) for pH 6.0 and pH 6.4, 10 mM EGTA, *N*-(hydroxyethyl)-ethylenediaminetriacetic acid (HEDTA) or nitrilotriacetic acid (NTA) adjusted to expected pH with HCl. Calcium chelator (EGTA, HEDTA, NTA) was selected appropriately according to their chelating capacitance. To make 0.1 ~1, 3 ~ 30, 100 ~ 1,000 μM Ca^{2+} solution, 10 mM EGTA, HEDTA and NTA were added to the solution, respectively. Calcium was added as calculated with the program WEBMAXC (http://www.stanford.edu/~cpatton/webmaxcS.htm, T=22℃, ionic equivalent = 0.15). Calculated Ca^{2+} and Mg^{2+} concentration was shown in Table 2. For whole-cell current recording, the pipette solution contained 140 mM NMDG, 2 mM $MgCl_2$, 10 mM HEPES, 2 mM ATP and 300 μM GTP adjusted to pH 7.2 with HCl.

(mM)

pH 8.0		pH 7.2		pH 6.8		pH 6.4		pH 6.0	
Ca^{2+}	Mg^{2+}	Ca^{2+}	Mg^{2+}	Ca^{2+}	Mg^{2+}	Ca^{2+}	Mg^{2+}	Ca^{2+}	Mg^{2+}
0.0	7.6	0.0	2.8	0.0	2.3	0.0	2.1	0.0	2.0
9.0	2.5	3.5	2.5	0.9	2.3	0.1	2.1	0.0	2.0
9.7	2.2	6.2	2.3	2.2	2.2	0.4	2.1	0.1	2.0
9.9	2.1	8.5	2.1	4.8	2.2	1.3	2.1	0.2	2.0
0.2	11.7	0.2	11.3	0.2	10.7	0.2	9.4	0.1	7.1
0.7	11.2	0.7	10.9	0.6	10.4	0.5	9.1	0.4	7.0
1.8	10.1	1.8	9.9	1.7	9.4	1.5	8.5	1.1	6.6
3.1	8.2	2.1	6.2	1.4	4.7	0.8	3.4	0.4	2.7
5.9	5.9	4.6	5.0	3.4	4.2	2.1	3.3	1.2	2.6
9.1	3.7	8.2	3.5	7.0	3.3	5.2	2.9	3.4	2.5

Table 2. Ca^{2+} and Mg^{2+} concentration in the NMDG-Cl solution

All chemicals for electrophysiology experiments were purchased from Sigma. E_{act} was provided by Prof. Namkung Wan in Yonsei University, Korea.

4. Ca^{2+}-imaging

HEK293T cells were co-transfected with ANO1 and ET_AR. After 24 hrs, Ca^{2+} increase was measured by the cell-permeable Ca^{2+}-sensitive fluorscence dye. Cells were loaded with Fluo3-AM (5 μM, Invitrogen) containing 0.1% Pluronic F-127 (Invitrogen). Basal intracellular Ca^{2+} (F_0) was determined by measuring fluorescent intensities after 40 min Fluo3-AM incubation. Intensities of

fluorescent images were measured at 488 nm every 5 s for 3 min.

5. Structure modeling

Amino acids of α6, α7 and α8 helix in mouse ANO1, which contains calcium binding sites, were selected as the target sequence. In *Nectria haematococcoa* TMEM16 crystal structure (accession code: 4WIS), the region between α6 and α6' is missing. The conserved amino acids were excluded in the target sequence according to alignment with mouse ANO1 protein sequence (accession number: NP_848757.4) and *Nectria haematococcoa* TMEM16 protein sequence (accession number: XP_003046028.1) by CLUSTALW2. Sequence alignment was shown by JalView. Model structure of mouse ANO1 was generated by MODWEB (https://modbase.compbio.ucsf.edu/modweb/), a web server for automated comparative protein structure modeling. Crystal structure and model structure were edited by PyMol.

6. Data analysis

Dose response relationships were fitted with the Hill equation of the form:

$$\frac{\mathrm{I}}{\mathrm{I}_{\max}} = \frac{1}{(1 + \frac{[\mathrm{Ca}^{2+}]}{\mathrm{EC}_{50}})^{n}}$$

I_{max} is the maximum current of each patches. [Ca^{2+}] is Ca^{2+} concentration. EC_{50} is the half-maximal concentration of Ca^{2+}. *n* denotes the Hill coefficient.

For G/G_{max} vs V_m curves, the data was fitted with the Boltzmann equation of the form:

$$\frac{G}{G_{max}} = \frac{1}{1 + e^{(V_m - V_{1/2})\frac{zF}{RT}}}$$

G, the conductance, was obtained from tail current at 100-200 μs after voltage pulses, step pulses from -200 mV to +200 mV in 10 mV increments. G_{max} was determined by a fit of averaged G. G/G_{max} is the normalized conductance, z is the equivalent gating charge associated with voltage-dependent channel opening. $V_{1/2}$ is the membrane potential producing half-maximal activation, F is the Faraday constant, R is the gas constant, and the T is the absolute temperature. Curves were fitted with SigmaPlot 10.0 (Systat Software Inc.).

7. Statistics

Data are presented as mean±SEM, with n indicating the number of cells. Statistical significance was determined using unpaired student *t* tests for comparison of two groups and one-way ANOVA followed by Tukey's post-hoc test for multiple comparisons.

Results

1. Intracellular acid inhibits ANOs

It has been known that endogenous calcium-activated chloride currents are inhibited by intracellular acid (Arreola et al., 1995; Park and Brown, 1995). Properties of ANO1 are similar with those of endogenous CaCCs that have been observed in T84 cells. In order to investigate whether ANO1 is blocked by intracellular proton, we performed single channel recordings with the inside-out patch configuration at -80 mV. Cl^- was a main carrier ion because the pipette and bath solutions contained 140 mM NMDG-Cl. The currents were elicited twice with 10 μM Ca^{2+} at the same excised membrane. ANO1 currents showed the weak tachyphylaxis. However, ANO1 current was inhibited completely at pH 6.0 (Fig. 5A, B).

To test whether the proton-mediated inhibition is effective at extracellular side of cells or not, we recorded whole-cell currents evoked by 50 nM endothelin-1 (ET-1). To induce ANO1 activation by ET-1, endothelin receptor subtype A (ET_AR) and ANO1 were cotransfected in HEK293T cells. Application of ET-1 in pH 6.0 evoked robust ANO1 current (Fig. 5C), similar to that in pH 7.2 (Fig. 5D, E). In addition, the intracellular Ca^{2+} increase via GPCR activation was not altered by extracellular acid. The increase of fluorscence intensity was almost identical between pH 7.2 and pH 6.0 (Fig. 6). Thus, the extracellular acid did not modulate ANO1 activation.

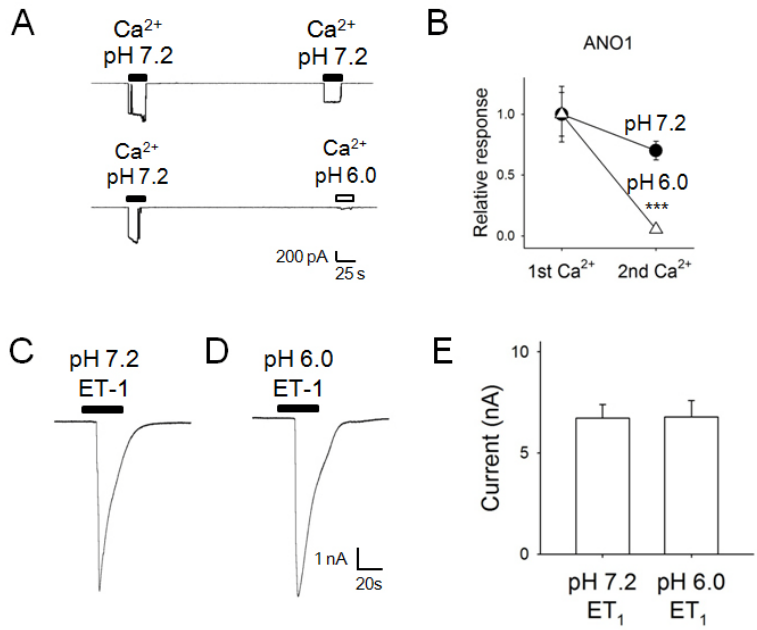

Fig. 5. Intracellular acid inhibits ANO1 current, whereas extracellular acid does not affect ANO1 current.

(A) Representative macroscopic single-channel currents of ANO1 activated by 10 μM Ca^{2+} with indicated intracellular pH, pH 7.2 or pH 6.0. Ca^{2+}-induced chloride current was completely inhibited in pH 6.0. Single-channel currents were recorded in inside-out membrane patches isolated from mouse ANO1 expressed HEK293T cells. Pipette and bath solution contained 140 mM NMDG-Cl. Holding potential (E_{hold}) was -80 mV

(B) Summary of the acid-mediated inhibition of ANO1 currents (n= 6-7). Currents were normalized to first Ca^{2+}-evoked currents. ***, $p<0.001$ compared to relative responses activated by 10 μM Ca^{2+} at pH 7.2. Student's unpaired two-tailed t-test. Error bars represent SEM

(C-D) Example traces of 50 nM endothelin-1 (ET-1) induced whole-cell currents at pH 7.2(C) or pH 6.0(D) in HEK293T cells transfected with mouse ANO1 and endothelin receptor subtype A (ET_AR). ET-1 was applied to the bath. E_{hold} = -60 mV.

(E) Summary of ET-1 induced ANO1 currents at pH 7.2 or pH 6.0. (n=9)

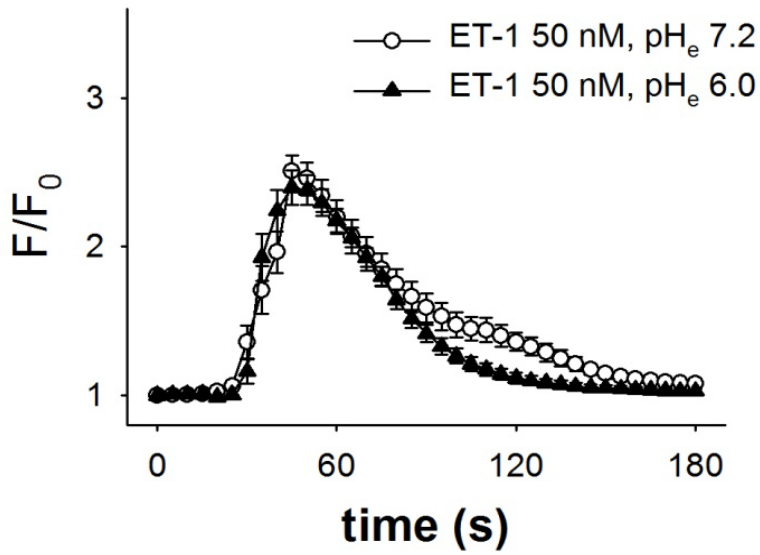

Fig. 6. Extracellular acid does not affect the GPCR-mediated Ca^{2+} increase.

ET-1 50 nM increased intracellular Ca^{2+} at pH_e 7.2 or pH_e 6.0 in HEK293T cells co-transfected with ET_AR and ANO1. (n=3)

ANO2 is also known to be a CaCC. We tested whether Ca^{2+}-activated ANO2 current is blocked by intracellular acid. Repeated application of 30 μM Ca^{2+} at pH 7.2 rapidly activated ANO2 with a slight desensitization (Fig. 7A). However, the application of 30 μM Ca^{2+} at pH 6.0 did not elicit ANO2 current (Fig. 7B). These results suggested that ANO1 and ANO2 are blocked by intracellular protons.

Other members of ANO family have channel activity, but they are activated by high Ca^{2+} concentration at positive membrane potential. We attempted whether intracellular acid affects other ANOs, ANO6, ANO7 and ANO9. ANO6 current was elicited by 300 μM Ca^{2+} at +80 mV in HEK293T cells, transfected with mouse ANO6. Repeated application of Ca^{2+} induces outward current without desensitization at pH 7.4. However, Ca^{2+} hardly activated the current by at pH 5.8 (Fig. 8A, B). HEK293T cells transfected with human ANO7 had small current, which was activated by 300 μM Ca^{2+} at +80 mV. There was no desensitization at pH 7.4. No current was elicited by 300 μM Ca^{2+} at pH 5.8 (Fig. 8C, D). Intracellular acid inhibits ANO6 and ANO7 current, similar to ANO1 and ANO2. Small current was elicited by 300 μM Ca^{2+} at +80 mV in HEK293T cells, expressing mouse ANO9. Repeated application of Ca^{2+} evoked the current with no desensitization at pH 7.4 and pH 5.8 (Fig 9A, B). Contrast to other ANOs, intracellular acid does not affect the ANO9 current.

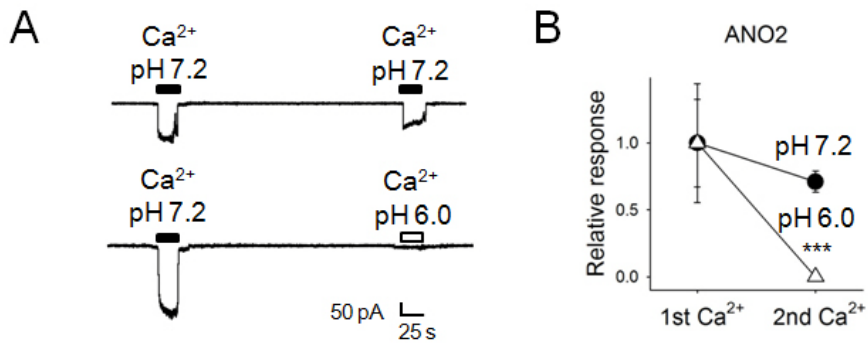

Fig. 7. ANO2 current is blocked by intracellular acid.

(A) Example traces of ANO2 currents induced by 30 μM Ca^{2+} at pH 7.2 or pH 6.0. Single-channel currents were recorded in inside-out patches isolated from HEK293T cells transfected with mouse ANO2. E_{hold} = -80 mV.

(B) Summary of the acid-mediated inhibition of ANO2 currents (n=7)

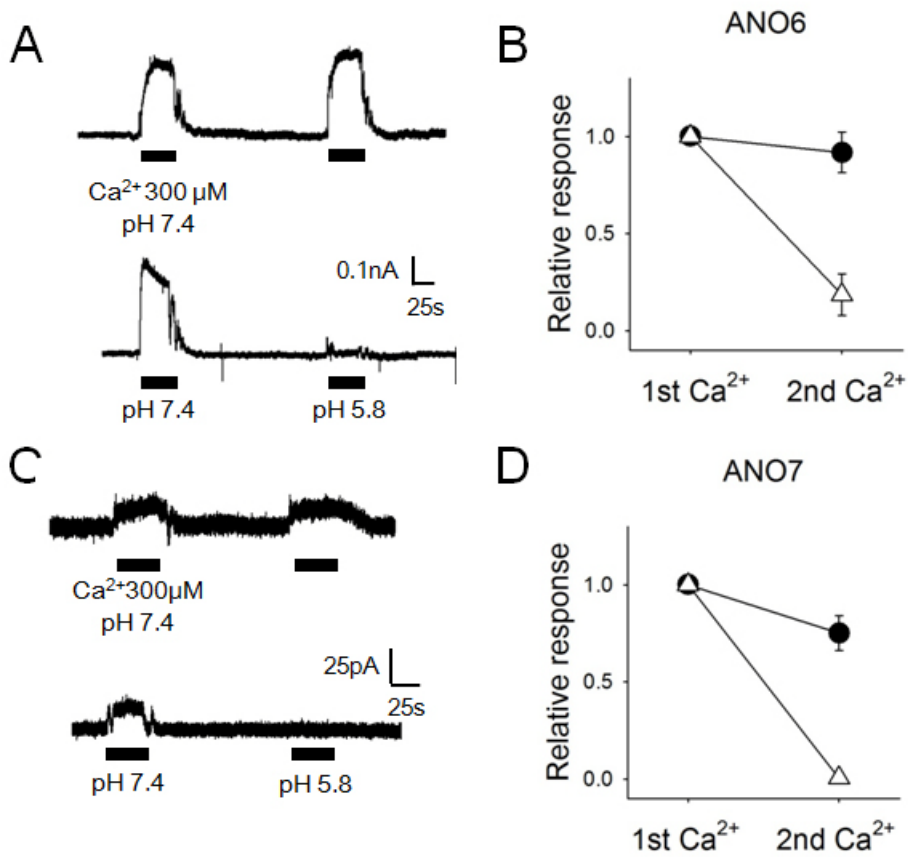

Fig. 8. Intracellular acid blocks the activation of mouse ANO6 and human ANO7.

(A) Example traces of ANO6 induced by 300 μM Ca^{2+} at pH 7.4 or pH 5.8. Currents were recorded in inside-out patches of HEK293T cells, which expressed mouse ANO6. E_{hold} = +80 mV.

(B) Summary of the acid-mediated inhibition of ANO6 currents (n=5-10)

(C) Example traces of ANO7 induced by 300 μM Ca^{2+} at pH 7.4 or pH 5.8. Currents were recorded in inside-out patches of HEK293T cells, which expressed human ANO7. E_{hold} = +80 mV.

(D) Summary of the acid-mediated inhibition of ANO7 currents (n=4).

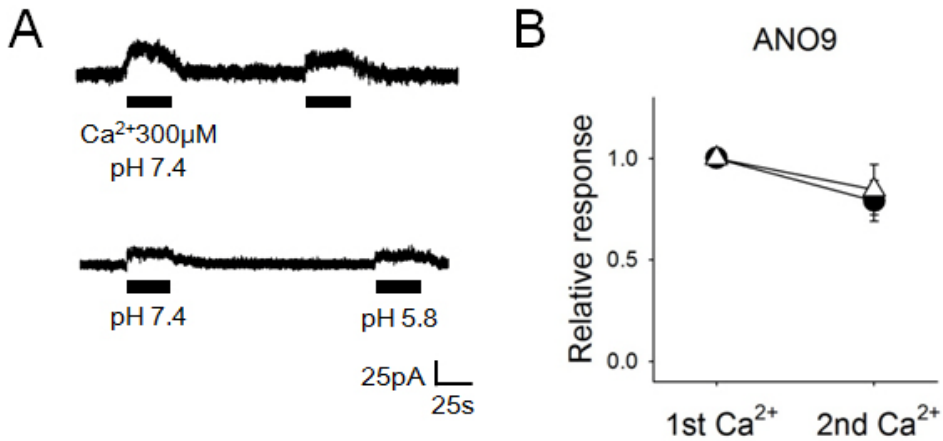

Fig. 9. Intracellular acid does not alter the ANO9 activation.

(A) Example traces of ANO9 activated by 300 μM Ca^{2+} at pH 7.4 or pH 5.8. Currents were recorded in inside-out patches of HEK293T cells, which expressed mouse ANO9. E_{hold} = +80 mV. Different to another ANOs, ANO9 was not inhibited by intracellular acid.

(B) Summary of ANO9 currents in two points of pHs, pH 7.4 and pH 5.8. E_{hold} = +80 mV (n=6-8)

To investigate whether the Ca^{2+} sensitivity of ANO1 was shifted by intracellular pH or not, the current activated by various Ca^{2+} concentrations was measured at different pHs in HEK293T cells overexpressed with mouse ANO1. The threshold Ca^{2+} concentration to activate ANO1 was less than 1 μM at pH 7.2. It was increased to about 10 μM at pH 6.0 (Fig. 10A). Half maximal effective Ca^{2+} concentration (EC_{50}) was obtained from fitting to Hill equation (Fig. 10B). Intracellular acid led to a right-shift of the EC_{50} in ANO1, from 5.4±0.4μM at pH 7.2 to 33.4 ± 1.9 μM at pH 6.0 (n=7). The dose-response curves shifted rightward significantly at pH 6.4 and pH 6.0 compared to pH 7.2 (Fig. 5C, EC_{50} 15.4 ± 2.3 μM at pH 6.4 (n=8)). However, intracellular alkali does not alter the Ca^{2+} sensitivity of ANO1, EC_{50} was 4.6 ± 0.4 μM at pH 8.0 (n=7). The higher Ca^{2+} concentration was required for ANO1 activation in acidic condition. A similar result was derived from ANO2. The current was elicited by various Ca^{2+} concentrations at different pHs in HEK293T cells transfected with mouse ANO2. With the increase of acidity from 7.2 to pH 6.0, EC_{50} was increased significantly from 13.5 ± 1.5 μM to 77.9 ± 6.5 μM (n=6, $p<0.001$) (Fig. 11A, B, C). The dose-response curve was shifted at pH 6.4, EC_{50} was 36.8 ± 5.6 μM (n=7, $p<0.01$). Similar to ANO1, the application of alkaline solution (pH 8.0) failed to modulate the Ca^{2+} sensitivity of ANO2 (EC_{50} 8.8 ± 0.5 μM at pH 8.0 (n=7)) (Fig. 11B, C). We noticed that the activation of ANO1 and ANO2 need more Ca^{2+} under the increase of intracellular acidity.

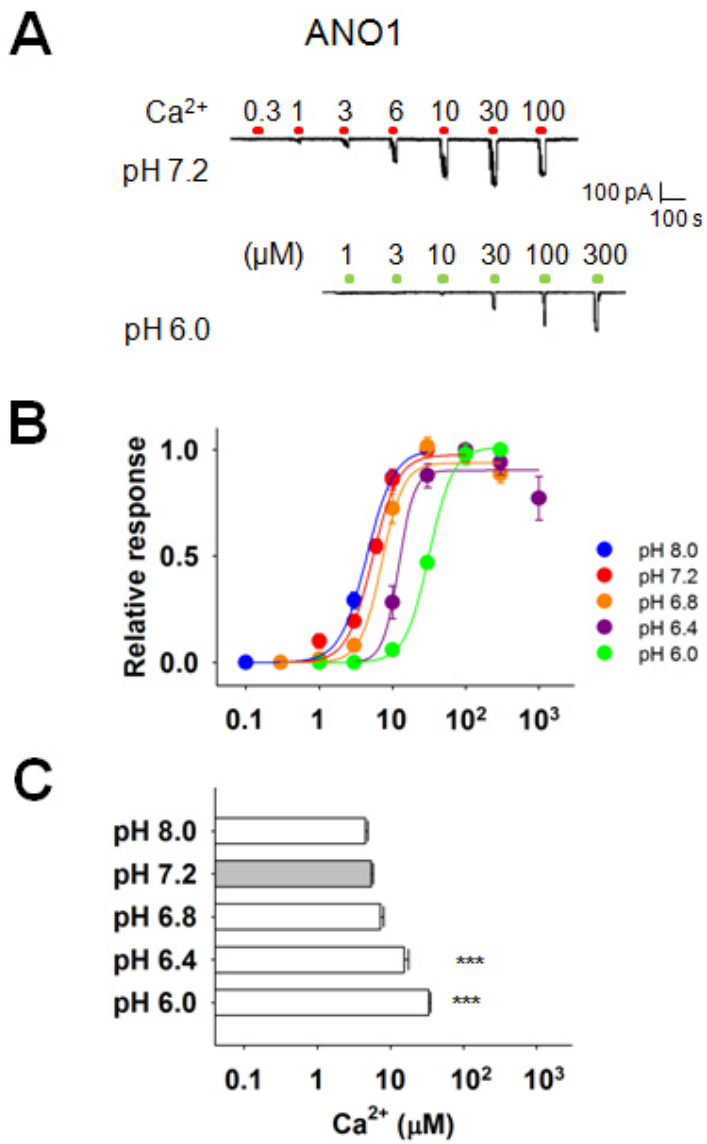

Fig. 10. Intracellular acid reduces the Ca^{2+} sensitivity of ANO1

(A) Example traces of ANO1 currents activated by various Ca^{2+} (μM) concentration at pH 7.2 or pH 6.0. E_{hold}= -80 mV

(B) The dose-response curves of ANO1 activated by various Ca^{2+} (μM) concentration at various pHs. Each current was normalized to the maximum current. Averaged data were fitted with the Hill equation (n= 7-8).

(C) Summary of Ca^{2+} EC_{50}s at various pHs. ***p<0.001 compared to the EC_{50} at pH 7.2. One-way ANOVA followed by Tukey's post-hoc test.

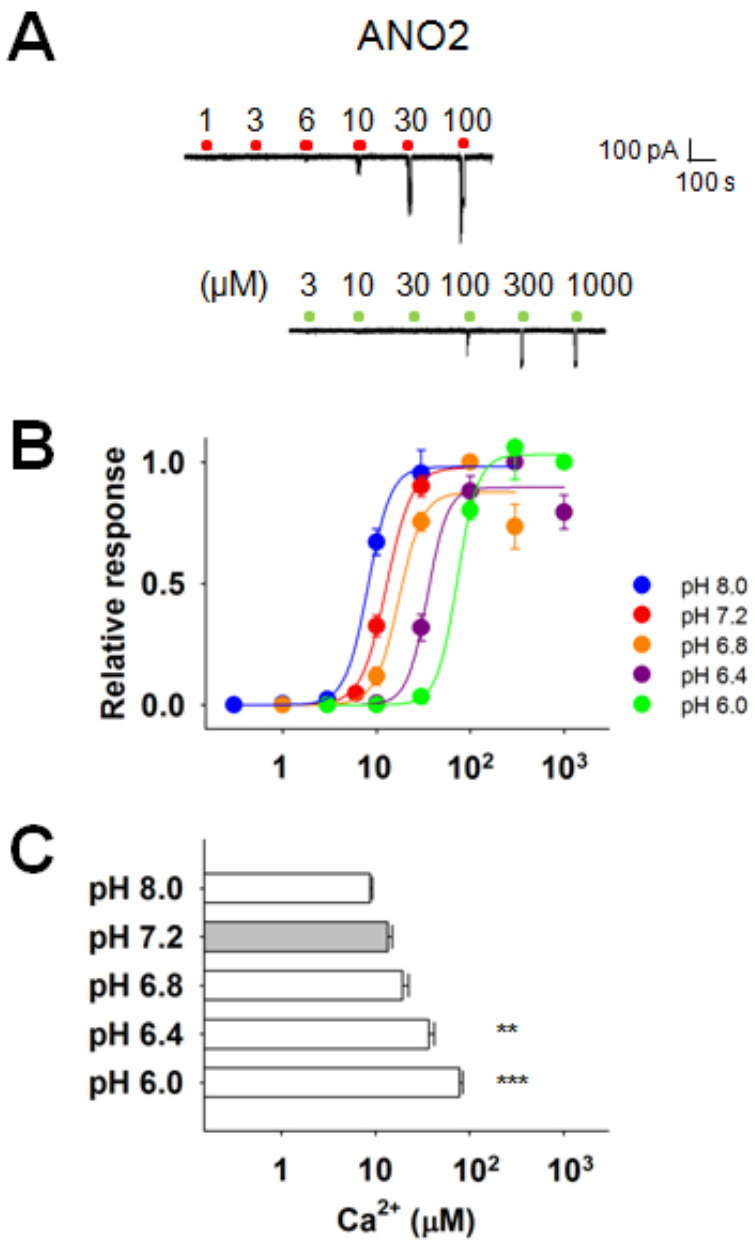

Fig. 11. Intracellular acid reduces the Ca^{2+} sensitivity of ANO2.

(A) Example traces of ANO2 currents activated by various Ca^{2+} (μM) concentration at pH 7.2 or pH 6.0. E_{hold}= -80 mV

(B) The dose-response curves of ANO2 activated by various Ca^{2+} (μM) concentration at various pHs. (n= 6-7).

(C) Summary of Ca^{2+} EC_{50}s at various pHs. **p<0.01

To get further understanding of the acid-induced ANO1 inhibition, we analyzed the half-maximal concentrations for inhibition (IC_{50}) in ANO1 current at a given Ca^{2+} concentrations. The slight change of intracellular pH inhibited the ANO1 current. The IC_{50}s varied according to the Ca^{2+} concentration in activating ANO1. At -80 mV, IC_{50} of the ANO1 current activated by 1 μM Ca^{2+} is pH 7.09 ± 0.003 (n=8). With the increase of Ca^{2+} concentration, the IC_{50} become acidic (pH 7.03 ±0.02 at 3 μM Ca^{2+}, $p<0.05$, n=7 and pH 6.92 ±0.05 at 10 μM Ca^{2+}, $p<0.01$, n=7) (Fig. 12A). The more intracellular protons were required to inhibit the ANO1 activation by higher Ca^{2+} concentration. We obtained similar results at +80 mV (Fig. 12B). The IC_{50} at 1 μM Ca^{2+} is pH 7.08 ± 0.02 whereas it is pH 7.02 ± 0.06 at 3 μM ($p<0.05$, n=6). The IC_{50} was not affected by voltage. But it was dependent on the Ca^{2+} concentration.

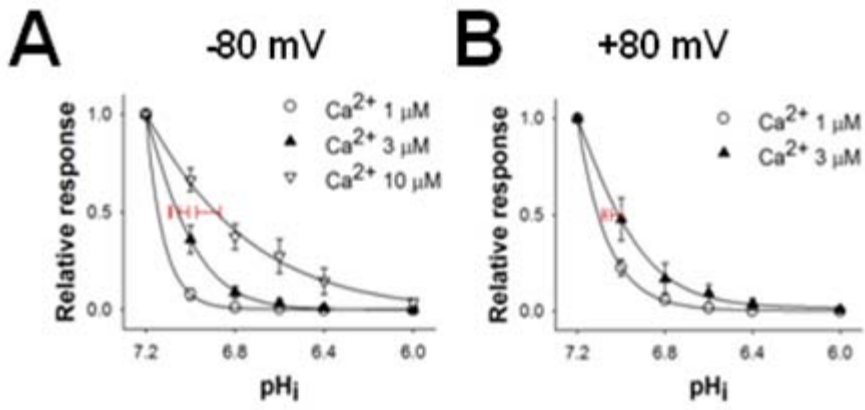

Fig. 12. The half maximal inhibitory concentration (IC_{50}) changes according to the Ca^{2+} concentration in activating ANO1.

(A) The dose-response curves of ANO1 inhibited by various pHs at a given Ca^{2+} concentration. Each current was normalized to the maximal current. Currents were recorded with inside-out patches isolated from ANO1 transfected HEK293T cells. E_{hold} = -80 mV. (n=7-8)

(B) The dose-response curves of ANO1 inhibited by various pHs at a given Ca^{2+} concentration. E_{hold} = +80 mV. (n=6)

2. Voltage-mediated and heat-mediated ANO1 activation is not inhibited by intracellular acid.

ANO1 is well known that it is dually gated by voltage (V_m) and intracellular Ca^{2+} (Xiao et al., 2011). Therefore, we investigated whether the voltage-dependent ANO1 activation is altered at intracellular acid. ANO1 whole-cell currents were recorded in HEK293T cells expressing mouse ANO1 and elicited by Ca^{2+} 10 μM in the pipette. The activation of ANO1 was enhanced by membrane depolarization. And intracellular acid (pH 6.8) inhibited voltage-dependent ANO1 activation (Fig. 13B). Tail currents were recorded at -100 mV after prepulses between -200 mV and +200 mV in 10 mV increment. The voltage dependence of steady-state activation (G-V relation) was analyzed by measuring tail currents. The data was fitted with the Boltzmann equation. As shown in Fig. 13C, the G-V curve of ANO1 at Ca^{2+} 10 μM was shifted rightward at pH 6.8. The half-maximal voltage ($V_{1/2}$) was changed from -144.6 ± 11.7 mV at pH 7.2 to 103.7 ± 28.4 mV at pH 6.8. Because ANO1 was fully activated by only Ca^{2+} at 10 μM, it was hard to represent the voltage-dependence of ANO1. To get insight that intracellular acid alters the voltage-evoked current, ANO1 current was measured at Ca^{2+} 3 μM in pH 7.2 or pH 6.8. It was enhanced by positive membrane potential (Fig. 13A). Similar to Ca^{2+} 10 μM, the G-V curve shifted rightward at

intracellular acid. $V_{1/2}$ at pH 7.2 was 12.4 ± 27.5 mV but changed to 103.7 ± 28.4 mV at pH 6.8 ($p<0.001$, n= 5-6) (Fig. 13C). However, the intracellular acid failed to change the equivalent gating charge (z). At pH 7.2, z was 0.33 ± 0.06 and at pH 6.8, z was 0.31 ± 0.03. Because $V_{1/2}$ infers voltage-independent channel opening, the shift of $V_{1/2}$ suggests that intracellular acid affects the Ca^{2+} sensing. And z represents voltage-dependent channel opening, the fixed z value indicates that intracellular acid fails to alter the voltage-sensing.

To confirm the result, the voltage-induced ANO1 activation without Ca^{2+} was investigated. ANO1 is slightly activated by positive membrane potentials without Ca^{2+} (Fig. 14A). Severe depolarization (>100 mV) evoked outward-rectifying ANO1 whole-cell currents after dialyzing with 0 μM Ca^{2+}. The intracellular acid did not affect this Ca^{2+}-independent activation (Fig. 14B). The result supports our hypothesis that the acid-mediated ANO1 inhibition is involved in the Ca^{2+}-sensing.

Heat is another Ca^{2+}-independent ANO1 activator (Cho et al., 2012). The temperature above 44 ℃ activates ANO1. Heat-induced ANO1 activation is not related to the Ca^{2+}-binding (Lee et al., 2014b). Whether intracellular acid inhibits the heat-evoked ANO1 current or not was assessed. At 0 μM Ca^{2+} in the pipette with pH 7.2, the high temperature induced ANO1 currents (13.38±1.97 pA/pF) (Fig. 15A, B). Heat-evoked ANO1 current was not changed by intracellular acid (pH 6.0) (14.37±2.49

pA/pF). Intracellular acid did not inhibit the heat-evoked ANO1 current. Thus, we noticed that intracellular acid failed to inhibit the Ca^{2+}-independent ANO1 activation, whereas the Ca^{2+}-induced activation was inhibited by intracellular acid.

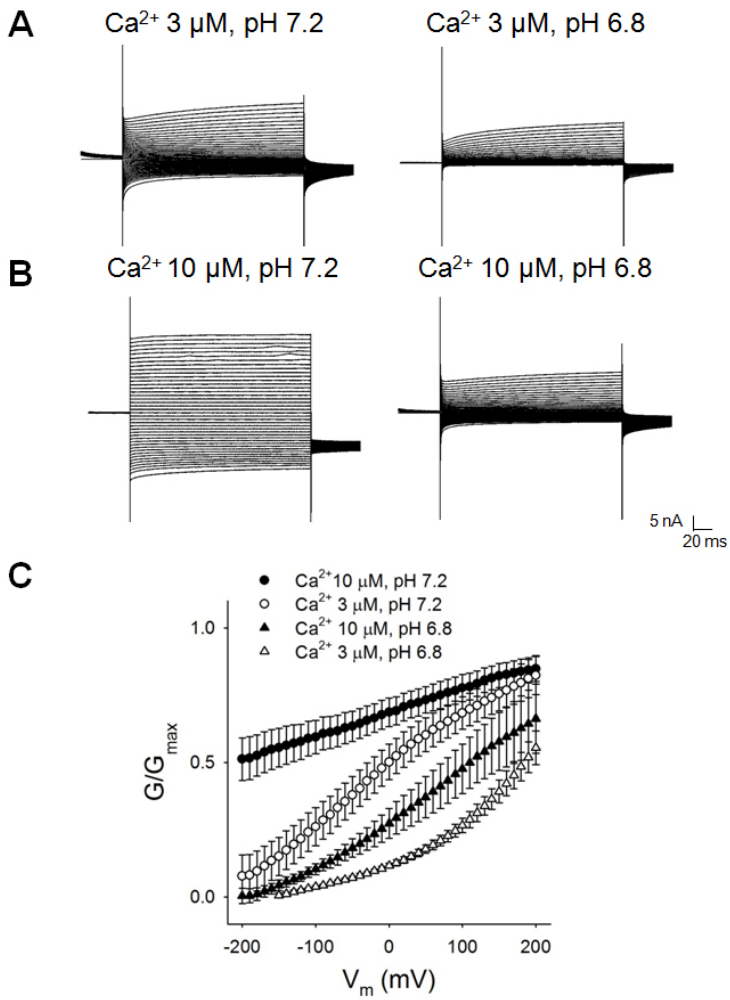

Fig. 13. Voltage-dependent ANO1 activation remains at intracellular acid.

(A) ANO1 whole-cell currents in response to voltage steps (from -200 mV to +200 mV in 10 mV increment). Whole-cell currents were recorded at indicated pHs, pH 7.2 or pH 6.8, in HEK293T cells expressing mouse ANO1. Pipette solution contained Ca^{2+} 3 μM in the NMDG-Cl solution.

(B) ANO1 whole-cell currents in response to voltage steps. Pipette solution contained Ca^{2+} 10 μM.

(C) The conductance-voltage (G-V) curves of ANO1 at Ca^{2+} 3 μM and 10 μM with pH 7.2 or pH 6.8. The normalized conductances (G/G_{max}s) were plotted against membrane potential (V_m).

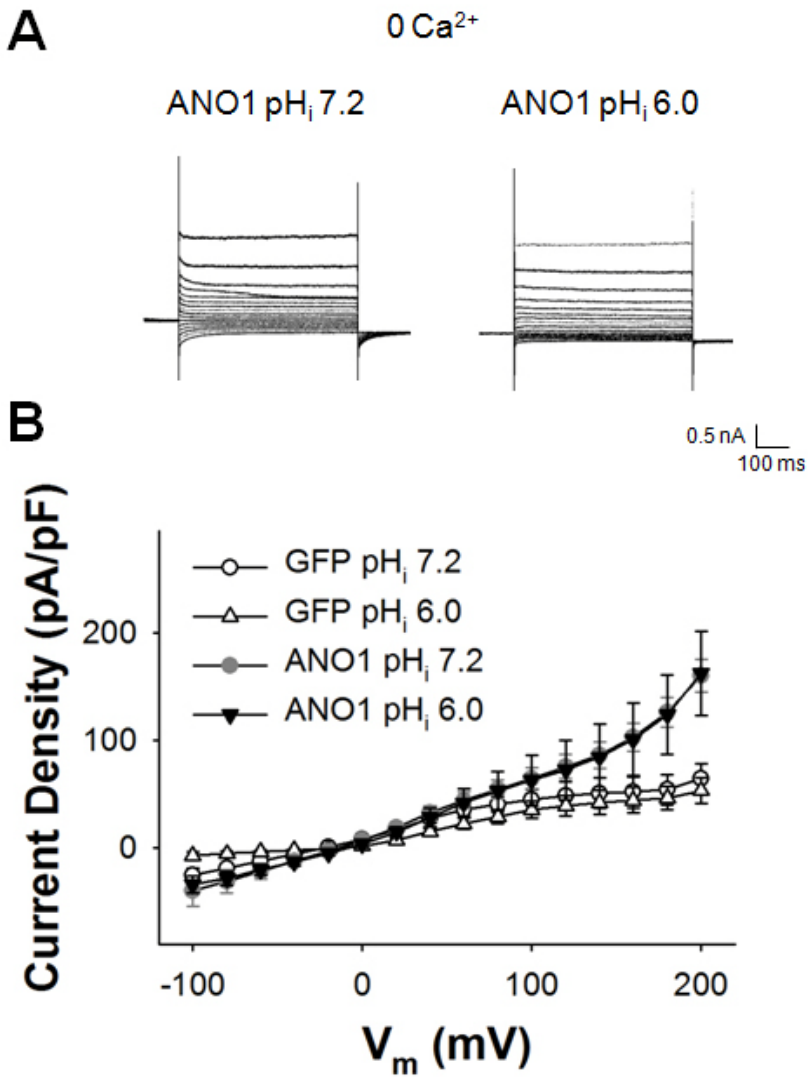

Fig. 14. The intracellular acid fails to inhibit the voltage-dependent ANO1 activation.

(A) Representative ANO1 whole-cell currents in response to voltage steps (from -100 mV to +200 mV in 20 mV increment). Whole-cell currents were recorded at indicated pHs, pH 7.2 or pH 6.0, in HEK293T cells expressing mouse ANO1. Pipette solution did not contain Ca^{2+} in the NMDG-Cl solution. (B) The current density-voltage (I-V) curves of ANO1 without Ca^{2+} at pH 7.2 or pH 6.0.

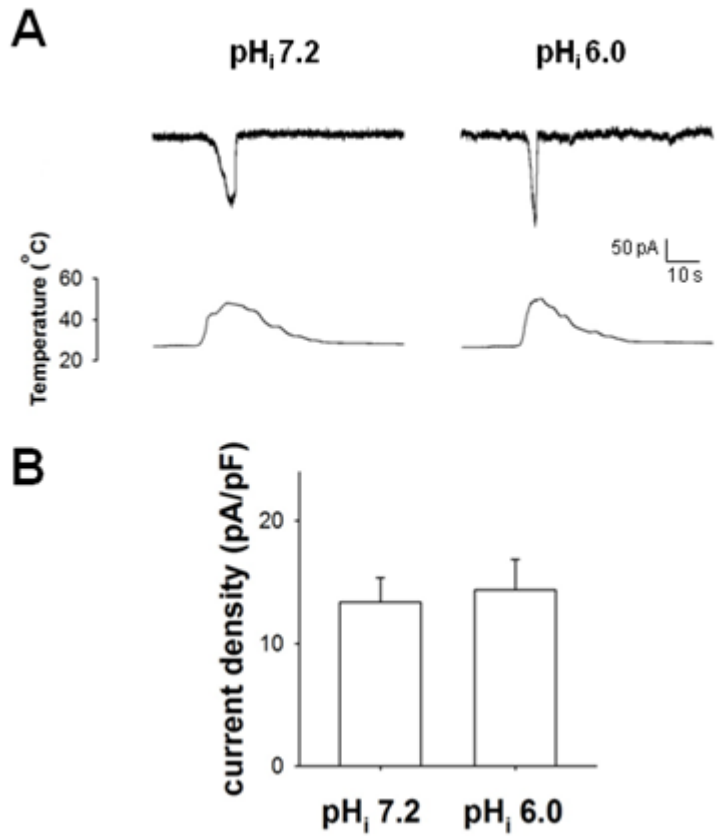

Fig. 15. Heat-evoked ANO1 currents are not inhibited by intracellular acid.

(A) Traces of heat-evoked ANO1 whole-cell currents at pH 7.2 or pH 6.0. The pipette solution contained 0 μM Ca^{2+} in the NMDG-Cl solution with 10 mM EGTA at pH 7.2 or pH 6.0.

(B) A summary of heat-evoked ANO1 whole-cell currents at pH_i7.2 and pH 6.0. (n=9)

3. His residues are not critical for ANO1 inhibition by intracellular acid.

To search for sites involved in the intracellular acid-dependent ANO1 inhibition, we generated a series of point mutants of mouse ANO1. His residue has an adequate pK_a value 6.04 to be protonated at physiological relevant range (pH 6-7). This may in turn cause alterations in channel conformation and function. Recently, the crystal structure of *Nectria haematococca* (*nh*) TMEM16 was resolved (Brunner et al., 2014). The expected topology of ANO1 had 8 transmembrane domains, whereas the topology of *nh*TMEM16 has 10 transmembrane domains with α helices. Therefore, we revised the mouse ANO1 topology by alignment with *nh*TMEM16 amino acid sequence (Fig. 16). As shown in the topology, there are 21 His residues. 4 His residues in the purple circles were excluded because they were predicted to be located at the extracellular region. 17 His residues are expected to locate in the intracellular or intramembrane region. We generated 17 His/Arg mutants, replacing His residues with Arg residues. The large inward current was elicited by 10 μM Ca^{2+} in wild-type(WT) ANO1. The repeated application desensitized slightly. However, no current was activated by Ca^{2+} at pH 6.0 (Fig. 17A). 10 μM Ca^{2+} evoked the robust current in H18, 69, 70, 120, 151, 163, 183, 212, 230, 426, 453, 898, 936, 941 and 956R single-point ANO1 mutants. And it was inhibited

completely at pH 6.0 similar to WT (Fig. 17B, C). Because H159R and H284R were not activated by maximal Ca^{2+} concentration, we could not test the acid-mediated inhibition on them. These results indicated that His residues of ANO1 do not have ability to sense proton to inhibit the channel function.

4. Mutations of Glu and Asp in multiple acidic amino acid regions do not affect the acid-induced inhibition.

Glu and Asp residues are titrable at low pH (Jordt et al., 2000). Based on this, Glu and Asp residues were suggested that they have possibility of sensing protons. Because they were also candidates for the calcium sensor, we tested two mutants, which were previously reported (Xiao et al., 2011; Lee et al., 2014b). First, we assessed the acid-mediated inhibition of ANO1 Δ5E mutant. 5 Glu residues (444-EEEEE-448) are clustered at the intracellular loop between transmembrane(TM)2 and TM3 of mouse ANO1 (Fig. 18). We deleted the cluster of 5E (Δ5E mutant) in mouse ANO1. The current was evoked by 10 μM Ca^{2+} in Δ5E mutant (Fig. 19A). The repeated application of Ca^{2+} induced the current with little desensitization at pH 7.2 whereas Ca^{2+} failed to evoke the current at pH 6.0 (Fig. 19A, B). The acid-mediated inhibition was occurred in the mutant similar to ANO1 WT. Next, another cluster of acidic amino acids in ANO1, named ED-rich region (121-**EDD**KRFRR**EE**Y**E**GNLL**E**AGL**E**L**E**N**DED**-147) was assessed. The ED-rich

region is located at N-terminus of mouse ANO1 (Fig. 18). Asp and Glu residues in this region were substituted into Asn and Glu, respectively (121-**QNN**KRFRR**QQ**Y**Q**GNLL**Q**AGL**Q**L**Q**N**NQN**-147, ED rich mutant). 10 μM Ca^{2+} activated the large and robust inward-current in HEK293T cells transfected with mouse ANO1 ED-rich mutant (Fig. 20A). Second response showed no desensitization at pH 7.2. However, no current was elicited by the second 10 μM Ca^{2+} application at pH 6.0 (Fig. 20A, B). The acid-mediated inhibition of ED-rich mutant remained. The data indicated that the multiple acidic amino-acids are not related to the ANO1 inhibition by intracellular acid.

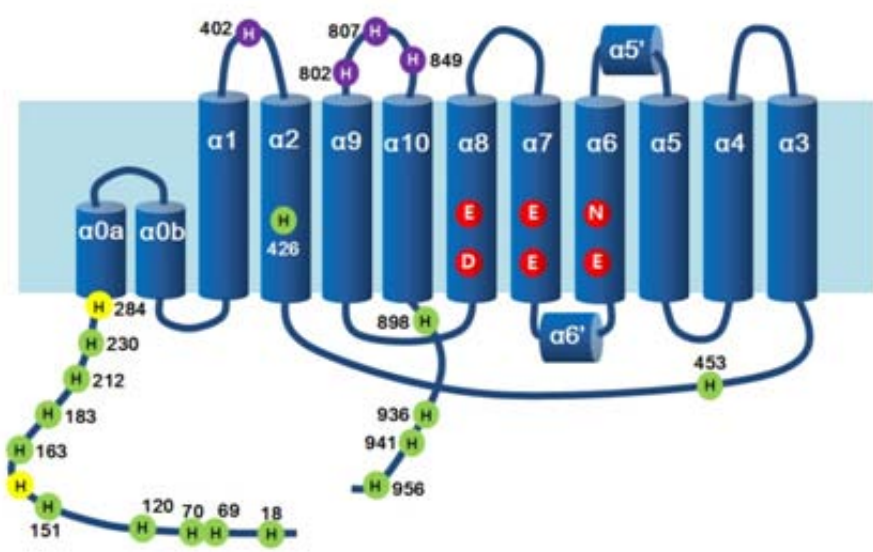

Fig. 16. The topology of mouse ANO1 with His residues

There are 21 His residues in ANO1. The topology of mouse ANO1 was derived from the alignment with *nh*TMEM16. ●, His residues located at the extracellular region; ●, His residues located at the intracellular and intramembrane region; ●, Mutants in these residues failed to evoke the current by maximal Ca^{2+}.

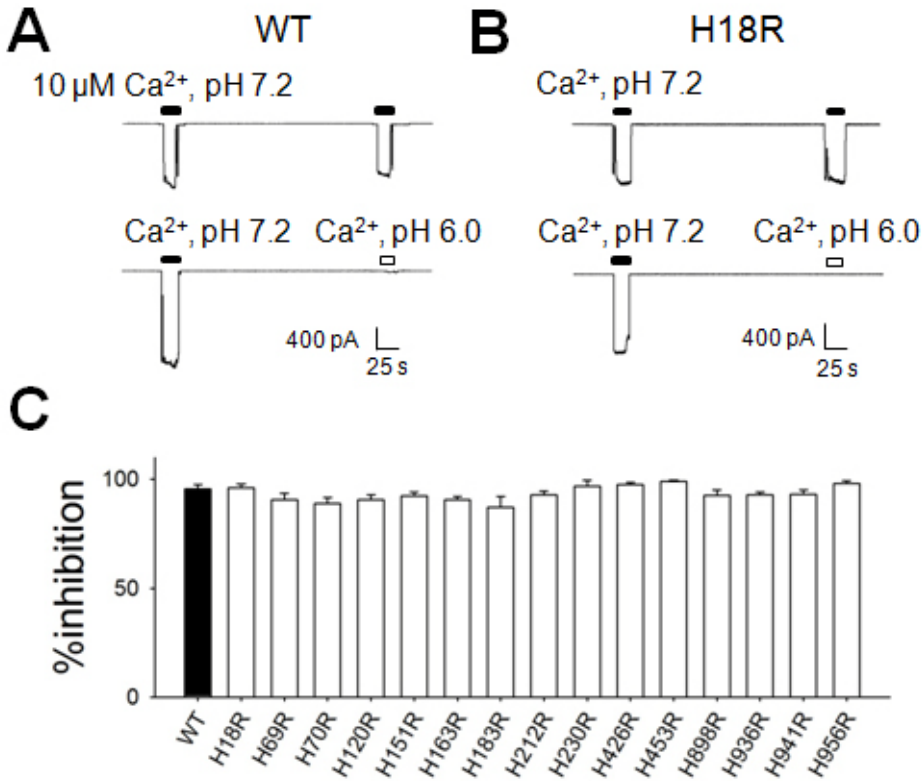

Fig. 17. His residues are dispensable for the acid-mediated ANO1 inhibition.

(A) Example macroscopic single-channel traces of ANO1 WT elicited by Ca^{2+} 10 μM at pH 7.2 and pH 6.0. E_{hold} = -80 mV.

(B) Example macroscopic single-channel traces of ANO1 H18R mutant elicited by Ca^{2+} 10 μM at pH 7.2 and pH 6.0.

(C) Summary of the acid-mediated inhibition of ANO1 WT and ANO1 His/Arg mutants. His residues at 18, 69, 70, 120, 151, 163, 183, 212, 230, 426, 453, 898, 936, 941 and 956 in mouse ANO1 were replaced with Arg. All mutants exhibited similar inhibition by intracellular acid to WT. One-way ANOVA; Tukey's post-hoc test.

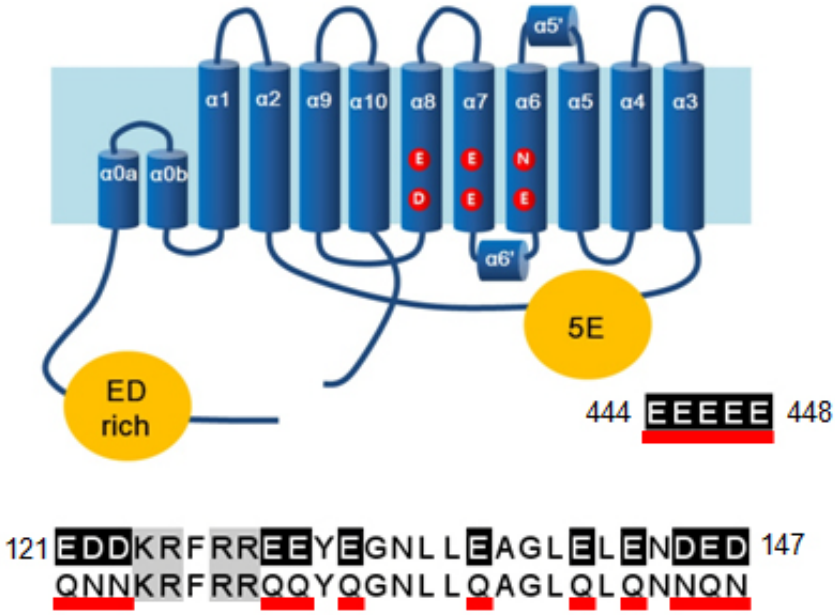

Fig. 18. Locations of the 5E cluster and the ED rich region in the mouse topology

The 5E cluster and the ED rich region are shown in orange. The 5E cluster (444-**EEEEE**-448) was deleted. Glu and Asp residues in the ED rich region (121-**EDD**KRFRR**EE**Y**E**GNNLL**E**AGL**E**L**E**N**DED**-147) were replaced with Gln or Asn, indicated with red lines.

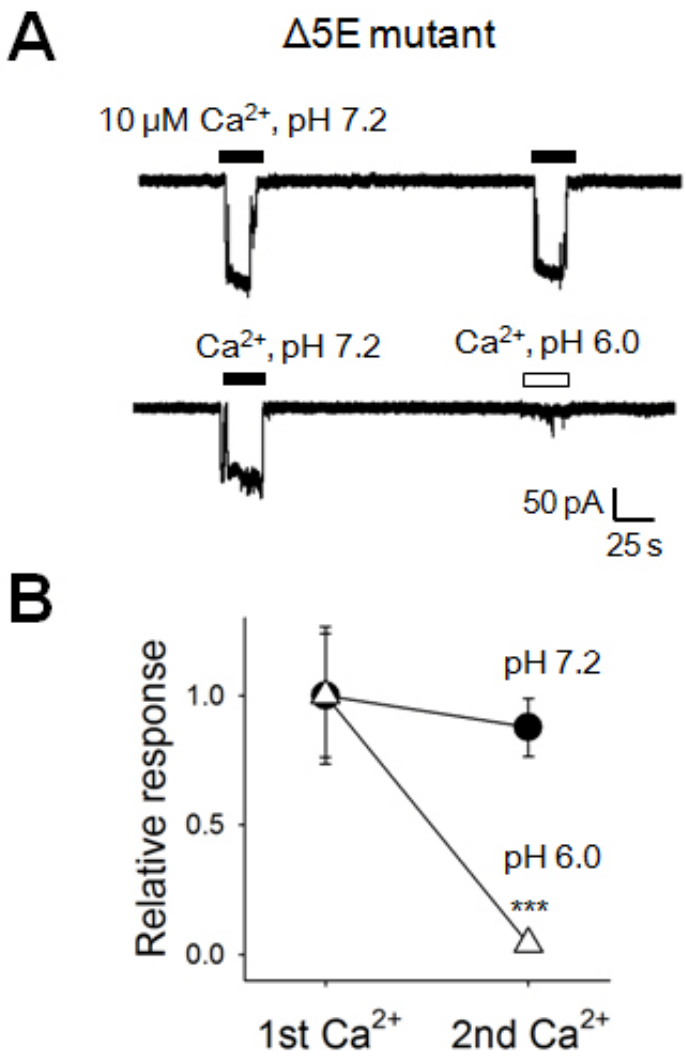

Fig. 19. Clustered Glu residues are dispensable for the acid-mediated inhibition.

(A) Example traces of Δ5E ANO1 mutant elicited by Ca^{2+} 10 μM at pH 7.2 and pH 6.0. E_{hold} = -80 mV.

(B) Summary of the acid-induced current inhibition in Δ5E mutant (n=4-7). ***p<0.001 compared to the relative response at pH 7.2.

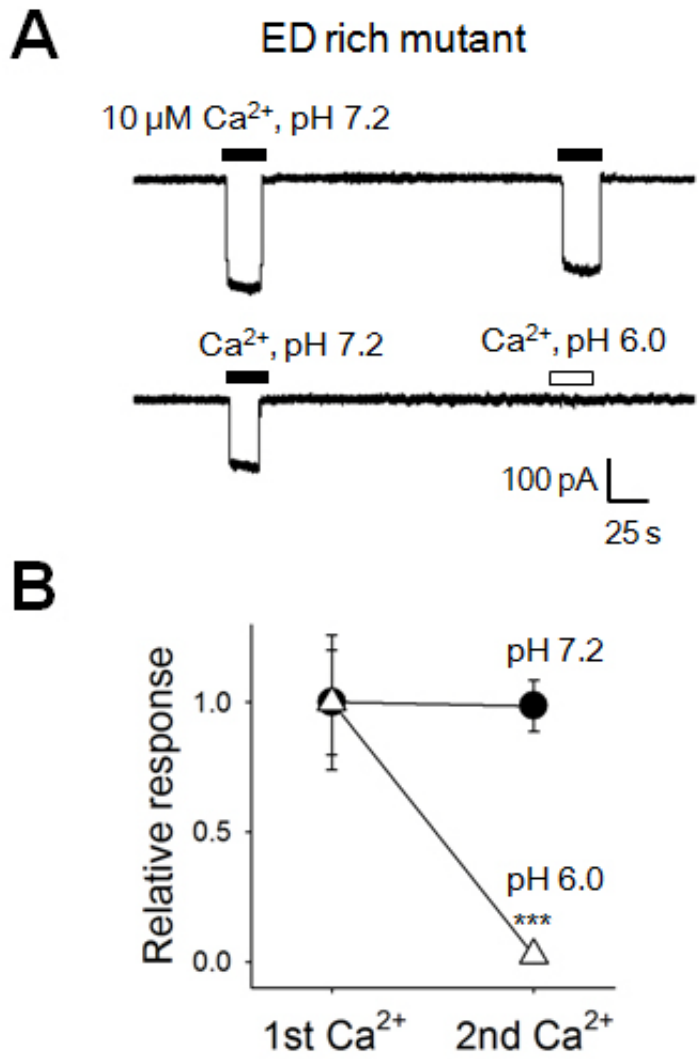

Fig. 20. The multiple acidic amino-acids region is not essential for the acid-mediated ANO1 inhibition.

(A) Current traces of the ANO1 ED-rich mutant activated by Ca^{2+} 10 μM at pH 7.2 and pH 6.0. E_{hold} = -80 mV.

(B) Summary of the acid-induced current inhibition in ED-rich mutant (n=5). ***p<0.001

5. Calcium binding sites in the hydrophobic core are essential for acid-mediated inhibition.

Recently, the X-ray structure of *nh*TMEM16 has been defined (Brunner et al., 2014). Lipid scramblase activity of a fungal TMEM16 requires Ca^{2+}. 6 residues embedded within the hydrophobic core are identified as the Ca^{2+} binding site of *nh*TMEM16. They are highly conserved throughout the TMEM16 homologs. Conserved residues, N650, E654, E702, E705, E734 and D738 of mouse ANO1 are essential for Ca^{2+} sensing to activate the current. As shown in Fig. 21, red colored residues at the α6, α7 and α8 helix are involved in the Ca^{2+} coordination in *nh*TMEM16 and *m*ANO1. The predicted structure of *m*ANO1 was obtained by computer modeling (Fig. 21C). Amino-acids composing α6, α7 and α8 helix were selected for modeling. The crystal structure of *nh*TMEM16 (PDB number: 4WIS) was chosen as a template (Fig. 21B). The residues in the Ca^{2+} binding site face each other as if they encase Ca^{2+}. It is well-known that mutations of the essential residues reduce the Ca^{2+} sensitivity (Yu et al., 2012; Brunner et al., 2014; Tien et al., 2014). We further assessed that residues in the Ca^{2+} binding site has the ability to sense intracellular acid in inhibiting ANO1 current.

First, the mutant of α6 helix was tested. N650 and E654 at α6 helix were substituted into Ala and Gln. The currents were recorded at +80 mV in

order to see the better response. The current of WT ANO1 was elicited by lower Ca^{2+} at +80 mV (EC_{50} 1.8 ± 0.6 μM at pH 7.2, n=10) (Fig. 29). The currents of mutants related to the Ca^{2+} binding site were evoked by higher Ca^{2+} concentration at the positive membrane potential. The EC_{50} of N650A/E654Q mutant was 17.6 ± 3.7 μM at pH 7.2 (n=6). Contrast to ANO1 WT (EC_{50} 12.0 ± 4.6 μM at pH 6.0, n=6), N650A/E654Q mutant failed to change the EC_{50} by intracellular acid (pH 6.0) (EC_{50} 19.1 ± 3.5 μM, n=5) (Fig. 22).

Second, the current was measured in the mutants of α7 helix. E702 and E705 are critical for binding Ca^{2+}. They were replaced with Gln. The E702Q/E705Q mutant exhibited a markedly reduction in the Ca^{2+} sensitivity (EC_{50} 14.5 ± 0.8 mM, n=5). The acid-mediated inhibition was diminished. The dose-response curve of Ca^{2+} is rather slightly left-shifted at pH 6.0 (EC_{50} 8.3 ± 1.0 mM, n=6) (Fig. 23). We then examined the effects of mutation of E702 and E705 individually. Single mutation was sufficient to reduce the Ca^{2+} sensitivity. The EC_{50} of E702Q mutant was 73.1 ± 6.2 μM and that of E705Q mutant was 3.9 ± 2.5 mM at pH 7.2 (n=6). However, an individual replacement was insufficient to alter the acid sensitivity. E702Q and E705Q showed a rightward shift by intracellular acid. The EC_{50} of E702Q mutant was 486.9 ± 110.2 μM (n=5) and that of E705Q mutant was 16.4 ± 7.1 mM (n=6) at pH 6.0 (Fig. 24 and 25). Moreover the substitution into Asp, another acidic amino-acid (E702D/E705D), did not affect the acid-mediated inhibition, whereas the Ca^{2+} sensitivity was reduced. The

threshold of Ca^{2+} to activate the mutant was ~30 μM at pH 7.2. But ~100 μM Ca^{2+} was acquired to evoke the current at pH 6.0 (Fig. 26A). It was half-activated by 135.6 ± 36.8 μM at pH 7.2 (n=6). The dose-response curve of E702D/E705D was shifted right slightly pH 6.0 (EC_{50} 358.7 ± 92.0 μM, n=6) (Fig. 26B). The data proposed that both E702 and E705 are required to the acid-mediated inhibition, distinct to the Ca^{2+} binding.

Finally, we assessed the effect of mutations at α8 helix. Two acidic amino-acids (E734 and D738) are embedded in α8 helix. We generated the mutant to replace Glu at 734 and Asp at 738 into Gln and Asn, respectively. Because E734 and D738 are important to sense Ca^{2+}, the EC_{50} of Ca^{2+} in activating the E734Q/D738N mutant was higher than WT (13.5 ± 4.4 μM, n=9). Similar to other double-mutations of the Ca^{2+} binding site, the double mutations on E734 and D738 induced to diminish the acid-mediated inhibition (18.9 ± 3.4 μM, n=8) (Fig. 27). Indeed, substitutions into Ala (E734A/D738A) also revealed the same results. The EC_{50} of the E734A/D738A mutant was similar to that of the E734Q/D738N mutant at pH 7.2 (18.7 ± 8.1 μM, n=8). And it was not affected by intracellular acid (18.4 ± 12.0 μM at pH 6.0, n=7) (Fig. 29B). However, the single Glu mutant (E734Q) still had the acid-mediated inhibition. The EC_{50} of Ca^{2+} in activating the E734Q at pH 6.0 was right-shifted compared to neutral solution (pH 7.2), from 15.1 ± 2.4 μM to 45.1 ± 12.4 μM (n=7) (Fig. 28A, B). Note that the EC_{50} of E734Q was almost identical to the EC_{50} of E734Q/D738N or E734A/D738A at pH 7.2 (Fig. 29B). This result was in agreement with those

of E702Q or E705Q, which possessed a single mutation at α7 helix.

Double mutations on the Ca^{2+} binding-related helix (α6, α7 and α8 helix) diminished the acid-induced ANO1 inhibition (Fig. 29). It was inferred that residues in the Ca^{2+} binding site involve the acid-mediated inhibition.

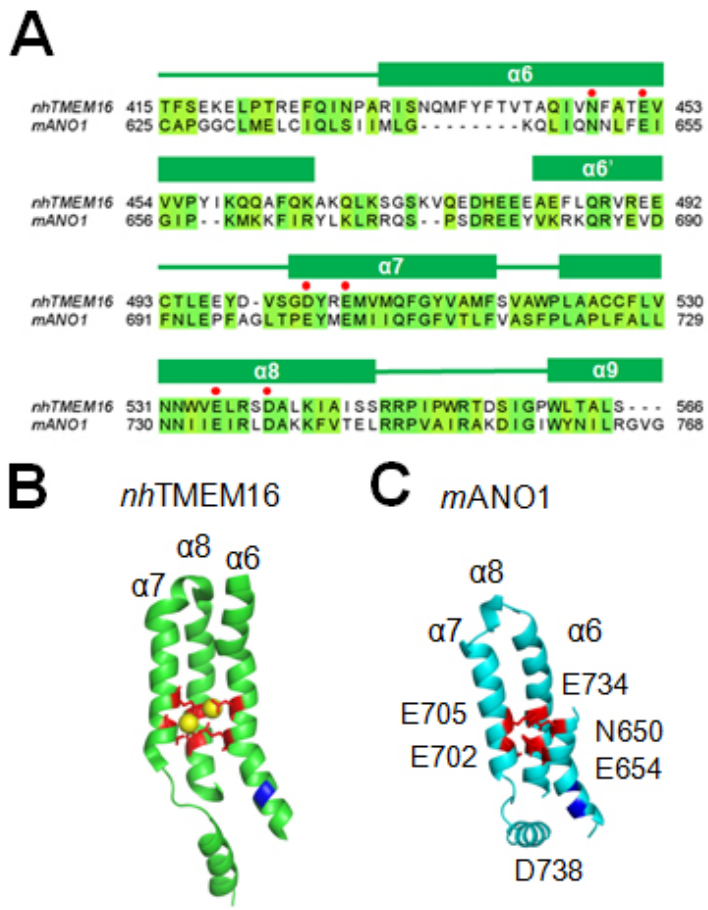

Fig. 21. Prediction of the mouse ANO1 structure

(A) Sequence alignment of *nh*TMEM16 and *m*ANO1. Identical and homologous residues are shown in green and yellowish green. Green boxes above the alignment indicate α-helices, the membrane spanning regions. The critical residues for the Ca^{2+} binding to activate ANO1 were marked with red circles.

(B) Location of Ca^{2+} binding site of *nh*TMEM16. The structure was editing to depicit α6, α7 and α8 helix, which possesses the essential residues to sense Ca^{2+}. The Glu, Asp and Asn residues are shown in red with sticks. Yellow spheres represent Ca^{2+}.

(C) Location of Ca^{2+} binding site of *m*ANO1. The model was predicted by ModWeb. N650, E654, E702, E705, E734 and D738, which are suggested as Ca^{2+} binding sites, are shown in red with sticks.

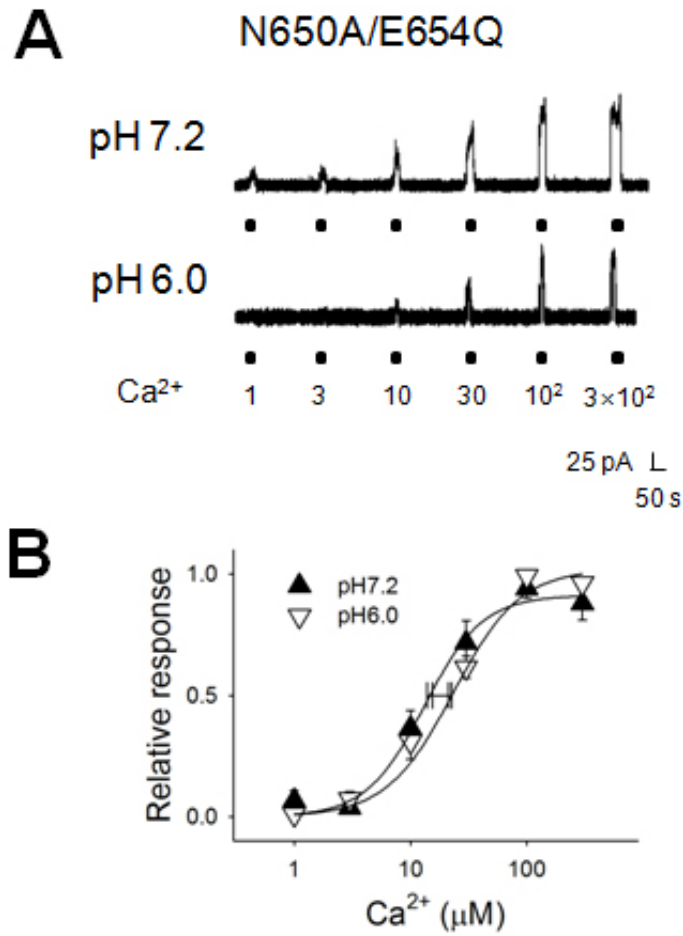

Fig. 22. Asn and Glu residues at α6 helix are essential for the acid-mediated ANO1 inhibition.

(A) Representative traces of N650A/E654Q mutant. Various concentrations of Ca^{2+} in 140 mM NMDG-Cl at pH 7.2 and pH 6.0 were perfused on inside-out patches. E_{hold} = +80 mV.

(B) The dose-response curves of Ca^{2+} in activating N650A/E654Q mutant (n=5-6). Each current was normalized to maximal responses. Horizontal error bars indicate EC_{50}s.

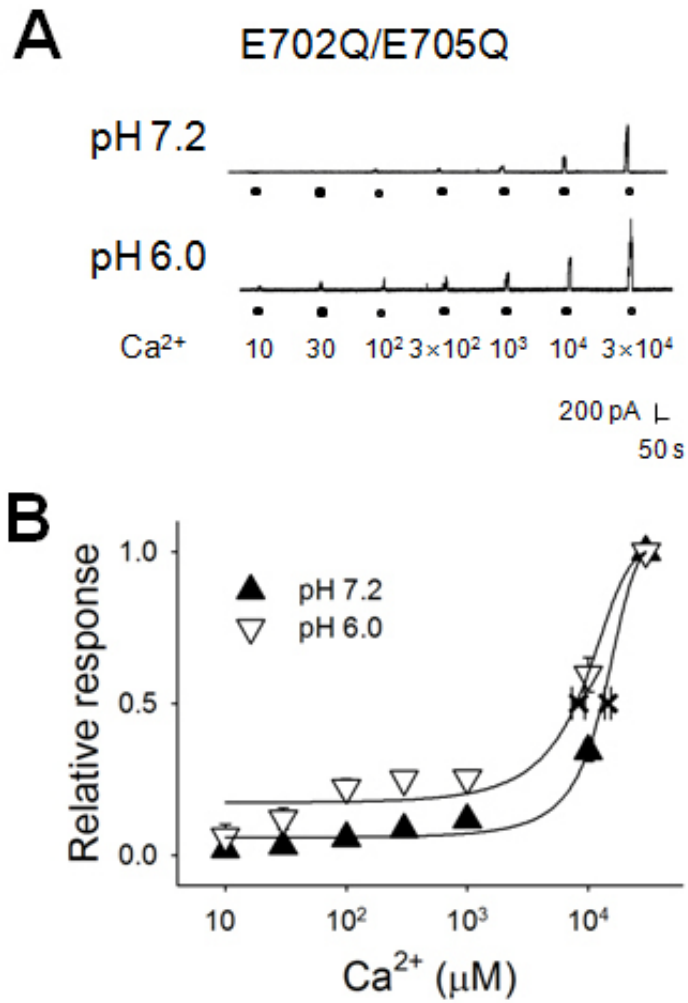

Fig. 23. 2 Glu residues at α7 helix are critical for sensing intracellular acid.

(A) Current traces of E702Q/E705Q mutant.

(B) The dose-response curves of Ca^{2+} in activating E702Q/E705Q mutant (n=5-6). Relative response was obtained by dividing each current to maximal current. Horizontal error bars with × represent EC_{50}s.

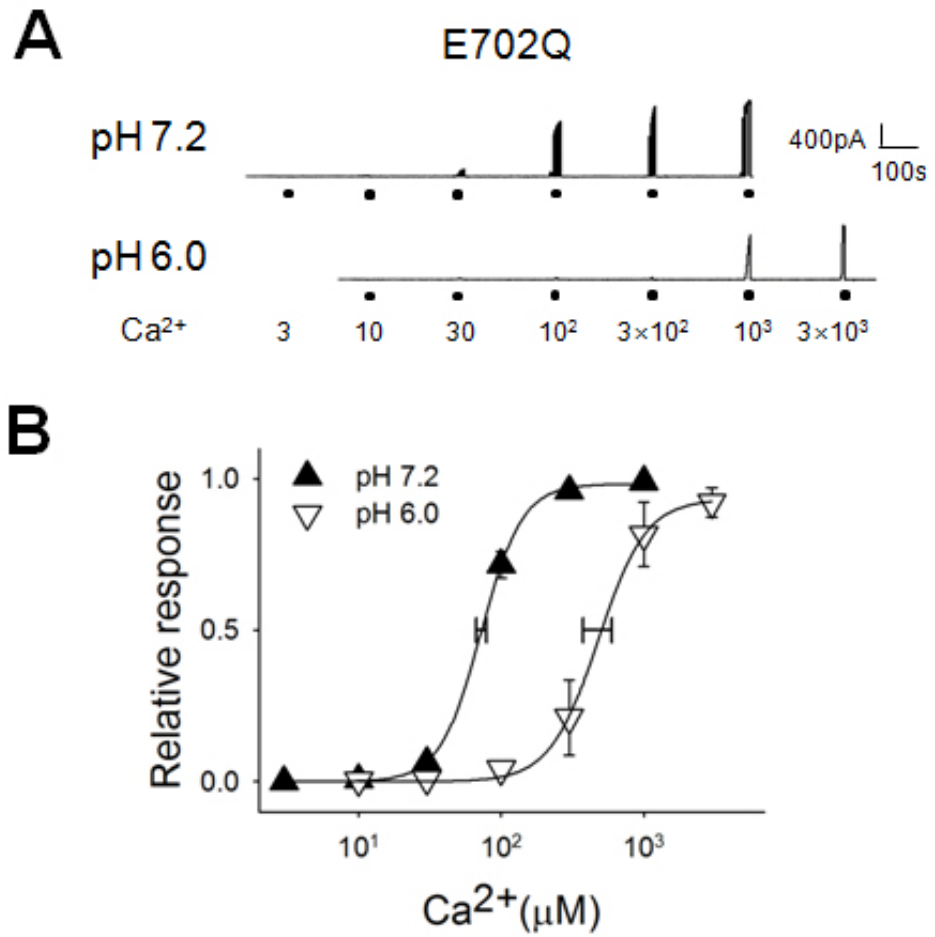

Fig. 24. Mutation of single Glu residue at α7 helix is insufficient to alter the acid-mediated ANO1 inhibition.

(A) Example single-channel current traces of E702Q mutant.

(B) The dose-response curves of Ca^{2+} in activating E702Q mutant (n=5-6). Each current was normalized to the maximal current. Horizontal error bars present EC_{50}s.

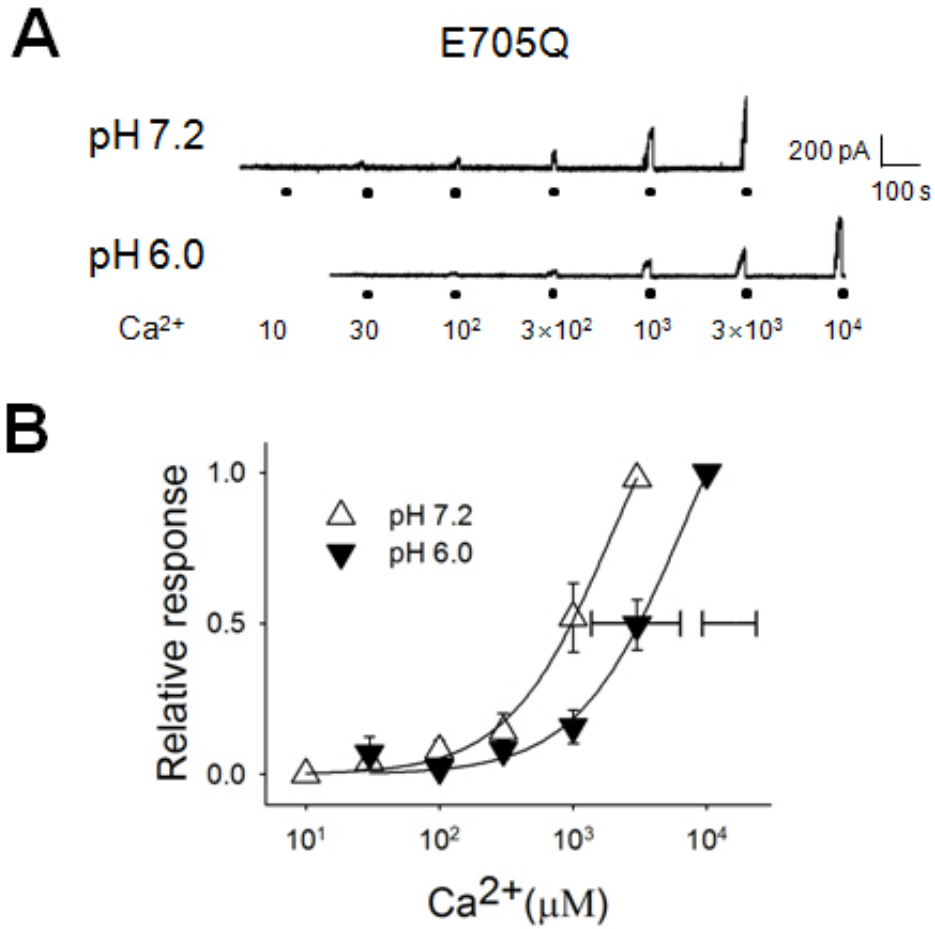

Fig. 25. A Glu residue in the Ca^{2+} binding site does not have ability to sense intracellular proton.

(A) Representative traces of E705Q mutant.

(B) The dose-response curves of Ca^{2+} in activating E702Q mutant (n=6). Each current was normalized to the maximal response. EC_{50}s are shown with horizontal error bars.

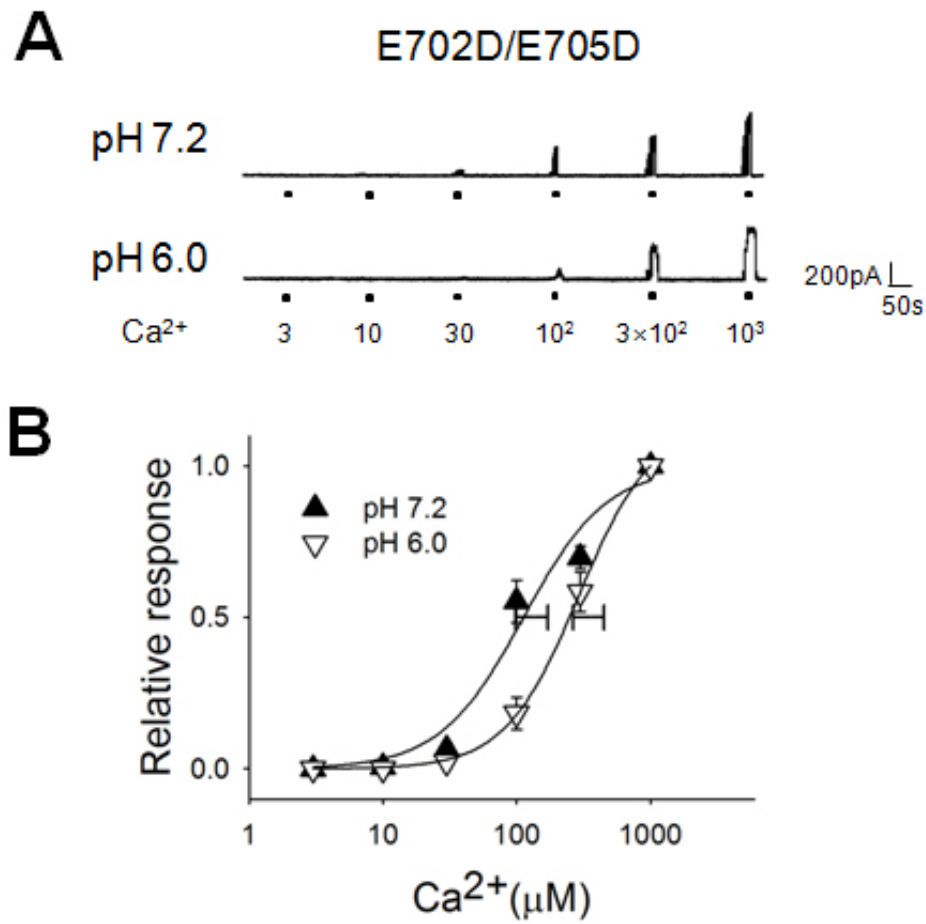

Fig. 26. The acid-mediated inhibition remains after the replacement of Glu residues into Asp residues at α7 helix.

(A) Example traces of E702D/E705D mutant at pH 7.2 and pH 6.0.

(B) The dose-response curves of Ca^{2+} in E702D/E705D mutant (n=6). Each current was normalized to the maximal current. EC_{50}s are shown with horizontal error bars.

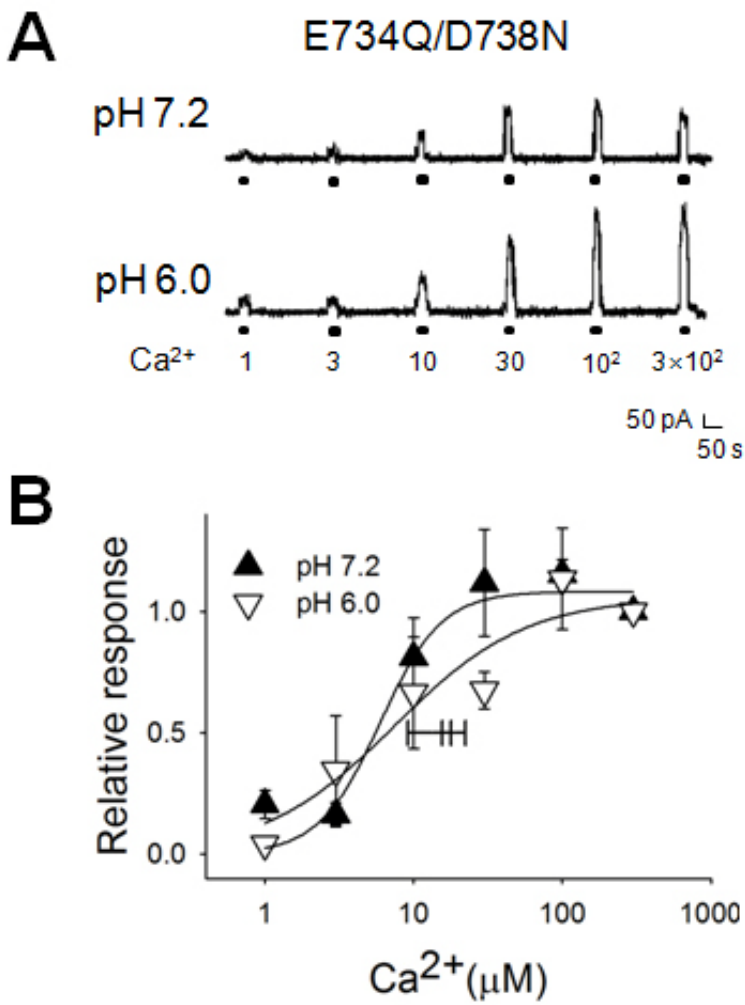

Fig. 27. Mutations on Glu and Asp residues at α8 helix diminish the acid-mediated inhibition.

(A) Single-channel current traces of E734Q/D738N mutant at pH 7.2 and pH 6.0.

(B) The dose-response curves of Ca^{2+} in activating E734Q/D738N mutant (n=8-9). Each current was normalized to the maximal current. EC_{50}s are shown with horizontal error bars.

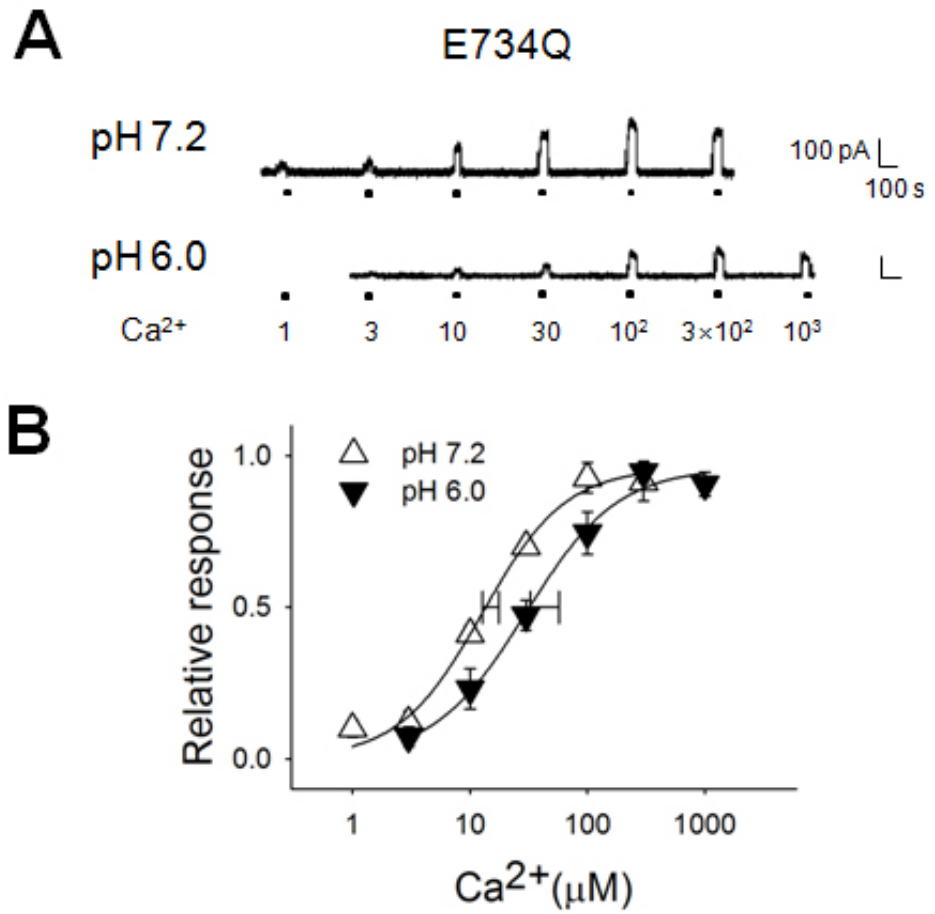

Fig. 28. A Glu residue at α8 helix is insufficient to sense intracellular acid.

(A) Representative traces of E734Q mutant at pH 7.2 and pH 6.0.

(B) The dose-response curves of Ca^{2+} in E734Q mutant (n=7). Each current was normalized to the maximal response. Horizontal error bars represent EC_{50}s.

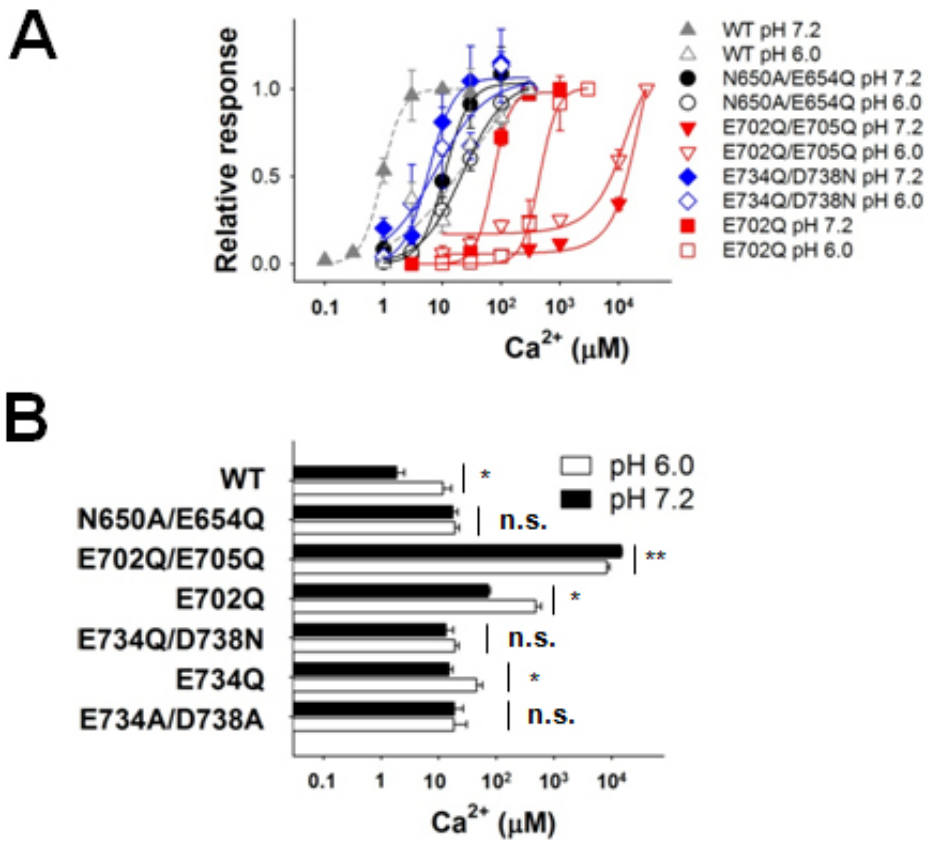

Fig. 29. Glu, Asp and Asn residues in the Ca^{2+} binding site are involved in the acid-mediated ANO1 inhibition.

(A) The dose-response curves of Ca^{2+} in activating WT (▲, △, n=6-10), N650A/E654Q (●, ○, n=5-6), E702Q/E705Q (▼, ▽, n=5-6), E702Q (■, □, n=5-6) and E734Q/D738N (◆, ◇, n=8-9) mutants at pH 7.2 (closed) or pH 6.0 (open).

(B) Summary of the EC_{50}s of WT, N650A/E654Q, E702Q/E705Q, E702Q, E734Q/D738N, E734Q and E734A/D738A mutants. *p<0.05 compared to the EC_{50} at pH 7.2. Student's unpaired two-tailed t-test.

6. Reference helix is not responsible to sense intracellular acid.

We previously reported that the gating of ANO1 is modulated by movement of the reference helix (Lee et al., 2014b). The reference helix is composed of positive charged amino-acids, Lys or Arg. As shown in the model structure of mouse ANO1, it is located between α6 and α7 helix (Fig. 30). It was imagined that Ca^{2+} pushes the reference helix away because both are positive-charged. The entrance for Ca^{2+} might be exposed by repelling the reference helix. The Ca^{2+} sensitivity was slightly decreased in the mutant on the reference helix (K659Q/K661Q/K662Q). The EC_{50} of in activating K659Q/K661Q/K662Q mutant at pH 7.2 was 9.3 ± 1.7 μM (n=10) (Fig. 31). To observe whether the acid-mediated inhibition of the mutant remains or not, the current was measured at pH 6.0. The dose-response curve of K659Q/K661Q/K662Q mutant at pH 6.0 exhibited the rightward shift, similar to WT (58.2 ± 29.5 μM, n=5) (Fig. 31). Therefore, we proposed that the disrupted reference helix does not affect the acid-mediated inhibition, whereas it affects the Ca^{2+}-mediated gating.

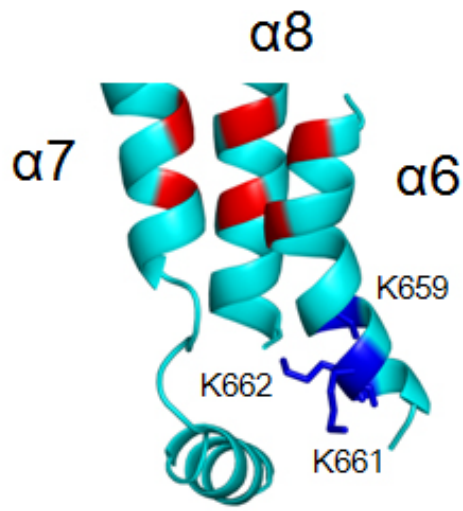

Fig. 30. Location of the reference helix in the mouse ANO1 model structure

The model structure was edited to present the reference helix, colored in blue. It was located between α6 and α7 helix. It contains basic amino-acids, K659, K661 and K662.

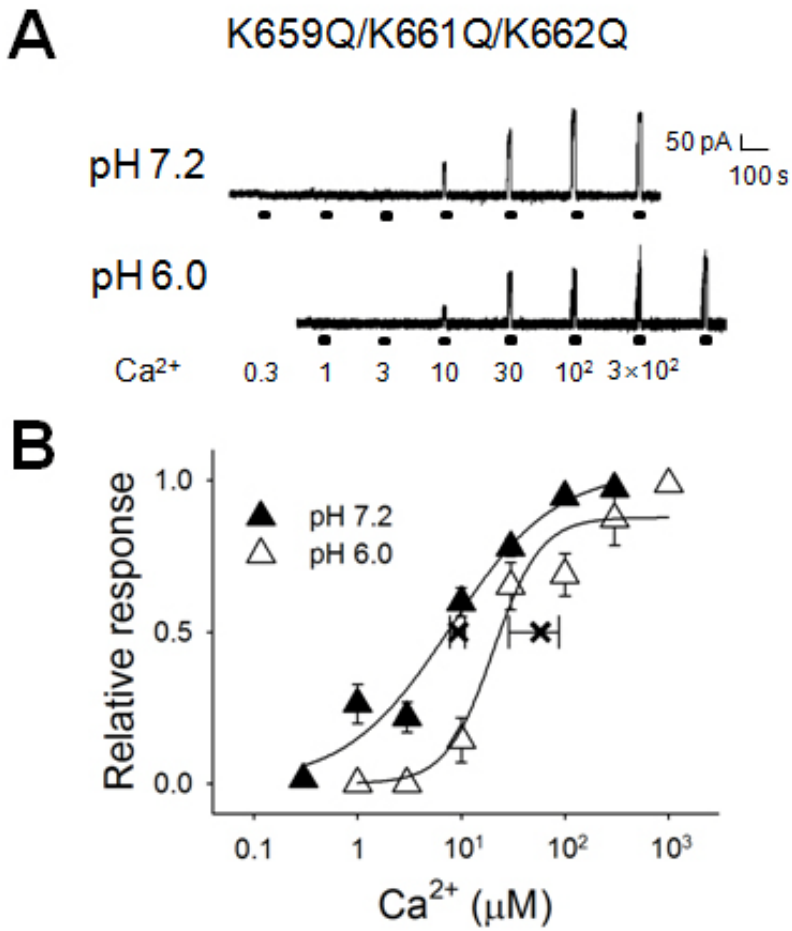

Fig. 31. Mutations on the reference helix fail to eliminate the acid-mediated ANO1 inhibition.

(A) Current traces of K659Q/K661Q/K662Q mutant at pH 7.2 and pH6.0.

(B) The dose-response curves of Ca^{2+} in activating K659Q/K661Q/K662Q mutant (n=5-10). Relative response was obtained by dividing each current to maximal current. Horizontal error bars with × represent EC_{50}s.

7. Acid inhibits the E_{act}-activated ANO1 currents.

E_{act} was designed and synthesized as an activator of ANO1 (Namkung et al., 2011b). It was suggested that E_{act} binds to the Ca^{2+} binding site to activate ANO1 (Lee et al., 2014b). The treatment of 1 μM E_{act} in inside-out patches evoked large, robust inward currents at pH 7.2 in HEK293T cells expressing mouse ANO1. The repeated application induced remarkable desensitization (Fig. 32A). Although the current was completely blocked at pH 6.0, the acid-mediated ANO1 inhibition was indistinct because of the desensitization (Fig. 32B). We applied 10 nM E_{act} to the patches of mouse ANO1 expressed HEK293T cells. 10 nM E_{act} was sufficient to activate the channel. The desensitization still remained, but it was alleviated (Fig. 33A, B). Therefore, we tested again whether E_{act}-activated current is inhibited by intracellular acid or not using 10 nM E_{act}. 10 nM E_{act} in pH 6.0 failed to evoke the current. The current was completely blocked (Fig. 33A, B). Thus, these results further support that intracellular protons act on and compete with Ca^{2+} at the Ca^{2+} binding site of ANO1.

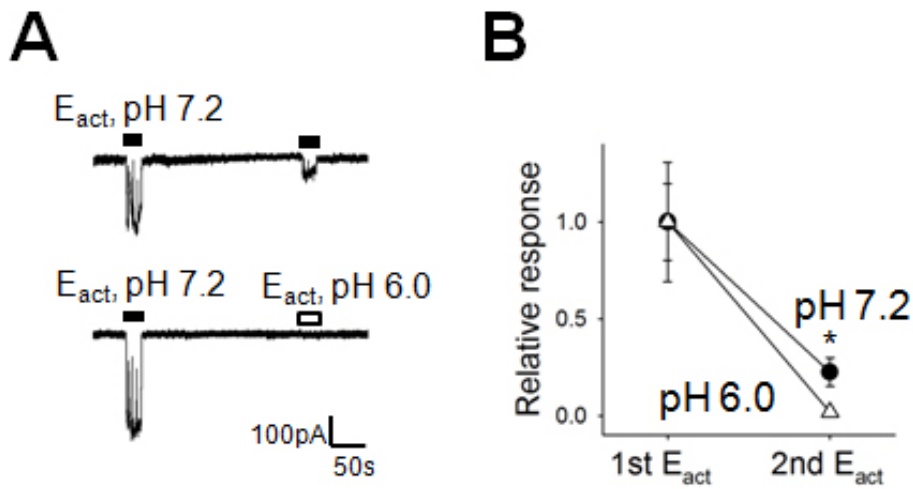

Fig. 32. 1 μM E_{act}-activated ANO1 currents are also inhibited by intracellular acid.

(A) Example traces of single-channel currents of ANO1 elicited by 1 μM E_{act} at pH 7.2 or pH 6.0. E_{hold} = -80 mV.

(B) Summary of the normalized current of ANO1 elicited by 1 μM E_{act} at pH 7.2 or pH 6.0. *p<0.05, Student's unpaired two-tailed t-test.

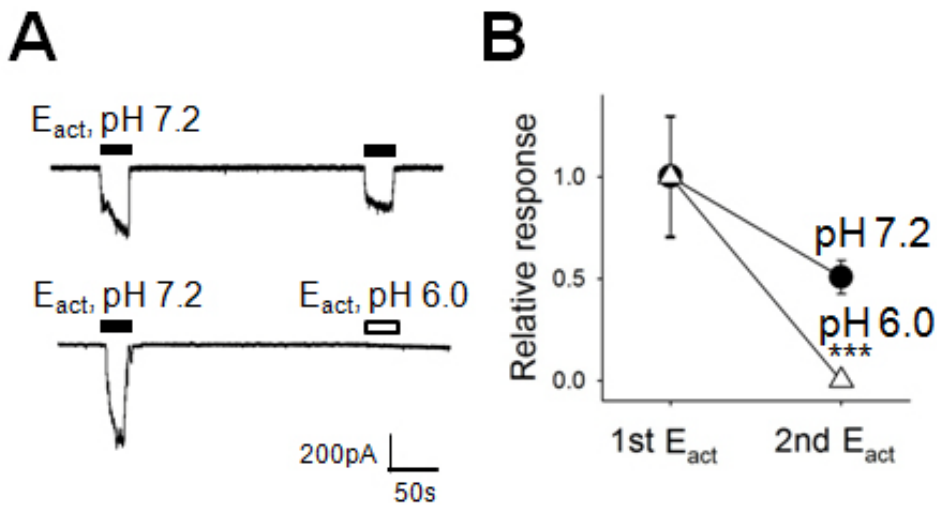

Fig. 33. ANO1 currents are not evoked by 10 nM E_{act} at acidic solution.

(A) Example traces of single-channel currents of ANO1 elicited by 10 nM E_{act} at pH 7.2 or pH 6.0. E_{hold} = -80 mV.

(B) Summary of the relative responses of ANO1 activated by 10 nM E_{act} at pH 7.2 or pH 6.0. ***p<0.001

Discussion

The present study demonstrates that intracellular acid inhibited the Ca^{2+}-activated ANO1 and ANO2. Ca^{2+} applications to the inside-out patches directly activated ANO1 and ANO2. The ANO1 and ANO2 activation was strongly inhibited by intracellular acid, whereas alkaline intracellular pH slightly affected. However, intracellular acid fails to inhibit the Ca^{2+}-independent ANO1 activation. The voltage-evoked and the heat-evoked ANO1 current are not inhibited by intracellular acid. Indeed, site-directed mutagenesis study revealed that the Ca^{2+} binding residues, located at α6, α7 and α8 helix respectively (N650, E654, E702, E705, E734, and D738), are the primary determinant of the acid-mediated ANO1 inhibition (Yu et al., 2012; Brunner et al., 2014; Tien et al., 2014). Intracellular acid inhibits the E_{act}-activated ANO1current. Because E_{act} is known to act on the Ca^{2+}-binding site, it is supported that protons might interrupt Ca^{2+} binding to the Ca^{2+}-binding site.

1. Intracellular acid-mediated modulations of ANOs.

ANO1 and ANO2 current were not elicited by Ca^{2+} when the intracellular solution was acidic. But in acid extracellular solution, ANO1 current was evoked by Ca^{2+} normally. Intracellular acid blocked the ANO1 and ANO2 activation. Although only ANO1 and ANO2 are accounted for CaCC, the

currents of other ANOs are evoked by higher intracellular Ca^{2+} at positive membrane potential. It is uncertain that other ANOs encode Cl^- channels.

The acid-mediated modulations of other ANOs were evaluated. As a result, the outward current of mouse ANO6 and human ANO7 were inhibited by intracellular acid, similar to ANO1 and ANO2. ANO6 also has scramblase activity. However, whether the scramblase activity was inhibited by intracellular acid was not assessed in this study. The relationship between the scramblase activity and acid are elusive. Thus, it is worth studied in further research.

However, mouse ANO9 was not affected by the intracellular acid. It might be different modulations on ANO9. In our present studies, the Ca^{2+} binding residues are critical for the acid-mediated ANO1 inhibition. Because the Ca^{2+} binding residues are conserved in ANOs, it is expected that other ANOs are inhibited by intracellular acid. The reason of acid-insensitivity in ANO9 is elusive. ANO9 also contains the conserved Ca^{2+} binding residues. But it is possible that the Ca^{2+} binding residues could not form the cavity-like structure presented in the *nh*TMEM crystal structure or the mouse ANO1 model structure. Another possibility is that ANO9 has other functions. The ANO9 current was recorded with NMDG-Cl solutions. The main carrier is Cl^-. However, ANO9 may not be an anion channel. Thus, the inhibition might be undetectable in the anion current. The observed ANO9 current was smaller than that of other ANOs. ANO9 might be a little permeable to Cl^-.

2. Mechanisms of acid-mediated ANO1 inhibition

Intracellular acid reduce the Ca^{2+} sensitivity of ANO1. The more Ca^{2+} was required to activate ANO1 in the acid solution. A slight change of pH completely inhibited ANO1. Interestingly, the more protons were required to inhibit the ANO1 current activated by the more Ca^{2+}. It is suggested that protons act on the same site of Ca^{2+} to reduce the Ca^{2+} sensitivity. Intracellular acid inhibit the Ca^{2+}-mediated ANO1 activation.

However, intracellular acid failed to inhibit the voltage-induced and heat-induced ANO1 activation. In the presence of Ca^{2+}, the ANO1 conductance was inhibited by the intracellular acid, but voltage-dependent properties were remained. The voltage-activated ANO1 current without Ca^{2+} was not inhibited by intracellular acid. Moreover, heat-evoked ANO1 current was not inhibited by intracellular acid. ANO1 is activated by heat without Ca^{2+} and the ANO1 mutant of Ca^{2+}-binding sites is activated by heat. Thus, heat-mediated ANO1 activation is different to Ca^{2+}-mediated activation. According to these results, intracellular acid does not affect the Ca^{2+}-independent ANO1 activation.

2.1. Critical residues for acid-mediated ANO1 inhibition

To investigate which residues are essential for the acid-induced inhibition, the mutation studies were performed. In several channels modulated by the intracellular pH such as ROMK1 or HCN2 channels, His residue is critical

for sensing the intracellular protons (Chanchevalap et al., 2000; Zong et al., 2001). Unlike these channels, all His residues of ANO1 are not involved in the acid-mediated ANO1 inhibition. In addition, Glu residues of TRPV1 are essential for the acid-mediated TRPV1 potentiation (Jordt et al., 2000) and Asp residues of ASIC channels plays the acid-sensing roles (Ishikita, 2011). However, Δ5E and mutations on ED-rich region failed to modulate the acid-mediated ANO1 inhibition. Recently, it was reported that residues with opposite charges between two helices plays important roles in the channel gating (Lee et al., 2014b). However, the mutant with substitutions on the helix showed the acid-mediated inhibition, whereas the Ca^{2+} sensitivity was slightly decreased. Thus, we noticed that the intracellular acid affects the Ca^{2+} binding directly, without altering the helix movement. Intracellular protons might be non-allosteric inhibitors.

Interestingly, acid-induced ANO1 inhibition was disappeared in ANO1 mutants of Ca^{2+}-binding sites. Although they represented decrease of the Ca^{2+} sensitivity, intracellular acid failed to decrease the Ca^{2+} sensitivity more. Double mutations on the Ca^{2+}-binding sites diminished the acid-induced inhibition. But single mutation on the Ca^{2+}-binding sites did not affect the acid-induced inhibition. From these results, intracellular protons act on the Ca^{2+}-binding site to inhibit the Ca^{2+}-induced activation. Protons might compete with the Ca^{2+} or modify the electrostatic environment and the structure of the Ca^{2+}-binding site. Because Ca^{2+} and proton are positive charged ions, they might compete on the binding site in the case of

sarcoplasmic reticulum ATPase (Inesi and Hill, 1983). However, to confirm the hypothesis that proton interfere Ca^{2+} binding to its site is experimentally difficult. There is also a possibility of modifying the microenvironment and the structure near the Ca^{2+}-binding site.

2.2. Supporting evidences

It was proposed that proton inhibit ANO1 current acting on the Ca^{2+}-binding site through the mutation studies. Note that the IC_{50} of ANO1 depended on Ca^{2+} concentration in activating. It supports that proton and Ca^{2+} might bind to the same site. Those two ions might compete with each other to bind its site. High concentration of protons might interfere with Ca^{2+} binding to its site.

It is generally considered that the activators of CaCC may be useful for the cure of the pathological symptoms in cystic fibrosis. Thus, E_{act} was designed and synthesized as an activator of ANO1. E_{act} acts on the two of Ca^{2+}-binding residues, E702 and E705. In this study, the intracellular acid inhibits the E_{act}-mediated ANO1 activation. This result supports our hypothesis that the Ca^{2+}-binding sites are involved in the intracellular acid-mediated ANO1 inhibition.

Extracellular acid failed to inhibit ANO1 activation. Inhibition was occurred by acid application at the intracellular side. It is consistent with the observation that the Ca^{2+} application is effective to evoke the ANO1 current. Moreover, intracellular acid reduces channel open probability of CaCCs but

not the single-channel current amplitude (Arreola et al., 1995). It supports our hypothesis that protons inhibit the Ca^{2+} binding in the competitive manner.

In addition, the Ca^{2+}-independent activation, heat- and voltage-mediated ANO1 activation was not inhibited by intracellular acid. Heat and voltage activates ANO1 without Ca^{2+}. Heat- and voltage-mediated ANO1 activation might have the different mechanism to open the channel. Thus, it is evidence for supporting our hypothesis.

3. Desensitization influences

In our study, the ANO1 current presented a consistent 30-35% current rundown (desensitization) at the repetitive application of Ca^{2+}. The property might negatively affect to obtain EC_{50}s. But in some mutants, rundown was not observed. Even though there was no rundown, the acid-mediated inhibition was present. Thus, two processes might be different. It is possible that intracellular acid greatly enhance the rundown. However, we failed to take the rundown into account in determining the EC_{50}s and IC_{50}s. For this weakness, lower EC_{50}s and higher IC_{50}s might be obtained in our results.

4. Crosslights on intracellular-mediated ANO1 modulation

Contrast to our result, it was suggested recently that ANO1 is activated by the intracellular acid in renal tubular cells (Faria et al., 2014). ANO1

currents was increased in pH 6.5 by the application of carbonyl cyanide 3-chlorophenylhydrazone (CCCP), the protonophore. Because the conductance of protonophore and H^+ ATPase were not ruled out in their experiments, our data which were observed directly in the excised patch might be more convincing. Moreover, the inhibition of ANO1 is consistent with the result of endogenous calcium activated chloride current (Arreola et al., 1995).

5. Pathophysiological implications

The physiological implication of the acid-mediated ANO1 inhibition is clearly not understood. However, we could expect the physiological implication of this regulatory properties, Fluid secretion is largely dependent on Cl^- efflux through CaCC or CFTR. And HCO_3^- is abundant anions in epithelial cells. It is also involved in the fluid secretion. Moreover, it serves as a pH buffer in cells (Fig. 34A). The increase of Ca^{2+} through the physiological signals induces the intracellular acidosis. When the sympathetic nervous system was excited, acetylcholine, an agonist of muscarinic receptor, was released. Acetylcholine increases the intracellular Ca^{2+} thorough GPCR pathway. The increase of Ca^{2+} induces an acidification in acinar cells (Lee et al., 2012). It might be caused by HCO_3^- efflux. ANO1 is also permeable to HCO_3^-. The ANO1 activation permits the acidification of cells (Fig. 34B). The severe acidification is harmful to cell viability. Thus, the acid-mediated inhibition of ANO1 would be a feedback

mechanism that prevents the excessive HCO_3^- efflux (Fig. 34C).

According to several studies, decline of intracellular pH is observed during ischemia at heart and brain. Insufficiency of glucose and oxygen increases anaerobic metabolism and then leads to acidosis. Intracellular pH is decreased to near pH 6.4 (Steenbergen et al., 1977; Mabe et al., 1983). This pH value is adequate to inhibit ANO1 activation. Thus, it may be related to intracellular pH homeostasis in pathological condition. The fact that the elevation of intracellular calcium is observed in hippocampus neurons during anoxia could support our hypothesis (Diarra et al., 1999). ANO1 expression is increased in cardiac vascular endothelial cells at the chronic hypoxia (Sun et al., 2012; Wu et al., 2014). The increase of this channel might protect from chronic acidosis of hypoxia and then the cells could maintain their vasocontractility.

In summary, this study demonstrates the intracellular acid-mediated modulations of ANOs and the molecular basis of the inhibition. Defining the regulatory properties in ANO1 and determination of the structure-function relationship by site-directed mutation analysis may contribute to the advance of our knowledge in ANO1 gating mechanisms. It might aid to develop the anti-cystic fibrosis drugs.

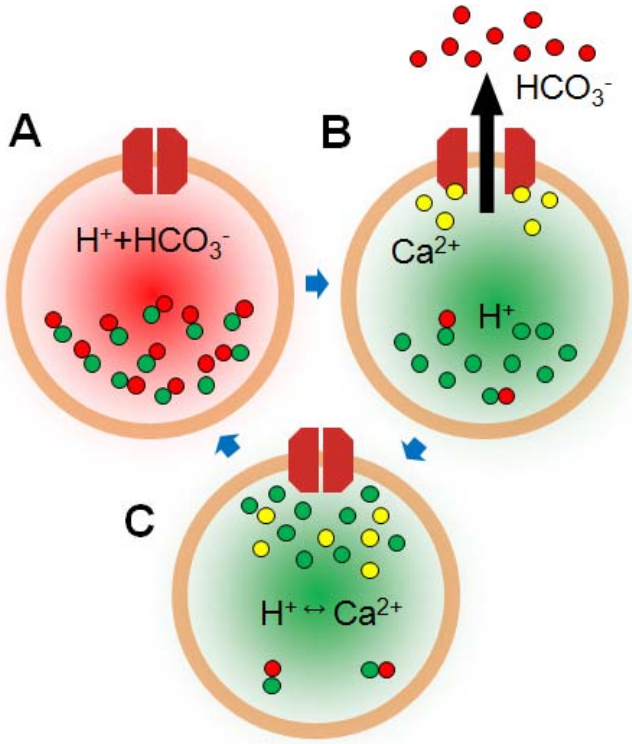

Fig. 34. Acid-mediated ANO1 inhibition might be important to maintain adequate pH in epithelial cells.

(A-C) The scheme of acid-mediated ANO1 inhibition in cell (A) Cytosol is buffered with H^+ (●) and HCO_3^- (●) at the resting state. Intracellular pH is about pH 7.2, represented with red. (B) Increase of intracellular Ca^{2+} (●) activates ANO1. The efflux of HCO_3^- (●) is occurred. Because H^+ (●) are remained in the cell, cytosol becomes acidic. Acidic cytosol is represented with green. (C) However, the channel is closed because H^+ hinders binding Ca^{2+} to its site. Therefore, the cell reverts to (A).

Reference

Al-Nakkash L, Iserovich P, Coca-Prados M, Yang H, Reinach PS (2004) Functional and molecular characterization of a volume-activated chloride channel in rabbit corneal epithelial cells. J Membr Biol 201:41-49.

Ameen NA, Ardito T, Kashgarian M, Marino CR (1995) A unique subset of rat and human intestinal villus cells express the cystic fibrosis transmembrane conductance regulator. Gastroenterology 108:1016-1023.

Anderson MP, Welsh MJ (1991) Calcium and cAMP activate different chloride channels in the apical membrane of normal and cystic fibrosis epithelia. Proc Natl Acad Sci U S A 88:6003-6007.

Arreola J, Melvin JE, Begenisich T (1995) Inhibition of Ca(2+)-dependent Cl- channels from secretory epithelial cells by low internal pH. J Membr Biol 147:95-104.

Arreola J, Melvin JE, Begenisich T (1996) Activation of calcium-dependent chloride channels in rat parotid acinar cells. J Gen Physiol 108:35-47.

Arreola J, Melvin JE, Begenisich T (1998) Differences in regulation of Ca(2+)-activated Cl- channels in colonic and parotid secretory cells. Am J Physiol 274:C161-166.

Ashton N, Argent BE, Green R (1991) Characteristics of fluid secretion from isolated rat pancreatic ducts stimulated with secretin and bombesin. J Physiol 435:533-546.

Ashton N, Evans RL, Elliott AC, Green R, Argent BE (1993) Regulation of fluid secretion and intracellular messengers in isolated rat pancreatic ducts by acetylcholine. J Physiol 471:549-562.

Barish ME (1983) A transient calcium-dependent chloride current in the immature Xenopus oocyte. J Physiol 342:309-325.

Barker JL, Ransom BR (1978) Amino acid pharmacology of mammalian central neurones grown in tissue culture. J Physiol 280:331-354.

Barnes S (1994) After transduction: response shaping and control of transmission by ion channels of the photoreceptor inner segments. Neuroscience 58:447-459.

Barrett KE, Keely SJ (2000) Chloride secretion by the intestinal epithelium:

molecular basis and regulatory aspects. Annu Rev Physiol 62:535-572.

Begenisich T, Melvin JE (1998) Regulation of chloride channels in secretory epithelia. J Membr Biol 163:77-85.

Billig GM, Pal B, Fidzinski P, Jentsch TJ (2011) Ca2+-activated Cl- currents are dispensable for olfaction. Nat Neurosci 14:763-769.

Bolton TB (1979) Mechanisms of action of transmitters and other substances on smooth muscle. Physiol Rev 59:606-718.

Boucher RC (1994) Human airway ion transport. Part one. Am J Respir Crit Care Med 150:271-281.

Britschgi A et al. (2013) Calcium-activated chloride channel ANO1 promotes breast cancer progression by activating EGFR and CAMK signaling. Proc Natl Acad Sci U S A 110:E1026-1034.

Brunner JD, Lim NK, Schenck S, Duerst A, Dutzler R (2014) X-ray structure of a calcium-activated TMEM16 lipid scramblase. Nature 516:207-212.

Byrne NG, Large WA (1985) Evidence for two mechanisms of depolarization associated with alpha 1-adrenoceptor activation in the rat anococcygeus muscle. Br J Pharmacol 86:711-721.

Caputo A, Caci E, Ferrera L, Pedemonte N, Barsanti C, Sondo E, Pfeffer U, Ravazzolo R, Zegarra-Moran O, Galietta LJ (2008) TMEM16A, a membrane protein associated with calcium-dependent chloride channel activity. Science 322:590-594.

Carew MA, Yang X, Schultz C, Shears SB (2000) myo-inositol 3,4,5,6-tetrakisphosphate inhibits an apical calcium-activated chloride conductance in polarized monolayers of a cystic fibrosis cell line. J Biol Chem 275:26906-26913.

Carmines PK (1995) Segment-specific effect of chloride channel blockade on rat renal arteriolar contractile responses to angiotensin II. Am J Hypertens 8:90-94.

Catalan M, Niemeyer MI, Cid LP, Sepulveda FV (2004) Basolateral ClC-2 chloride channels in surface colon epithelium: regulation by a direct effect of intracellular chloride. Gastroenterology 126:1104-1114.

Chambers LA, Rollins BM, Tarran R (2007) Liquid movement across the surface epithelium of large airways. Respir Physiol Neurobiol 159:256-270.

Chan HC, Kaetzel MA, Gotter AL, Dedman JR, Nelson DJ (1994) Annexin IV

inhibits calmodulin-dependent protein kinase II-activated chloride conductance. A novel mechanism for ion channel regulation. J Biol Chem 269:32464-32468.

Chanchevalap S, Yang Z, Cui N, Qu Z, Zhu G, Liu C, Giwa LR, Abdulkadir L, Jiang C (2000) Involvement of histidine residues in proton sensing of ROMK1 channel. J Biol Chem 275:7811-7817.

Chipperfield AR, Harper AA (2000) Chloride in smooth muscle. Prog Biophys Mol Biol 74:175-221.

Chmiel JF, Davis PB (2003) State of the art: why do the lungs of patients with cystic fibrosis become infected and why can't they clear the infection? Respir Res 4:8.

Cho H, Yang YD, Lee J, Lee B, Kim T, Jang Y, Back SK, Na HS, Harfe BD, Wang F, Raouf R, Wood JN, Oh U (2012) The calcium-activated chloride channel anoctamin 1 acts as a heat sensor in nociceptive neurons. Nat Neurosci 15:1015-1021.

Clarke LL, Boucher RC (1992) Chloride secretory response to extracellular ATP in human normal and cystic fibrosis nasal epithelia. Am J Physiol 263:C348-356.

Cohn JA, Friedman KJ, Noone PG, Knowles MR, Silverman LM, Jowell PS (1998) Relation between mutations of the cystic fibrosis gene and idiopathic pancreatitis. N Engl J Med 339:653-658.

Colledge WH, Abella BS, Southern KW, Ratcliff R, Jiang C, Cheng SH, MacVinish LJ, Anderson JR, Cuthbert AW, Evans MJ (1995) Generation and characterization of a delta F508 cystic fibrosis mouse model. Nat Genet 10:445-452.

Cook DI, Day ML, Champion MP, Young JA (1988) Ca2+ not cyclic AMP mediates the fluid secretory response to isoproterenol in the rat mandibular salivary gland: whole-cell patch-clamp studies. Pflugers Arch 413:67-76.

Cooke HJ (1994) Neuroimmune signaling in regulation of intestinal ion transport. Am J Physiol 266:G167-178.

Cressman VL, Lazarowski E, Homolya L, Boucher RC, Koller BH, Grubb BR (1999) Effect of loss of P2Y(2) receptor gene expression on nucleotide regulation of murine epithelial Cl(-) transport. J Biol Chem 274:26461-26468.

Criddle DN, de Moura RS, Greenwood IA, Large WA (1996) Effect of niflumic acid on noradrenaline-induced contractions of the rat aorta. Br J Pharmacol 118:1065-1071.

Dalton S, Gerzanich V, Chen M, Dong Y, Shuba Y, Simard JM (2003) Chlorotoxin-sensitive Ca2+-activated Cl- channel in type R2 reactive astrocytes from adult rat brain. Glia 42:325-339.

Dartt DA (2002) Regulation of mucin and fluid secretion by conjunctival epithelial cells. Prog Retin Eye Res 21:555-576.

Davis MJ, Hill MA (1999) Signaling mechanisms underlying the vascular myogenic response. Physiol Rev 79:387-423.

Delay RJ, Dubin AE, Dionne VE (1997) A cyclic nucleotide-dependent chloride conductance in olfactory receptor neurons. J Membr Biol 159:53-60.

Denning GM, Ostedgaard LS, Cheng SH, Smith AE, Welsh MJ (1992) Localization of cystic fibrosis transmembrane conductance regulator in chloride secretory epithelia. J Clin Invest 89:339-349.

Deschenes M, Feltz P, Lamour Y (1976) A model for an estimate in vivo of the ionic basis of presynaptic inhibition: an intracellular analysis of the GABA-induced depolarization in rat dorsal root ganglia. Brain Res 118:486-493.

Devor DC, Pilewski JM (1999) UTP inhibits Na+ absorption in wild-type and DeltaF508 CFTR-expressing human bronchial epithelia. Am J Physiol 276:C827-837.

Diarra A, Sheldon C, Brett CL, Baimbridge KG, Church J (1999) Anoxia-evoked intracellular pH and Ca2+ concentration changes in cultured postnatal rat hippocampal neurons. Neuroscience 93:1003-1016.

Doughty JM, Miller AL, Langton PD (1998) Non-specificity of chloride channel blockers in rat cerebral arteries: block of the L-type calcium channel. J Physiol 507 (Pt 2):433-439.

Duchen MR (1990) Effects of metabolic inhibition on the membrane properties of isolated mouse primary sensory neurones. J Physiol 424:387-409.

Duvvuri U, Shiwarski DJ, Xiao D, Bertrand C, Huang X, Edinger RS, Rock JR, Harfe BD, Henson BJ, Kunzelmann K, Schreiber R, Seethala RS, Egloff AM, Chen X, Lui VW, Grandis JR, Gollin SM (2012) TMEM16A induces MAPK and contributes directly to tumorigenesis and cancer progression. Cancer

Res 72:3270-3281.

Evans MG, Marty A (1986) Calcium-dependent chloride currents in isolated cells from rat lacrimal glands. J Physiol 378:437-460.

Fallah G, Romer T, Detro-Dassen S, Braam U, Markwardt F, Schmalzing G (2011) TMEM16A(a)/anoctamin-1 shares a homodimeric architecture with CLC chloride channels. Mol Cell Proteomics 10:M110 004697.

Faria D, Rock JR, Romao AM, Schweda F, Bandulik S, Witzgall R, Schlatter E, Heitzmann D, Pavenstadt H, Herrmann E, Kunzelmann K, Schreiber R (2014) The calcium-activated chloride channel Anoctamin 1 contributes to the regulation of renal function. Kidney Int 85:1369-1381.

Farinas J, Kneen M, Moore M, Verkman AS (1997) Plasma membrane water permeability of cultured cells and epithelia measured by light microscopy with spatial filtering. J Gen Physiol 110:283-296.

Foskett JK (1990) [Ca2+]i modulation of Cl- content controls cell volume in single salivary acinar cells during fluid secretion. Am J Physiol 259:C998-1004.

Frings S, Reuter D, Kleene SJ (2000) Neuronal Ca2+ -activated Cl- channels--homing in on an elusive channel species. Prog Neurobiol 60:247-289.

Frizzell RA, Rechkemmer G, Shoemaker RL (1986) Altered regulation of airway epithelial cell chloride channels in cystic fibrosis. Science 233:558-560.

Fujikawa-Adachi K, Nishimori I, Sakamoto S, Morita M, Onishi S, Yonezawa S, Hollingsworth MA (1999) Identification of carbonic anhydrase IV and VI mRNA expression in human pancreas and salivary glands. Pancreas 18:329-335.

Gibson RL, Burns JL, Ramsey BW (2003) Pathophysiology and management of pulmonary infections in cystic fibrosis. Am J Respir Crit Care Med 168:918-951.

Greenwood IA, Large WA (1995) Comparison of the effects of fenamates on Ca-activated chloride and potassium currents in rabbit portal vein smooth muscle cells. Br J Pharmacol 116:2939-2948.

Grubb BR, Vick RN, Boucher RC (1994) Hyperabsorption of Na+ and raised Ca(2+)-mediated Cl- secretion in nasal epithelia of CF mice. Am J Physiol 266:C1478-1483.

Grubb S, Poulsen KA, Juul CA, Kyed T, Klausen TK, Larsen EH, Hoffmann EK

(2013) TMEM16F (Anoctamin 6), an anion channel of delayed Ca(2+) activation. J Gen Physiol 141:585-600.

Hartzell C, Putzier I, Arreola J (2005) Calcium-activated chloride channels. Annu Rev Physiol 67:719-758.

Hazama A, Shimizu T, Ando-Akatsuka Y, Hayashi S, Tanaka S, Maeno E, Okada Y (1999) Swelling-induced, CFTR-independent ATP release from a human epithelial cell line: lack of correlation with volume-sensitive cl(-) channels. J Gen Physiol 114:525-533.

Heinze C, Seniuk A, Sokolov MV, Huebner AK, Klementowicz AE, Szijarto IA, Schleifenbaum J, Vitzthum H, Gollasch M, Ehmke H, Schroeder BC, Hubner CA (2014) Disruption of vascular Ca2+-activated chloride currents lowers blood pressure. J Clin Invest 124:675-686.

Herness MS, Sun XD (1999) Characterization of chloride currents and their noradrenergic modulation in rat taste receptor cells. J Neurophysiol 82:260-271.

Hiraoka M, Kawano S, Hirano Y, Furukawa T (1998) Role of cardiac chloride currents in changes in action potential characteristics and arrhythmias. Cardiovasc Res 40:23-33.

Hogan DL, Ainsworth MA, Isenberg JI (1994) Review article: gastroduodenal bicarbonate secretion. Aliment Pharmacol Ther 8:475-488.

Hogan DL, Crombie DL, Isenberg JI, Svendsen P, Schaffalitzky de Muckadell OB, Ainsworth MA (1997) CFTR mediates cAMP- and Ca2+-activated duodenal epithelial HCO3- secretion. Am J Physiol 272:G872-878.

Hosoya K, Ueda H, Kim KJ, Lee VH (1999) Nucleotide stimulation of Cl(-) secretion in the pigmented rabbit conjunctiva. J Pharmacol Exp Ther 291:53-59.

Huang F, Wang X, Ostertag EM, Nuwal T, Huang B, Jan YN, Basbaum AI, Jan LY (2013) TMEM16C facilitates Na(+)-activated K+ currents in rat sensory neurons and regulates pain processing. Nat Neurosci 16:1284-1290.

Huang F, Zhang H, Wu M, Yang H, Kudo M, Peters CJ, Woodruff PG, Solberg OD, Donne ML, Huang X, Sheppard D, Fahy JV, Wolters PJ, Hogan BL, Finkbeiner WE, Li M, Jan YN, Jan LY, Rock JR (2012a) Calcium-activated chloride channel TMEM16A modulates mucin secretion and airway smooth muscle contraction. Proc Natl Acad Sci U S A 109:16354-16359.

Huang WC, Xiao S, Huang F, Harfe BD, Jan YN, Jan LY (2012b) Calcium-activated chloride channels (CaCCs) regulate action potential and synaptic response in hippocampal neurons. Neuron 74:179-192.

Huang X, Godfrey TE, Gooding WE, McCarty KS, Jr., Gollin SM (2006) Comprehensive genome and transcriptome analysis of the 11q13 amplicon in human oral cancer and synteny to the 7F5 amplicon in murine oral carcinoma. Genes Chromosomes Cancer 45:1058-1069.

Hussy N (1992) Calcium-activated chloride channels in cultured embryonic Xenopus spinal neurons. J Neurophysiol 68:2042-2050.

Ianowski JP, Choi JY, Wine JJ, Hanrahan JW (2007) Mucus secretion by single tracheal submucosal glands from normal and cystic fibrosis transmembrane conductance regulator knockout mice. J Physiol 580:301-314.

Inesi G, Hill TL (1983) Calcium and proton dependence of sarcoplasmic reticulum ATPase. Biophys J 44:271-280.

Ishiguro H, Steward MC, Naruse S, Ko SB, Goto H, Case RM, Kondo T, Yamamoto A (2009) CFTR functions as a bicarbonate channel in pancreatic duct cells. J Gen Physiol 133:315-326.

Ishikita H (2011) Proton-binding sites of acid-sensing ion channel 1. PLoS One 6:e16920.

Jang Y, Oh U (2014) Anoctamin 1 in secretory epithelia. Cell Calcium 55:355-361.

January CT, Fozzard HA (1988) Delayed afterdepolarizations in heart muscle: mechanisms and relevance. Pharmacol Rev 40:219-227.

Jentsch TJ, Steinmeyer K, Schwarz G (1990) Primary structure of Torpedo marmorata chloride channel isolated by expression cloning in Xenopus oocytes. Nature 348:510-514.

Jentsch TJ, Stein V, Weinreich F, Zdebik AA (2002) Molecular structure and physiological function of chloride channels. Physiol Rev 82:503-568.

Jordt SE, Tominaga M, Julius D (2000) Acid potentiation of the capsaicin receptor determined by a key extracellular site. Proc Natl Acad Sci U S A 97:8134-8139.

Jung J, Nam JH, Park HW, Oh U, Yoon JH, Lee MG (2013) Dynamic modulation of ANO1/TMEM16A HCO3(-) permeability by Ca2+/calmodulin. Proc Natl Acad Sci U S A 110:360-365.

Kaetzel MA, Chan HC, Dubinsky WP, Dedman JR, Nelson DJ (1994) A role for annexin IV in epithelial cell function. Inhibition of calcium-activated chloride conductance. J Biol Chem 269:5297-5302.

Kleene SJ (1997) High-gain, low-noise amplification in olfactory transduction. Biophys J 73:1110-1117.

Kompella UB, Kim KJ, Shiue MH, Lee VH (1996) Cyclic AMP modulation of active ion transport in the pigmented rabbit conjunctiva. J Ocul Pharmacol Ther 12:281-287.

Koumi S, Sato R, Aramaki T (1994) Characterization of the calcium-activated chloride channel in isolated guinea-pig hepatocytes. J Gen Physiol 104:357-373.

Kuijpers GA, De Pont JJ (1987) Role of proton and bicarbonate transport in pancreatic cell function. Annu Rev Physiol 49:87-103.

Kuruma A, Hartzell HC (2000) Bimodal control of a Ca(2+)-activated Cl(-) channel by different Ca(2+) signals. J Gen Physiol 115:59-80.

Lamb FS, Barna TJ (1998) Chloride ion currents contribute functionally to norepinephrine-induced vascular contraction. Am J Physiol 275:H151-160.

Large WA (1984) The effect of chloride removal on the responses of the isolated rat anococcygeus muscle to alpha 1-adrenoceptor stimulation. J Physiol 352:17-29.

Large WA, Wang Q (1996) Characteristics and physiological role of the Ca(2+)-activated Cl- conductance in smooth muscle. Am J Physiol 271:C435-454.

Lazarowski ER, Boucher RC, Harden TK (2000) Constitutive release of ATP and evidence for major contribution of ecto-nucleotide pyrophosphatase and nucleoside diphosphokinase to extracellular nucleotide concentrations. J Biol Chem 275:31061-31068.

Lee B, Cho H, Jung J, Yang YD, Yang DJ, Oh U (2014a) Anoctamin 1 contributes to inflammatory and nerve-injury induced hypersensitivity. Mol Pain 10:5.

Lee J, Jung J, Tak MH, Wee J, Lee B, Jang Y, Chun H, Yang DJ, Yang YD, Park SH, Han BW, Hyun S, Yu J, Cho H, Hartzell HC, Oh U (2014b) Two helices in the third intracellular loop determine anoctamin 1 (TMEM16A) activation by calcium. Pflugers Arch.

Lee MG, Ohana E, Park HW, Yang D, Muallem S (2012) Molecular mechanism of

pancreatic and salivary gland fluid and HCO3 secretion. Physiol Rev 92:39-74.

Lee MG, Xu X, Zeng W, Diaz J, Wojcikiewicz RJ, Kuo TH, Wuytack F, Racymaekers L, Muallem S (1997) Polarized expression of Ca2+ channels in pancreatic and salivary gland cells. Correlation with initiation and propagation of [Ca2+]i waves. J Biol Chem 272:15765-15770.

Lipecka J, Bali M, Thomas A, Fanen P, Edelman A, Fritsch J (2002) Distribution of ClC-2 chloride channel in rat and human epithelial tissues. Am J Physiol Cell Physiol 282:C805-816.

Liu B, Linley JE, Du X, Zhang X, Ooi L, Zhang H, Gamper N (2010) The acute nociceptive signals induced by bradykinin in rat sensory neurons are mediated by inhibition of M-type K+ channels and activation of Ca2+-activated Cl- channels. J Clin Invest 120:1240-1252.

Lomax RB, Warhurst G, Sandle GI (1996) Characteristics of two basolateral potassium channel populations in human colonic crypts. Gut 38:243-247.

Lowe G, Gold GH (1993) Contribution of the ciliary cyclic nucleotide-gated conductance to olfactory transduction in the salamander. J Physiol 462:175-196.

Mabe H, Blomqvist P, Siesjo BK (1983) Intracellular pH in the brain following transient ischemia. J Cereb Blood Flow Metab 3:109-114.

Maertens C, Wei L, Droogmans G, Nilius B (2000a) Inhibition of volume-regulated and calcium-activated chloride channels by the antimalarial mefloquine. J Pharmacol Exp Ther 295:29-36.

Maertens C, Wei L, Voets T, Droogmans G, Nilius B (1999) Block by fluoxetine of volume-regulated anion channels. Br J Pharmacol 126:508-514.

Maertens C, Wei L, Tytgat J, Droogmans G, Nilius B (2000b) Chlorotoxin does not inhibit volume-regulated, calcium-activated and cyclic AMP-activated chloride channels. Br J Pharmacol 129:791-801.

Maricq AV, Korenbrot JI (1988) Calcium and calcium-dependent chloride currents generate action potentials in solitary cone photoreceptors. Neuron 1:503-515.

Marino CR, Matovcik LM, Gorelick FS, Cohn JA (1991) Localization of the cystic fibrosis transmembrane conductance regulator in pancreas. J Clin Invest 88:712-716.

Martinez-Pinna J, McLachlan EM, Gallego R (2000) Distinct mechanisms for activation of Cl- and K+ currents by Ca2+ from different sources in mouse sympathetic neurones. J Physiol 527 Pt 2:249-264.

Martins JR, Faria D, Kongsuphol P, Reisch B, Schreiber R, Kunzelmann K (2011) Anoctamin 6 is an essential component of the outwardly rectifying chloride channel. Proc Natl Acad Sci U S A 108:18168-18172.

Mayer ML (1985) A calcium-activated chloride current generates the after-depolarization of rat sensory neurones in culture. J Physiol 364:217-239.

McEwan GT, Hirst BH, Simmons NL (1994) Carbachol stimulates Cl- secretion via activation of two distinct apical Cl- pathways in cultured human T84 intestinal epithelial monolayers. Biochim Biophys Acta 1220:241-247.

McRoberts JA, Beuerlein G, Dharmsathaphorn K (1985) Cyclic AMP and Ca2+-activated K+ transport in a human colonic epithelial cell line. J Biol Chem 260:14163-14172.

Melvin JE, Moran A, Turner RJ (1988) The role of HCO3- and Na+/H+ exchange in the response of rat parotid acinar cells to muscarinic stimulation. J Biol Chem 263:19564-19569.

Melvin JE, Yule D, Shuttleworth T, Begenisich T (2005) Regulation of fluid and electrolyte secretion in salivary gland acinar cells. Annu Rev Physiol 67:445-469.

Morth JP, Pedersen BP, Buch-Pedersen MJ, Andersen JP, Vilsen B, Palmgren MG, Nissen P (2011) A structural overview of the plasma membrane Na+,K+-ATPase and H+-ATPase ion pumps. Nat Rev Mol Cell Biol 12:60-70.

Muallem S, Loessberg PA (1990) Intracellular pH-regulatory mechanisms in pancreatic acinar cells. II. Regulation of H+ and HCO3- transporters by Ca2(+)-mobilizing agonists. J Biol Chem 265:12813-12819.

Namkung W, Phuan PW, Verkman AS (2011a) TMEM16A inhibitors reveal TMEM16A as a minor component of calcium-activated chloride channel conductance in airway and intestinal epithelial cells. J Biol Chem 286:2365-2374.

Namkung W, Thiagarajah JR, Phuan PW, Verkman AS (2010) Inhibition of Ca2+-activated Cl- channels by gallotannins as a possible molecular basis for health benefits of red wine and green tea. FASEB J 24:4178-4186.

Namkung W, Yao Z, Finkbeiner WE, Verkman AS (2011b) Small-molecule

activators of TMEM16A, a calcium-activated chloride channel, stimulate epithelial chloride secretion and intestinal contraction. FASEB J 25:4048-4062.

Nauntofte B (1992) Regulation of electrolyte and fluid secretion in salivary acinar cells. Am J Physiol 263:G823-837.

Nguyen HV, Shull GE, Melvin JE (2000) Muscarinic receptor-induced acidification in sublingual mucous acinar cells: loss of pH recovery in Na+-H+ exchanger-1 deficient mice. J Physiol 523 Pt 1:139-146.

Nilius B, Prenen J, Szucs G, Wei L, Tanzi F, Voets T, Droogmans G (1997) Calcium-activated chloride channels in bovine pulmonary artery endothelial cells. J Physiol 498 (Pt 2):381-396.

Nilius B, Prenen J, Voets T, Eggermont J, Bruzik KS, Shears SB, Droogmans G (1998) Inhibition by inositoltetrakisphosphates of calcium- and volume-activated Cl- currents in macrovascular endothelial cells. Pflugers Arch 435:637-644.

Nishimoto I, Wagner JA, Schulman H, Gardner P (1991) Regulation of Cl- channels by multifunctional CaM kinase. Neuron 6:547-555.

Oh SJ, Hwang SJ, Jung J, Yu K, Kim J, Choi JY, Hartzell HC, Roh EJ, Lee CJ (2013) MONNA, a potent and selective blocker for transmembrane protein with unknown function 16/anoctamin-1. Mol Pharmacol 84:726-735.

Okada T, Horiguchi H, Tachibana M (1995) Ca(2+)-dependent Cl- current at the presynaptic terminals of goldfish retinal bipolar cells. Neurosci Res 23:297-303.

Owen DG, Segal M, Barker JL (1984) A Ca-dependent Cl- conductance in cultured mouse spinal neurones. Nature 311:567-570.

Pacaud P, Loirand G, Baron A, Mironneau C, Mironneau J (1991) Ca2+ channel activation and membrane depolarization mediated by Cl- channels in response to noradrenaline in vascular myocytes. Br J Pharmacol 104:1000-1006.

Papp Z, Sipido KR, Callewaert G, Carmeliet E (1995) Two components of [Ca2+]i-activated Cl- current during large [Ca2+]i transients in single rabbit heart Purkinje cells. J Physiol 483 (Pt 2):319-330.

Park K, Brown PD (1995) Intracellular pH modulates the activity of chloride channels in isolated lacrimal gland acinar cells. Am J Physiol 268:C647-

650.

Payne JA, Forbush B, 3rd (1995) Molecular characterization of the epithelial Na-K-Cl cotransporter isoforms. Curr Opin Cell Biol 7:493-503.

Perez-Cornejo P, Arreola J (2004) Regulation of Ca(2+)-activated chloride channels by cAMP and CFTR in parotid acinar cells. Biochem Biophys Res Commun 316:612-617.

Peters CJ, Yu H, Tien J, Jan YN, Li M, Jan LY (2015) Four basic residues critical for the ion selectivity and pore blocker sensitivity of TMEM16A calcium-activated chloride channels. Proc Natl Acad Sci U S A 112:3547-3552.

Petersen OH (1986) Calcium-activated potassium channels and fluid secretion by exocrine glands. Am J Physiol 251:G1-13.

Pifferi S, Dibattista M, Menini A (2009) TMEM16B induces chloride currents activated by calcium in mammalian cells. Pflugers Arch 458:1023-1038.

Pilewski JM, Frizzell RA (1999) Role of CFTR in airway disease. Physiol Rev 79:S215-255.

Piper AS, Greenwood IA, Large WA (2002) Dual effect of blocking agents on Ca2+-activated Cl(-) currents in rabbit pulmonary artery smooth muscle cells. J Physiol 539:119-131.

Pressley TA (1996) Structure and function of the Na,K pump: ten years of molecular biology. Miner Electrolyte Metab 22:264-271.

Qiu Z, Dubin AE, Mathur J, Tu B, Reddy K, Miraglia LJ, Reinhardt J, Orth AP, Patapoutian A (2014) SWELL1, a plasma membrane protein, is an essential component of volume-regulated anion channel. Cell 157:447-458.

Qu Z, Hartzell HC (2000) Anion permeation in Ca(2+)-activated Cl(-) channels. J Gen Physiol 116:825-844.

Qu Z, Hartzell HC (2001) Functional geometry of the permeation pathway of Ca2+-activated Cl-channels inferred from analysis of voltage-dependent block. J Biol Chem 276:18423-18429.

Quinton PM (1999) Physiological basis of cystic fibrosis: a historical perspective. Physiol Rev 79:S3-S22.

Rattner A, Sun H, Nathans J (1999) Molecular genetics of human retinal disease. Annu Rev Genet 33:89-131.

Reinsprecht M, Rohn MH, Spadinger RJ, Pecht I, Schindler H, Romanin C (1995)

Blockade of capacitive Ca2+ influx by Cl- channel blockers inhibits secretion from rat mucosal-type mast cells. Mol Pharmacol 47:1014-1020.

Ridley PD, Curtis MJ (1992) Anion manipulation: a new antiarrhythmic approach. Action of substitution of chloride with nitrate on ischemia- and reperfusion-induced ventricular fibrillation and contractile function. Circ Res 70:617-632.

Riordan JR, Rommens JM, Kerem B, Alon N, Rozmahel R, Grzelczak Z, Zielenski J, Lok S, Plavsic N, Chou JL, et al. (1989) Identification of the cystic fibrosis gene: cloning and characterization of complementary DNA. Science 245:1066-1073.

Rogers CS et al. (2008) Disruption of the CFTR gene produces a model of cystic fibrosis in newborn pigs. Science 321:1837-1841.

Ruiz C, Martins JR, Rudin F, Schneider S, Dietsche T, Fischer CA, Tornillo L, Terracciano LM, Schreiber R, Bubendorf L, Kunzelmann K (2012) Enhanced expression of ANO1 in head and neck squamous cell carcinoma causes cell migration and correlates with poor prognosis. PLoS One 7:e43265.

Saluja A, Logsdon C, Garg P (2008) Direct versus indirect action of cholecystokinin on human pancreatic acinar cells: is it time for a judgment after a century of trial? Gastroenterology 135:357-360.

Schroeder BC, Cheng T, Jan YN, Jan LY (2008) Expression cloning of TMEM16A as a calcium-activated chloride channel subunit. Cell 134:1019-1029.

Sheridan JT, Worthington EN, Yu K, Gabriel SE, Hartzell HC, Tarran R (2011) Characterization of the oligomeric structure of the Ca(2+)-activated Cl- channel Ano1/TMEM16A. J Biol Chem 286:1381-1388.

Shi XP, Candia OA (1995) Active sodium and chloride transport across the isolated rabbit conjunctiva. Curr Eye Res 14:927-935.

Shimizu T, Iehara T, Sato K, Fujii T, Sakai H, Okada Y (2013) TMEM16F is a component of a Ca2+-activated Cl- channel but not a volume-sensitive outwardly rectifying Cl- channel. Am J Physiol Cell Physiol 304:C748-759.

Shiue MH, Kim KJ, Lee VH (1998) Modulation of chloride secretion across the pigmented rabbit conjunctiva. Exp Eye Res 66:275-282.

Smith JJ, Travis SM, Greenberg EP, Welsh MJ (1996) Cystic fibrosis airway

epithelia fail to kill bacteria because of abnormal airway surface fluid. Cell 85:229-236.

Staley K, Smith R, Schaack J, Wilcox C, Jentsch TJ (1996) Alteration of GABAA receptor function following gene transfer of the CLC-2 chloride channel. Neuron 17:543-551.

Steenbergen C, Deleeuw G, Rich T, Williamson JR (1977) Effects of acidosis and ischemia on contractility and intracellular pH of rat heart. Circ Res 41:849-858.

Stephan AB, Shum EY, Hirsh S, Cygnar KD, Reisert J, Zhao H (2009) ANO2 is the cilial calcium-activated chloride channel that may mediate olfactory amplification. Proc Natl Acad Sci U S A 106:11776-11781.

Steward MC, Ishiguro H, Case RM (2005) Mechanisms of bicarbonate secretion in the pancreatic duct. Annu Rev Physiol 67:377-409.

Stohr H, Heisig JB, Benz PM, Schoberl S, Milenkovic VM, Strauss O, Aartsen WM, Wijnholds J, Weber BH, Schulz HL (2009) TMEM16B, a novel protein with calcium-dependent chloride channel activity, associates with a presynaptic protein complex in photoreceptor terminals. J Neurosci 29:6809-6818.

Stott JB, deCourcey F, Ennis M, Zholos AV (2014) Functional and pharmacological characterization of volume-regulated anion channels in human normal and cystic fibrosis bronchial and nasal epithelial cells. Eur J Pharmacol 740:183-191.

Sun H, Xia Y, Paudel O, Yang XR, Sham JS (2012) Chronic hypoxia-induced upregulation of Ca2+-activated Cl- channel in pulmonary arterial myocytes: a mechanism contributing to enhanced vasoreactivity. J Physiol 590:3507-3521.

Suzuki J, Umeda M, Sims PJ, Nagata S (2010) Calcium-dependent phospholipid scrambling by TMEM16F. Nature 468:834-838.

Tanaka H, Matsui S, Kawanishi T, Shigenobu K (1996) Use of chloride blockers: a novel approach for cardioprotection against ischemia-reperfusion damage. J Pharmacol Exp Ther 278:854-861.

Tarran R, Button B, Boucher RC (2006) Regulation of normal and cystic fibrosis airway surface liquid volume by phasic shear stress. Annu Rev Physiol 68:543-561.

Tarran R, Button B, Picher M, Paradiso AM, Ribeiro CM, Lazarowski ER, Zhang L, Collins PL, Pickles RJ, Fredberg JJ, Boucher RC (2005) Normal and cystic fibrosis airway surface liquid homeostasis. The effects of phasic shear stress and viral infections. J Biol Chem 280:35751-35759.

Terashima H, Picollo A, Accardi A (2013) Purified TMEM16A is sufficient to form Ca2+-activated Cl- channels. Proc Natl Acad Sci U S A 110:19354-19359.

Thiemann A, Grunder S, Pusch M, Jentsch TJ (1992) A chloride channel widely expressed in epithelial and non-epithelial cells. Nature 356:57-60.

Tien J, Lee HY, Minor DL, Jr., Jan YN, Jan LY (2013) Identification of a dimerization domain in the TMEM16A calcium-activated chloride channel (CaCC). Proc Natl Acad Sci U S A 110:6352-6357.

Tien J, Peters CJ, Wong XM, Cheng T, Jan YN, Jan LY, Yang H (2014) A comprehensive search for calcium binding sites critical for TMEM16A calcium-activated chloride channel activity. Elife 3.

Turner HC, Alvarez LJ, Candia OA (2001) Identification and localization of acid-base transporters in the conjunctival epithelium. Exp Eye Res 72:519-531.

Turner HC, Alvarez LJ, Bildin VN, Candia OA (2000) Immunolocalization of Na-K-ATPase, Na-K-Cl and Na-glucose cotransporters in the conjunctival epithelium. Curr Eye Res 21:843-850.

Turner RJ, Sugiya H (2002) Understanding salivary fluid and protein secretion. Oral Dis 8:3-11.

Turvill JL, Farthing MJ (1999) Water and electrolyte absorption and secretion in the small intestine. Curr Opin Gastroenterol 15:108-112.

Vajanaphanich M, Schultz C, Rudolf MT, Wasserman M, Enyedi P, Craxton A, Shears SB, Tsien RY, Barrett KE, Traynor-Kaplan A (1994) Long-term uncoupling of chloride secretion from intracellular calcium levels by Ins(3,4,5,6)P4. Nature 371:711-714.

Verkman AS (2001) Lung disease in cystic fibrosis: is airway surface liquid composition abnormal? Am J Physiol Lung Cell Mol Physiol 281:L306-308.

Verkman AS, Song Y, Thiagarajah JR (2003) Role of airway surface liquid and submucosal glands in cystic fibrosis lung disease. Am J Physiol Cell Physiol 284:C2-15.

Voss FK, Ullrich F, Munch J, Lazarow K, Lutter D, Mah N, Andrade-Navarro MA,

von Kries JP, Stauber T, Jentsch TJ (2014) Identification of LRRC8 heteromers as an essential component of the volume-regulated anion channel VRAC. Science 344:634-638.

Wei L, Vankeerberghen A, Cuppens H, Eggermont J, Cassiman JJ, Droogmans G, Nilius B (1999) Interaction between calcium-activated chloride channels and the cystic fibrosis transmembrane conductance regulator. Pflugers Arch 438:635-641.

West RB, Corless CL, Chen X, Rubin BP, Subramanian S, Montgomery K, Zhu S, Ball CA, Nielsen TO, Patel R, Goldblum JR, Brown PO, Heinrich MC, van de Rijn M (2004) The novel marker, DOG1, is expressed ubiquitously in gastrointestinal stromal tumors irrespective of KIT or PDGFRA mutation status. Am J Pathol 165:107-113.

White MM, Aylwin M (1990) Niflumic and flufenamic acids are potent reversible blockers of Ca2(+)-activated Cl- channels in Xenopus oocytes. Mol Pharmacol 37:720-724.

Wu MM, Lou J, Song BL, Gong YF, Li YC, Yu CJ, Wang QS, Ma TX, Ma K, Hartzell HC, Duan DD, Zhao D, Zhang ZR (2014) Hypoxia augments the calcium-activated chloride current carried by anoctamin-1 in cardiac vascular endothelial cells of neonatal mice. Br J Pharmacol 171:3680-3692.

Xiao Q, Cui Y (2014) Acidic amino acids in the first intracellular loop contribute to voltage- and calcium- dependent gating of anoctamin1/TMEM16A. PLoS One 9:e99376.

Xiao Q, Yu K, Perez-Cornejo P, Cui Y, Arreola J, Hartzell HC (2011) Voltage- and calcium-dependent gating of TMEM16A/Ano1 chloride channels are physically coupled by the first intracellular loop. Proc Natl Acad Sci U S A 108:8891-8896.

Xie W, Solomons KR, Freeman S, Kaetzel MA, Bruzik KS, Nelson DJ, Shears SB (1998) Regulation of Ca2+-dependent Cl- conductance in a human colonic epithelial cell line (T84): cross-talk between Ins(3,4,5,6)P4 and protein phosphatases. J Physiol 510 (Pt 3):661-673.

Xu WX, Kim SJ, So I, Kang TM, Rhee JC, Kim KW (1997) Volume-sensitive chloride current activated by hyposmotic swelling in antral gastric myocytes of the guinea-pig. Pflugers Arch 435:9-19.

Yang H, Kim A, David T, Palmer D, Jin T, Tien J, Huang F, Cheng T, Coughlin SR,

Jan YN, Jan LY (2012) TMEM16F forms a Ca2+-activated cation channel required for lipid scrambling in platelets during blood coagulation. Cell 151:111-122.

Yang YD, Cho H, Koo JY, Tak MH, Cho Y, Shim WS, Park SP, Lee J, Lee B, Kim BM, Raouf R, Shin YK, Oh U (2008) TMEM16A confers receptor-activated calcium-dependent chloride conductance. Nature 455:1210-1215.

Yao Z, Namkung W, Ko EA, Park J, Tradtrantip L, Verkman AS (2012) Fractionation of a herbal antidiarrheal medicine reveals eugenol as an inhibitor of Ca2+-Activated Cl- channel TMEM16A. PLoS One 7:e38030.

Yau KW (1994) Phototransduction mechanism in retinal rods and cones. The Friedenwald Lecture. Invest Ophthalmol Vis Sci 35:9-32.

Yu K, Duran C, Qu Z, Cui YY, Hartzell HC (2012) Explaining calcium-dependent gating of anoctamin-1 chloride channels requires a revised topology. Circ Res 110:990-999.

Yu Y, Kuan AS, Chen TY (2014) Calcium-calmodulin does not alter the anion permeability of the mouse TMEM16A calcium-activated chloride channel. J Gen Physiol 144:115-124.

Yuan H, Gao C, Chen Y, Jia M, Geng J, Zhang H, Zhan Y, Boland LM, An H (2013) Divalent cations modulate TMEM16A calcium-activated chloride channels by a common mechanism. J Membr Biol 246:893-902.

Zhao H, Muallem S (1995a) Agonist-specific regulation of [Na+]i in pancreatic acinar cells. J Gen Physiol 106:1243-1263.

Zhao H, Muallem S (1995b) Na+, K+, and Cl- transport in resting pancreatic acinar cells. J Gen Physiol 106:1225-1242.

Zong X, Stieber J, Ludwig A, Hofmann F, Biel M (2001) A single histidine residue determines the pH sensitivity of the pacemaker channel HCN2. J Biol Chem 276:6313-6319.

Zsembery A, Strazzabosco M, Graf J (2000) Ca2+-activated Cl- channels can substitute for CFTR in stimulation of pancreatic duct bicarbonate secretion. FASEB J 14:2345-2356.

Zygmunt AC (1994) Intracellular calcium activates a chloride current in canine ventricular myocytes. Am J Physiol 267:H1984-1995.

Zygmunt AC, Gibbons WR (1992) Properties of the calcium-activated chloride current in heart. J Gen Physiol 99:391-414.

국 문 초 록

세포 내 칼슘 증가에 의해 활성화되는 염소이온채널인 CaCC (Ca^{2+}-activated chloride channel)는 분비 기능의 상피세포에서 염소 이온 분비 조절에 중요한 역할을 한다. 세포 내 산성도는 상피세포의 전해질과 수액 분비에 영향을 준다. CaCC의 활성은 세포 내 산성도에 의해 저해된다고 알려져 있다. 그러나 산성에 의한 저해 메커니즘은 아직 규명되지 않았다. CaCC의 기능을 담당하는 분자로 알려진 ANOCTAMIN1 (ANO1)은 침샘 같은 분비기관에서 수액 분비에 중요한 생리학적 기능을 수행한다. 그러나 세포 내 산성도에 의한 채널 활성 조절은 아직 연구되지 않았다. 따라서 세포 내 산성도가 ANO1과 그 동족체인 ANO2, ANO6, ANO7, ANO9의 채널 활성에 어떤 영향을 미치는지 알아보았다. ANO9을 제외한 ANO들은 세포 내 산성에 의해 채널 활성이 감소하였다. 그 중에서 CaCC의 역할을 하고 있다고 알려진 ANO1과 ANO2는 세포 내 산성이 증가할수록 채널의 활성화에 필요한 세포 내 칼슘농도가 높아졌다. ANO1은 세포막 전위차와 열에 의해서도 활성화된다. 하지만 세포 내 산성은 세포막 전위차와 열에 의한 ANO1 활성에는 영향을 미치지 않았다. 세포 내 산성에 의한 저해되는 특정 부위를 찾기 위해 분자생물학적 기법을 통해 여러 ANO1 돌연변이체를 제작하였다. 우선 산성용액에서 적정 가능한 해리 상수를 갖는 히스티딘

잔기를 다른 아미노산으로 대체하여 그 활성과 산성저해 정도를 알아본 결과, ANO1에 존재하는 히스티딘 잔기들은 모두 산성 저해 특성과 관련이 없었다. 또한 글루탐산과 아스파산 잔기의 집합체를 삭제 또는 대체해 본 결과, 산성 저해 정도에 변화를 주지 않았다. 최근 ANO1의 균류 동족체인 nhTMEM16의 X-선 결정구조가 밝혀졌다. 이 구조를 통해 채널의 활성을 위한 칼슘 결합 부위의 아미노산 잔기들이 확실해졌다. 이 잔기들을 다른 아미노산으로 대체한 결과, 칼슘 감도의 현저한 감소와 함께 세포 내 산성에 의한 저해도 사라졌다. 하지만 칼슘에 의한 반발력을 통해 활성에 도움을 주는 나선구조의 돌연변이체는 세포 내 산성도에 의해 영향을 받지 않았다. 이러한 연구 결과를 통해, 세포 내 수소이온이 칼슘과 같은 결합 부위에 작용한다는 것을 알 수 있었다. 이는 경쟁적인 방해나 구조적인 변화를 통해 일어난다고 생각된다. 본 연구는 분비 상피세포의 수액과 전해질의 분비에 영향을 미치는 세포 내 산성에 의한 ANO1과 그 동족체들의 활성 조절을 확인하고 ANO1 활성 저해의 분자수준의 메커니즘을 제시하였다.